MODELLING THE AZIMUTHAL DEPENDENCE OF THE TROPOSPHERIC DELAY ON GPS USING GAMIT/GLOBK AND THE UPDATED VIENNA MAPPING FUNCTION

BY:

BRIAN MAKABAYI

A Thesis submitted to the school of Graduate studies of Addis Ababa University in partial fulfillment of the requirements for the Degree of Master of Science in Civil Engineering under Geodesy

Addis Ababa, Ethiopia
April, 2013

APPROVAL SHEET

Addis Ababa University

Institute of Technology

Department of Civil Engineering

The undersigned here by certify that they have read and recommend to the school of technology for acceptance a thesis entitled "**Modelling the Azimuthal Dependence of the Tropospheric Delay On GPS Using GAMIT/GLOBK and the Updated Vienna Mapping Function**" by **Makabayi Brian** in partial fulfillment of the requirements for the degree of Master of Science.

Date: April, 2013

Supervisor/Advisor:

1. _____ _____ _____

Signature Date

Co-Advisor(s):

1. _____ _____ _____

2. _____ _____ _____

Signature Date

Examiner(s):

1. _____ _____ _____

2. _____ _____ _____

3. _____ _____ _____

Signature Date

ACKNOWLEDGEMENTS

I am indebted to so many people for this master's work. Even though all cannot be mentioned by name, I convey my gratitude anyhow.

I will always give glory to the almighty God for not only the privilege to study but also seeing me through this long journey in good shape. I thank Edulink for the sponsorship and study opportunity availed to me. My thanks also go to Makerere, the College of Engineering Design, Art and Technology and the Department of Geomatics and Land Management for the academic support rendered to me during my study. I would like to appreciate the above for granting me a study leave and continuing my employment with them after my study. My gratitude is extended to my supervisor, Dr. Addisu Hunegnaw for the patience, diligence and dedication to my work. I value the time we have spent working together. I recognize Drs. Tulu Besha and Lewi Elias for all the effort in trying to help me carry out my field work in Addis Ababa.

I am extremely grateful to Mr Sengendo Ronald for the help he gave me during the writing of my Thesis. I thank Drs Moses Musinguzi and Anthony Gidudu for the help they rendered me to manage to get this scholarship. I greatly appreciate the fatherly advice given to me by Dr Moses Musinguzi.

My colleagues at the Geomatics and Land Management Department of Makerere especially, Ms Dianah Abeho Rose, Ms Lydia Mazzi Kayondo and Ms Lilian Mono Wabineno for the diverse support rendered to me during the study period.

I also would like to thank my classmates of the Geodesy class in Addis Ababa for help they rendered in settling in after arrival in Addis Ababa and support as we studied especially; Mr. Asmamaw Chanie and, Berhanu Bekele

Makabayi Brian

April 2013

DEDICATION

To my dear father and friend, Mr. Kenneth Mafabi
You always shared with me of your hard study and urged me to follow suit
That has always kept on my heart,
To my dear Mother and friend, Mrs. Pheobe Mafabi
Thank you for all life's encouragement
To my Siblings, Brenda, Barbara, Bill and Bena
I urge you to follow your dreams passionately
To my Fiancée and friend Ms. Lindah Mbabazi
Thanks for all the support

TABLE OF CONTENTS

LIST OF ACRONYMS

GPS	Global Positioning System
VLBI	Very Long Baseline Interferometry
MIT	Massachusetts Institute of Technology
GAMIT	GPS Analysis at MIT
GLOBK	Global Kalman Filter
WVR	Water Vapour Radiometer
VMF1	Vienna Mapping Function
NMF	Niell Mapping Function
GMF	Global Mapping Function
GPT 50	Global Temperature Pressure
UFL	U-File
TEC	Total Electron Content
DOP	Dilution of Precision
GLONASS	Global Navigation Satellite System
C/A code	Clear/Access Coarse/Acquisition code
P code	Private/Precise code
DGPS	Differential GPS Positioning
GPST	GPS Time
NWM	Numerical Weather Model
ZPD	Zenith Path Delay
MF	Mapping Function
ZHD	Zenith Hydrostatic Delay
ZWD	Zenith Wet Delay
ECMWF	European Centre for Medium-Range Weather Forecasts
IMF	Isobaric Mapping Function
ERA	European Region Agency

DOY	Day of Year
SLR	Satellite Laser Ranging
VTEC	Vertical Total Electron Content
IGRF	International Geomagnetic Reference Field
IAGA	International Association of Geomagnetism and Aeronomy
STEC	Slant Total Electronic Content
CODE	Centre for Orbit Determination in Europe
GNSS	Global Navigation Satellite System
IGS	International GNSS Service
MCS	Master Control Station
PRN	Pseudo Random Noise
WGS84	World Geodetic System 1984
Block IIR	Block II Replenished/Replacement
Block IIF	Block II Forward
U.S	United States
I.D	Identification Number
Block IIA	Block II Advanced
Block IIM	Block II Modern
IONEX	Ionospheric Files
NAVSTAR	Navigation Satellite Timing and Ranging
RMS	Root Mean Square
WRMS	Weighted Root Mean Square
LS	Least Squares
NMFH	Hydrostatic NMF
NMFW	Wet NMF
VMFH	Hydrostatic VMF
VMFW	Wet VMF

LIST OF TABLES

LIST OF FIGURES

ABSTRACT

In order to improve the accuracy of point coordinates obtained by the Global Positioning System (GPS), it is important to model the atmospheric delay caused by the Troposphere (Neutral atmosphere). Until now the atmosphere has been considered to be horizontally layered and azimuthally symmetric. Although for most applications this assumption is appropriate, azimuthal asymmetry may introduce significant errors in geodetic measurements where high precision is required. Azimuthal variation of 20% is quite commonly observed in humid areas. The assumption of azimuthal symmetry may cause significant errors when the local troposphere has large lateral temperature, pressure or humidity gradient variations. Recent VLBI studies indicate that azimuth asymmetry effects at 15^0 Elevation typically produce a Root Mean Square (rms) variation of 7mm, but at times this effect can be as much as 5times. This research investigates the effect of azimuth asymmetry on Tropospheric delay modelling using GPS. The dependence of the Tropospheric Delay on azimuth of the satellites was modelled using GAMIT/GLOBK software and the application of the updated Vienna Mapping Function (VMF1) in Tropospheric Delay modelling was analyzed. A combination of different mapping functions (Vienna Mapping Function (VMF), Niell Mapping Function (NMF) and the Global Mapping Function (GMF)) with the corresponding a priori constraints (U-file (UFL) and Global Pressure Temperature (GPT 50) were used. The combination of VMF and UFL for a different number of gradients estimated per day was done for North America, Europe and Uganda GPS data. The combinations made were evaluated using the Repeatability graphs developed using GLOBK. The results were also presented using tables and line graphs. When the gradients are modelled, the accuracy of fixing the GPS points increases. The accuracy obtained is very low when the gradient is not estimated. The accuracy of the East and North offsets increased more than the up offset in this research since there was no serious storm surge. When the gradient estimated per day is two (2) the accuracy is sufficient for fixing the East and North offsets well as for the up offset, more gradients have to be estimated especially when there is a serious storm surge. VMF1 with GPT50 fix well the East and North offsets well as VMF1 and UFL fix the up offset better. When there is a serious storm surge, gradients more than three should be estimated per day to model the Tropospheric delay well. Different MF/APRIORI combinations should be varied with the number of gradients estimated per day. Meteorological Rinex Files (RNX) should be used as a priori zenith constraints in modelling the Tropospheric delay in the future.

Keywords Troposphere Modelling, Mapping Function, GPS, GAMIT/GLOBK.

CHAPTER 1

1.1 Background

The Global Positioning System (GPS) is a satellite-based radio GPS positioning system that has been fully operational since 1994. Although GPS was originally designed for (military) navigation purposes, the system has shown to be of great interest for surveying. Where for navigation applications metre-level accuracy is desired using GPS's pseudo-range observations, surveyors aim at centimetre accuracy or even better. To obtain this accuracy, they use the GPS phase observations and relative positioning techniques. The highest accuracy can be obtained with long observation times, by resolving the phase ambiguities, and by using accurate orbits in post processing.

For most survey purposes, cm-level accuracy is sufficient. For the height component however, the demands are often somewhat stricter than for the horizontal coordinates. Unfortunately, the intrinsic precision of GPS-derived heights is worse than that of the horizontal coordinates. This is caused by a combination of satellite geometry with all satellites on one side (above) the receiver, the presence of receiver clock errors, and disturbances in the neutral atmosphere also referred to as troposphere, that causes delays of the GPS signals. The first aspect can only partly be overcome by using low elevation satellites, but these observations to these satellites are of lower accuracy and are most sensitive to error sources like multipath.

The second aspect can only be overcome by using accurate atomic clocks, which would be very expensive to make GPS receivers suitable for everyday use. But by modelling of the delays caused by the troposphere, the accuracy of GPS derived heights will improve. It should however be noted that the physical limitation of the GPS satellites being only tracked above the receiver still contributes to the greatest error in the GPS derived heights.

The weather affects us all, sometimes disastrously with vicious storms; sometimes pleasantly with sunshine and warm breezes. It also affects GPS. But, whereas bad weather might disrupt our lives, causing us to curtail or postpone an activity, GPS continues to perform -it's an all-weather

system. Rain, snow, fog, and clouds all have a negligible effect on GPS. However, unseen weather - temperature, pressure, and humidity variations throughout the atmosphere does affect GPS observations. These parameters determine the propagation speed of radio waves, an important factor that must be accounted for when processing GPS or other radiometric observations. Because we cannot predict their exact values ahead of time, these invisible weather variables are a source of error in GPS positioning and navigation.

Modelling the propagation of the electromagnetic micro- wave signals through the electrically neutral part of the atmosphere (referred as troposphere) is of common interest for the space geodetic techniques.

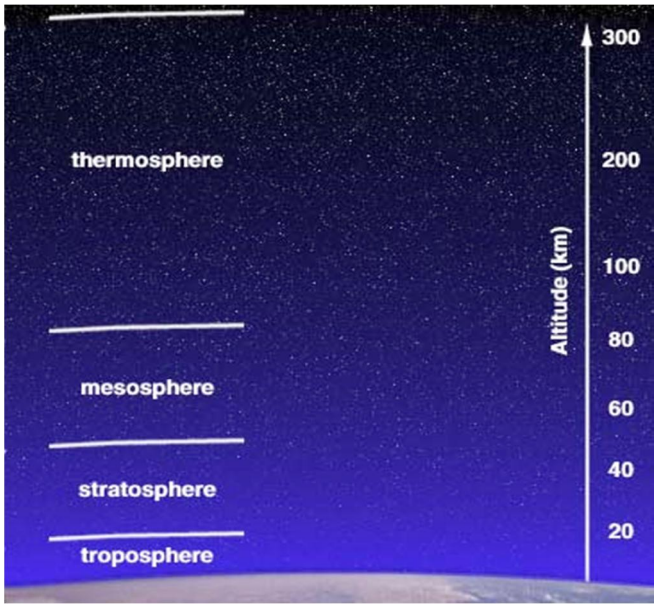

Figure1.1 The Basic Atmospheric Structure up to 300km

The troposphere is the lowest part of the earth's atmosphere up to *70km* altitude. The neutral atmosphere (troposphere, tropopause and stratosphere) is a non-dispersive medium with respect to the radio waves up to frequencies of *15GHz*. Thus the propagation is frequency independent unlike the ionopsheric refraction, consequently affects both the code and phase measurements the same way. The disadvantage is that an elimination of the tropospheric refraction by dual/triple frequency linear combination techniques is not possible. The effect is a delay that

reaches 2.0-2.5 metres in the zenith direction and increases approximately as a function of the cosecant of the elevation angle.

Many space geodetic measurement techniques, like Very Long Baseline Interferometry (VLBI) and GPS, use the propagation time of radio waves multiplied by the speed of light to get a measure of range. When a signal passes through the earth's atmosphere, the atmosphere affects the wave in three ways: (1) it causes a propagation delay; (2) it causes a bending of the ray path; and (3) it absorbs the signal. In this thesis only the propagation delay in the neutral atmosphere (or troposphere) is considered, including an indirect delay caused by the bending. Derivations and descriptions are given of several (components of) delay models that can be used to a priori correct the measured ranges.

1.2 Case Studies

1.2.1 North America

The plots of the IGS (International GNSS Service) stations in North America that were used for this research are shown in figure 1.2 below. The IGS stations used were Blythe (BLYT), Brand Basin (BRAN), Caltech (CIT1), JPL Mesa (JPLM) and Mt. Wilson (WLSN). These stations were selected because, after preliminary analyses was done using a combination with some other stations of North America – BILL, WIDC and SFDM the highest accuracy (lowest Root Mean Square (WRM)) of the repeatabilities of fixing the GPS points was obtained for the former points.

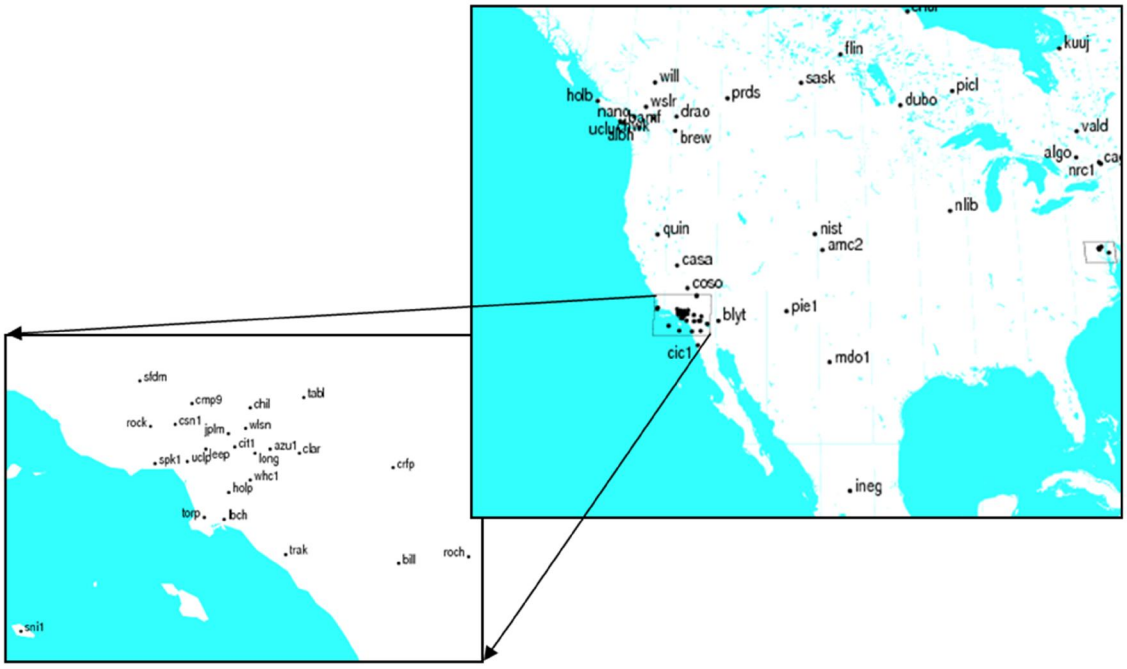

Figure1.2 The IGS Stations for the Network in North America

The IGS stations above are located in a dry environment. This enabled the analysis of the effect of the gradient and asymmetry of the atmosphere when the atmosphere does not have large pressure and humidity gradient variations.

1.2.2 Europe

The plots of the IGS stations in Europe that were used for this research are displayed in figure 1.3 below. The IGS stations used are Brussels (BRUS), Frankfurt (FFMJ), Matera (MATE), Onsala (ONSA), Braunschweig (PTBB), Villafranca (VILL) and Zimmerland (ZIMM).

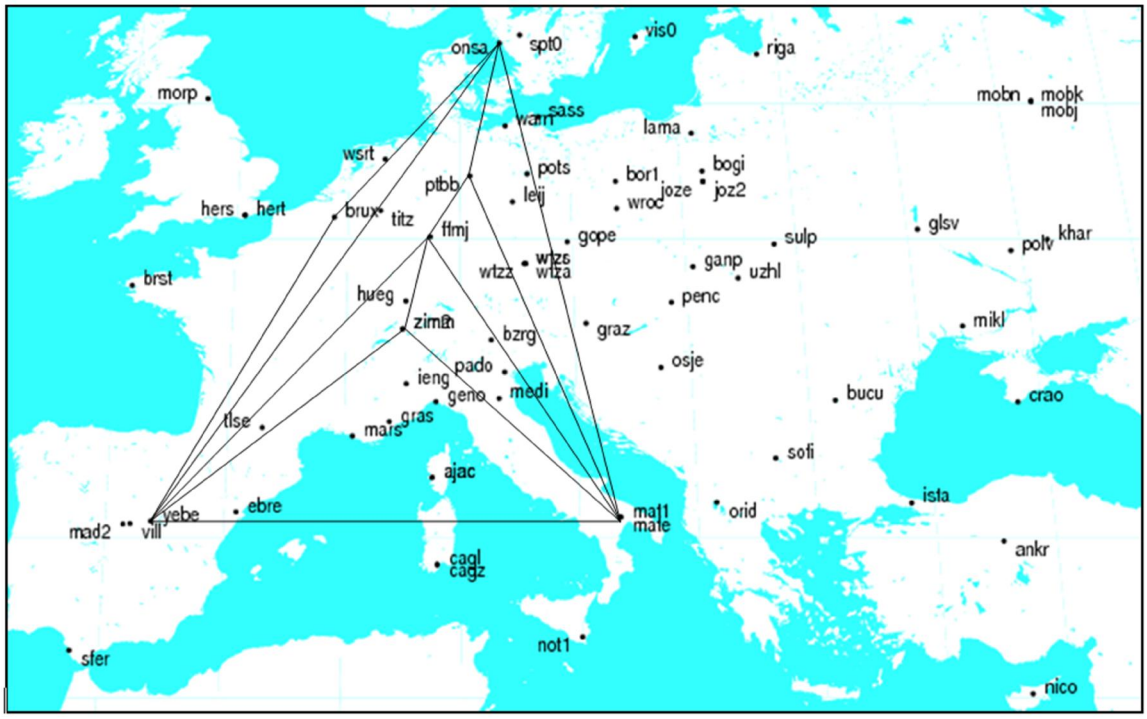

Figure1.3 The IGS Stations for the Network in Europe

The stations compared to the ones selected from North America are in a relatively humid area and thus enabled the investigation of the dependence of the Tropospheric delay on gradient when there is significant lateral and temporal variation in temperature, pressure and humidity.

1.2.3 Uganda

This compared to the above two networks, the dependence of the Tropospheric delay on gradient at a local level with a network having shorter distances.

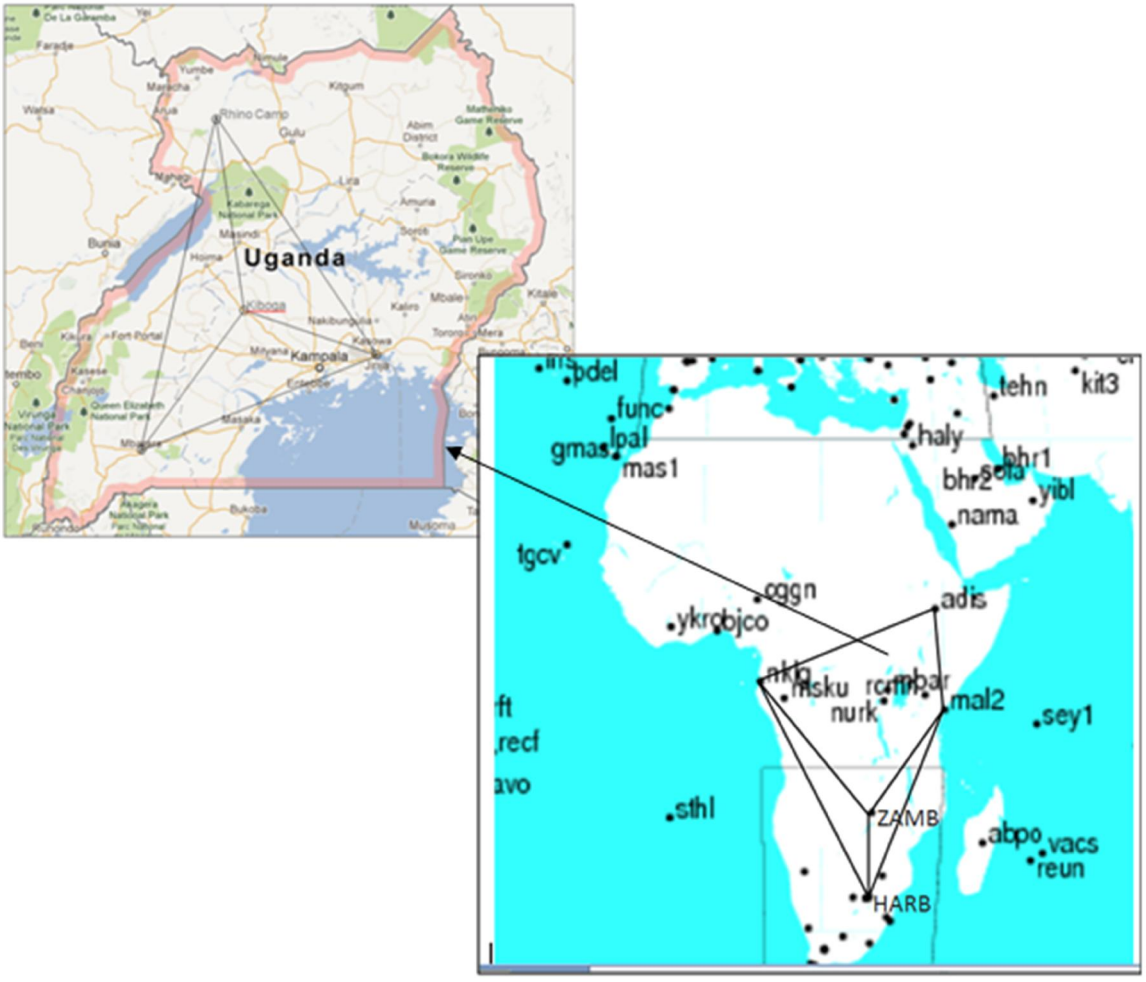

Figure1.4 The IGS Stations for the Network in Uganda

The GPS data used for the analyses was only for three days compared to year data collected for 2011 for North America and Europe. The stations used in Uganda included the local station and the near and most stable station in Africa. The local stations were Jinja (JINJ), Kiboga (KIBO), Mbarara (MBRA) and Rhino Camp (RHIN). Whereas the IGS station used were Addis Ababa University (ADDIS) in Ethiopia, Hartebeesthoek (HARB) in South Africa, Malindi (MAL2) in Kenya, N'Koltang (NKLG) in Gabon and Lusaka (ZAMB) in Zambia.

1.3 Significance of the Research

MacMillan (1995) showed that the position repeatability was significantly improved by using the gradient model. Similar results were reported for VLBI data by Chen and Herring (1997), who employed a more accurate gradient model, especially at low elevation angles. Similar efforts have also been made in GPS data analyses. Bar-Sever et al. (1998) implemented MacMillan's (1995) gradient model in GIPSY-OASIS II software and demonstrated that the model improved the repeatability in precise point positioning. On the basis of extensive point positioning experiments, they concluded that the best strategy is to use the elevation cut off of 7^0.From direct comparisons between data from GPS and a collocated (Water Vapour Radiometer) WVR, they further suggested that the GPS solution seemed to well reproduce the variation of the wet gradient component over timescales as short as 15 minutes. These conclusions suggest that the gradient model would significantly improve both of the accuracy and precision of position estimates.

1.4 Problem statement

The un modelled Tropospheric delay due to the azimuth (gradient) variation-the atmosphere assumed symmetric, will propagate to the coordinates of the GPS point being fixed. This millimetre error may be miss interpreted as movement in high precision Geodetic works like Deformation monitoring of large infrastructures like Dams, Bridges, Monumental Buildings and slow subsidizing geological sites.

1.5 Problem definition

The Tropospheric delay estimations assume azimuthal symmetry of the atmosphere in the vicinity of the given receiver, whereas azimuthal variations of 20% are quite commonly observed in humid areas.

Recent VLBI studies indicate that azimuth asymmetry effects at 15^0 typically produce a root mean square (RMS) variation of 7mm, but at times this effect can be as much as five times.

The assumption of azimuthal symmetry may cause significant errors when the local troposphere has large lateral temperature, pressure or humidity gradient variations leading to inaccurate conclusions in precise geodetic works.

1.6 General objective

Model the Azimuthal Dependence of the Tropospheric Delay on GPS Using GAMIT/GLOBK and the updated Vienna Mapping Function.

1.7 Specific objectives

- Investigate the dependence of the Tropospheric delay on azimuth of the satellite using GAMIT/GLOBK GPS processing software.
- Study the application of the updated Vienna Mapping Function (VMF) in Tropospheric delay modelling.

1.8Arrangement of Report

The remaining part of this Report contains the following chapters and contents.

Chapter Two focuses on the extensive literature review on aspects used in this research-Global Positioning System, GAMIT/GLOBK Software Processing- Atmospheric Models, Ocean Models, Ionospheric Files (IONEX) and Meteorological Files (Met Files), Different Tropospheric Delay Models and the Different Mapping Functions.

Chapter three describes the methodology followed in processing the collected GPS data from different stations.

Chapter four contains the presentation of the results obtained from this research including a detail analysis and discussion of the results.

Chapter five has the Conclusions and Recommendations made from the discussions and analyses from chapter four.

References are at the end showing the reading material used as an aid in this research.

Appendices contain the extra results that could not be included in the body of the report yet are important to be included in the report.

CHAPTER 2

2.1 GPS Introduction

The NAVSTAR Global Positioning System (GPS) is a satellite-based radio-positioning and time transfer system designed, financed, deployed, and operated by the U.S. Department of Defence (Rizos, 1990). GPS has benefitted the civilian community with the applications ever increasing today. The use of GPS is ever increasing because of the following reasons:

- The position accuracies obtained with this positioning method is relatively high ranging from metres to millimetres basing on the accuracy requirements, the surveying method and equipment used.
- It can be used to determine velocity and time alongside the position coordinates with accuracy close to that of the position coordinates.
- GPS signals can be accessed by the users everywhere on the earth (air, ground or at sea) provided there is no significant obstruction of the site being surveyed.
- No charges are to be paid the system is free except the initial charges that the user has to incur to buy the hardware (GPS receivers).
- It works in all weather conditions 24 hours a day making it suitable for monitoring applications.
- The position coordinates are both horizontal and vertical coordinates making it suitable for applications like navigation.

Due some of the reasons stated above the number of civilian users has now significantly grown superseding that of the military. However it is the U.S military that is still operating the GPS systems even if the civilian users have increased over the years. Even if GPS is controlled by the military the development and innovations within the civilian sector has continued to boom. Some of these innovations have been partly to overcome some of the constraints on the GPS system which were imposed or created by the military operatives.

Development work on GPS commenced within the U.S. Department of Defence in 1973, the motivation being to develop an all-weather, 24-hour, global positioning system to support the positioning requirements for the armed forces of the U.S. and its allies (Rizos, 1990). This system was to replace the different navigation systems that were then existent and emphasis was on the reliability of the system and how it would be able to survive for long. To fulfil this, a number of conditions had to be met:

- The system had to be usable on all classes of platforms: aircraft, ship, land and space,
- The velocity, Time and Position determined had to be at an appropriate accuracy basing on the need at hand,
- The determined position coordinates had to be referenced on a single global geodetic datum (World Geodetic Datum (WGS84)),
- A particular class of user would access the highest accuracy,
- The system was to be resistant to jamming whether intentional or unintentional jamming,
- More than required hardware (satellites) and components (signals) were to be considered,
- The user was not to transmit a signal to the satellite thus the system was to be passive,
- Able to be used by the global community simultaneously, and
- Much of the system complexity was to be build into the satellite segment.

This led to a design based on the following essential concepts:

- A system where the signal was transmitted from the satellite only (one-way ranging system) and the end user of the signal was unaware of. This implied the end user would not be detected for safety purposes and to be charged for the system.
- The use of very accurate clocks (atomic clocks) i.e. Caesium, Rubidium and Hydrogen maser.
- A system that makes range-like measurements with the aid of pseudo-random binary codes modulated on carrier signals (Rizos, 1990).
- The signals from the satellite had to be less affected by the rain and cloud.
- The system had to have a sufficient number of satellites in the constellation to ensure that at any point on the earth where one was, a sufficient number of satellites would be seen for positioning purposes.

What could have not been anticipated by the system designer was how the innovations to come later not would greatly improve GPS for precise positioning and navigation. For example, GPS with different positioning and measurement modes today, accuracies of tens of metres is possible for navigation purposes and sub-centimetre accuracy for relative positioning. GPS has so many applications in our daily lives today that it is difficult to imagine life without a GPS system. Rarely have so many seemingly unrelated technological advances been required to make a complex system such as GPS work. Briefly they are:

Space System Reliability: The U.S. space program had by 1973 demonstrated the reliability of space hardware. In particular, the Transit system had offered important lessons. The Transit (Transit is an early satellite-based navigation system based on Doppler measurements (Seeber, G., 1993.)) satellites were originally designed to last 2-3 years in orbit, yet some of the satellites have operated well beyond their design life. In fact Transit continued to perform reliably for over 25 years.

Atomic Clock Technology: The development of atomic clocks led to the invention of precise-time keeping which is very crucial for GPS positioning. However, the atomic clocks had never been tested in space before the start of the GPS system. The development of the atomic clocks, rubidium, caesium and hydrogen masers was thus a technological breakthrough. The atomic clocks used on GPS satellites have long-term frequency stability a few parts in 10^{14} per day which is about 1 second in 3,000,000 years. This long-term stability is one of the keys to GPS, as it allows for precise GPS positioning.

Quartz Crystal Oscillator Technology: Quartz crystal clocks as those used in digital watches are those that were proposed to be used in the GPS ground receivers compared to the atomic clocks. Using atomic clocks in the GPS receivers would make the cost of the receivers very expensive. Apart from the quartz clocks being cheap relative to the atomic clocks, they have very good stability over a short term. However, their long-term drift is determined in the fixing of the coordinates of a point.

Precise Satellite Tracking and Orbit Determination: For the GPS system to work efficiently, the coordinates of the GPS satellites must be accurately known and predicted based upon an earth-fixed reference system. Ground monitor stations collect tracking data which is collected approximately over a week and is analysed to determine the satellite orbit. The determined

reference ephemeris is extrapolated into the future and the data is up-loaded to the satellites. Satellite coordinates have been predicted to a few metres for a day.

Spread-Spectrum Technology: The ability to track and obtain any selected GPS satellite signal (a receiver will be required to track a number of satellites at the same time), in the presence of considerable ambient noise is a critical technology. This is now possible using spread-spectrum and pseudo-random-noise coding techniques (Spilker Jr., J.J., 1980.).

Large-Scale Integrated Circuit Technology: To realize the desired low cost, low power and small size necessary for much of the user equipment, the GPS program relies heavily on the successful application of VLSI circuits, and powerful computing capabilities built onto them (Rizos, 1990).

The GPS system comprises three segments:

- **The Space Segment**: this consists of the satellites and the signals emanating from the satellites.
- **The Control Segment**: this is where the satellites are tracked, the orbit of the satellites are computed and other satellite controls done.
- **The User Segment**: this consists the users who use the GPS signals to determine the coordinates of the different points.

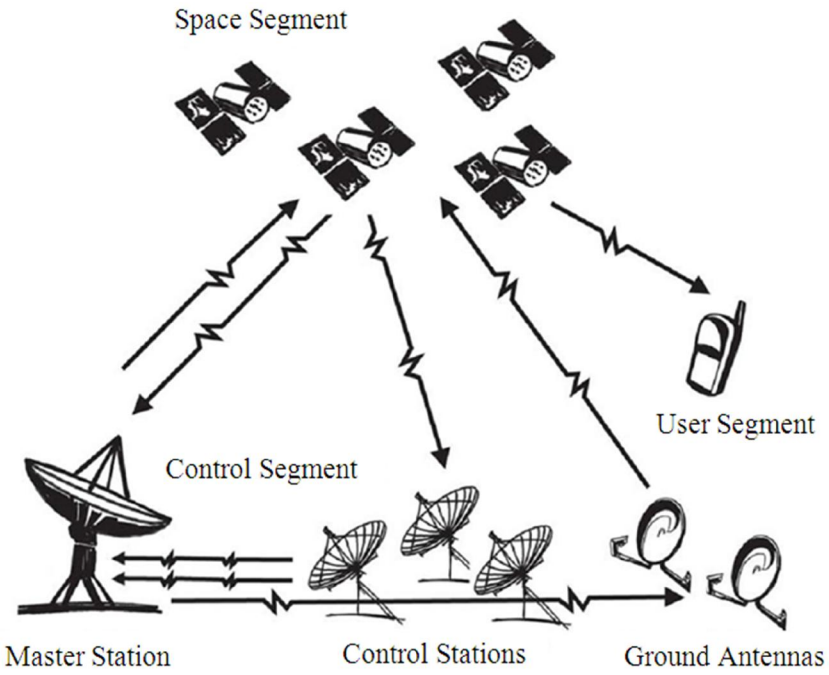

Figure2.1 GPS System Element

2.1.1 The Space Segment

The space segment is a constellation of GPS satellites (24) which emit signals that are used to position oneself in 3D, determine the velocity of moving vessels and the time of the positioning. The satellites in constellation are for the following functions:

- It receives and stores data that has been sent from the stations in the control segment.
- On board the satellites are the atomic clocks that are used to accurately measure GPS time.
- GPS signals on the carrier signals (L-band signals) are sent to the users from the satellites in the space segment.
- Contains the orbits in which the satellites revolve the earth transmitting signals to the end user.

The GPS satellites transmit signals on two L-band signals which enable the modelling of the ionospheric effect on GPS signals. This is done through linear combinations. However in the future there will be an introduction of the third L-band signal. Signals at this frequency can easily be reflected or blocked by solid materials. The clouds will be easily penetrated but leaves

of the trees are not easily penetrated as the clouds. The obstruction of the GPS signals by the tree leaves is dependent on the thickness of the tree leaves and whether they are wet or dry. It should be appreciated that the signals are transmitted with enough power because the signals travel a very long distance (20600km) before they reach the earth.

Below are the components of the satellite signals;

- L1 and L2 carrier waves.
- P and C/A codes which are modulated on the carrier waves (L1 and L2).

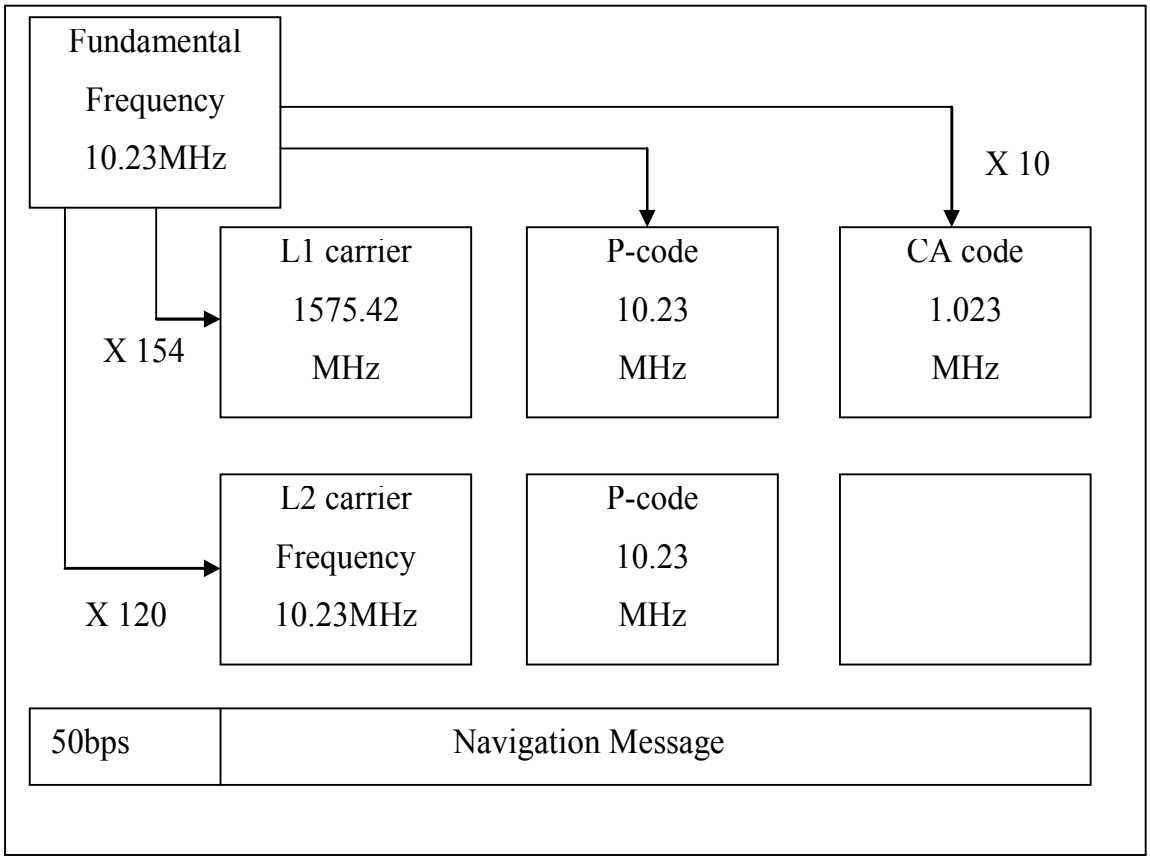

Figure2.2 GPS Satellite Signal Components

The ranging codes and the navigational message are modulated onto the carrier waves. The ranging codes are primarily used to measure the pseudo range by timing the travel time of the signal from the satellite to the user. This time of travel is multiplied by the velocity of light to yield the distance between the satellite and the receiver (user). The transmitted navigation message carries with it the satellite orbit information, satellite clock parameters and any other information necessary for determining the position of a point. The satellites normally carry four

atomic clocks. Two caesium and two rubidium atomic clocks, however not all are used some being spares. The other satellite positioning systems to come (GALILEO) plan to carry on board more precise atomic clocks (hydrogen masers).

2.1.2The Control Segment

The Control Segment consists of facilities necessary for satellite health monitoring, telemetry, tracking, command and control, satellite orbit and clock data computations, and data up linking (Rizos, 1990). There are five ground facility stations: Hawaii, Colorado Springs, Ascension Island, Diego Garcia and Kwajalein (Rizos, 1990). All are owned and operated by the U.S. Department of Defence and perform the following functions:

- The five stations are monitor stations. The monitor stations have GPS receivers that track the satellites. The data obtained from the tracking is sent to the Master Control Station.
- The Master Control Station (MCS) is located at Colorado Springs. At this Master Control Station the tracking data is processed to compute satellite ephemerides and clock corrections. It also carries out the following on the space segment, spacecraft manoeuvring, signal encryption, satellite clock keeping, etc.
- Upload stations are located at three stations (Ascension Island, Deigo Garcia, and Kwajalein). At these stations is where data is uplinked to the satellite using the s-band. In the uplinked data is the orbit and clock correction received by the user as a navigation message. Command telemetry is also received from the MCS.

The U.S Air Force command, Second Space Wing and Satellite Control Squadron at Falcon Air Force Base in Colorado is responsible for the operation of the Control and Space Segments. At least each day, each upload station views all the satellites. Uploads are therefore made to the satellite three times a day, this implies a new navigation message and command telemetry is transmitted to the GPS satellites every eight hours. The most essential functions of the control segment are; the computation of the satellite orbits (ephemerides) and the satellite clock errors. This is because the GPS satellites function as orbiting control stations in GPS positioning and their coordinates have to be known to a very high accuracy. Well as the satellite clock errors if well determined will reduce the measurement bias in the ranges.

The GPS satellites travel in almost a regular orbit pattern at a very high speed that is approximately 4km/second. After the satellite reaches its orbit after detaching from the launch rocket, this orbit is defined by the satellite's initial position and velocity and external force acting on the satellite from the other heavenly bodies. The satellites move in an elliptical orbit referred to as the keplerian ellipse. However the orbit of the satellite departs from the ideal keplerian ellipse due to non-spherical gravitational components of the earth's gravity field and non-gravitational forces that perturb the orbit.

Satellite motion is usually affected by the following forces:

- The gravitational attraction of the earth (spherical and non-spherical),
- The third body problem, the gravitational attractions from the sun, moon and planets towards the earth,
- The drag effect due to the atmosphere,
- Solar radiation pressure , and
- The gravitational effect due to the solid earth and ocean tides.

For the satellite orbit to be modelled accurately, the perturbing forces have to be computed accurately. If the perturbing forces are determined, knowing the initial position and velocity of the satellite will enable the computation of the satellite position and velocity in the future.
However, it is not normally the case to compute the perturbing forces very accurately. Satellite observations at the monitor stations are analyzed to produce an orbit that best fits the available observations. This will need the adjustment of the orbit parameters and the other external forces affecting the satellite orbit. The process of determining the satellite orbit is really complex but it is done continuously and automatically.
Orbit computations done at the Master Control Station avail the satellite ephemeris for use as orbiting control for GPS positioning. The satellite ephemeris contains the following parameters:

- 3-D coordinates and velocity at different intervals of time,
- Keplerian elements and their rate of change with time,
- The satellite trajectory in polynomial form,

The above orbit representations make up the broadcast ephemeris which is carried along with the satellite navigation message. The satellite coordinates are expressed in an earth-fixed reference system such as (World Geodetic System 1984 (WGS84)).

Each GPS satellite clock is monitored against GPS Time. This is done by atomic clocks at the GPS Master Control Station. The clock correction is made available to the users through the satellite clock coefficients. This clock correction is provided in polynomial form in the navigation message. It is however a prediction of the clock behaviour that is available to the users.

The developments in GPS are aiming at making the GPS system to operate independent from the Ground Control Segment without necessarily degrading the accuracy that should be obtained. For example it is planned that Block IIR and IIF will have crosslink capability which will make possible communication and ranging between satellites. This will enable the computation of the ephemeris within the space segment without involving the ground control segment.

2.1.3 The User Segment - Applications

This is the part of the GPS system that we have control over compared to the control and satellite segment that is still control by the U.S Department of defence. In the user segment emphasis is on the GPS applications, Equipment and the different positioning strategies. The development of the commercial GPS product has been driven by the growth in the different user applications or requirements. The GPS applications may be classified into the following categories:

1. Navigation on land, sea and air. This includes precise navigation, collision avoidance, cargo monitoring, vehicle tracking, and search and rescue operations. For these applications, the accuracy requirement is not that high but the results are needed in real time. This is the only handle that may be posed.
2. GPS is also used in Surveying and Mapping on land, sea and even in the air. Contrast to the navigation application, here the accuracy requirements are high.
3. In Military Applications, the reliability of the system is given high priority because this may imply loss of life.
4. Recreational Uses, used on land, sea and air need less accuracy and low cost equipment that is very easy to use.

5. Other uses that need specialized skills are: time transfer, attitude determination, spacecraft operations, atmospheric studies, etc. Which are high cost systems and need specialized skilled personnel.

GPS equipment has tremendously developed over the years that the GPS system has been operational. GPS equipment implies the total combination of the hardware, software and operational procedures (requirements).

2.2 The User Segment - Positioning Principles

Basically GPS positioning is by the measurement of ranges. The positioning principle is by the intersection of the loci. In two-dimensional positioning, the position of the point being fixed is at the intersection of two circles whose centres are the two satellites and the radius of the circles is the ranges measured form the satellites to the point being fixed. In three- dimensional positioning, the position of the point being fixed is the intersection of three spheres. The radii of these spheres are the three ranges measured from the satellites to the point being fixed (Figure 2.5). In case of GPS positioning the coordinates of the satellites are known (the coordinates are obtained from the satellite ephemeris that is within the navigation message that is received at the receiver). The combination of these satellite coordinates with the measured range distances, the position of the point being fixed is determined. In two dimensions the position of the point being fixed is the intersection of two distances (ranges) of two circles d1 and d2 Figure 2.4. It should be noted that the former scenery gives two positions of which only one is correct. One position is however easily discarded using the a priori approximate coordinates and velocity of the point being fixed. The other alternative is to measure three ranges instead of only two ranges. If these ranges are measured accurately without error then the position to be fixed is fixed without error.

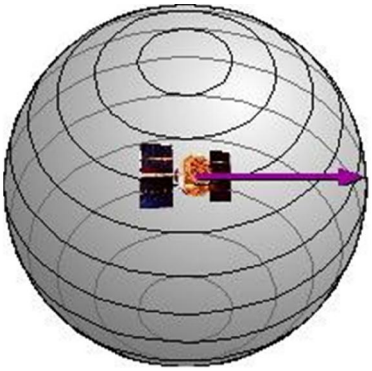

Figure2.3 Surfaces of Position for Range Measurements

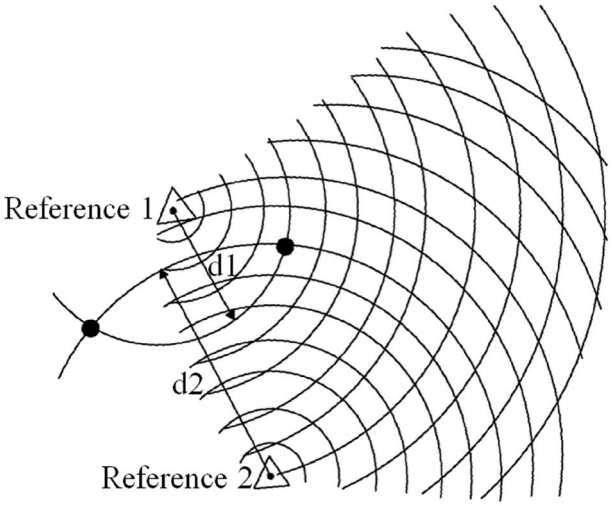

Figure2.4 The Intersection of Circular Lines of Position for 2-D Positioning

Similar is also for the three dimensional case except where the intersection of the three spheres gives two points of intersection in space where only one is the correct position of the point required (on the surface of the earth) (Figure 2.5). This then implies that measurement to three satellites (three spheres) will uniquely solve this mathematical problem. The accuracy of the point that is fixed is dependent on the accuracy with which the ranges are measured and the geometry of the intersection.

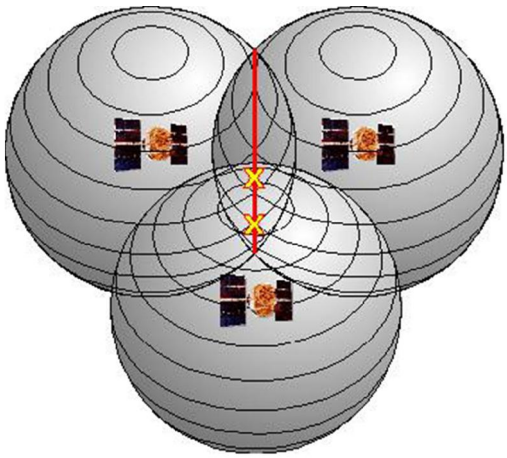

Figure2.5 Intersection of Surfaces of Position Based on Range Measurements

When the point being fixed is not moving, the two or three ranges do not need to be measured simultaneously. On the other hand if the point is in motion, the two or three ranges measured should be observed (measured) simultaneously. Because the GPS system was created in that at any particular time, a minimum of four satellites would be visible for positioning, satellite positioning is done by simultaneously measuring ranges to the satellites for most of the navigation application of GPS positioning.

2.3 GPS Satellite Constellation and Signals

The Block II/IIA satellites were to be fully launched in the late 1980's. However, this was not the case the system becoming operational in the 1990s. This was due to numerous problems including the space shuttle challenger disaster that occurred on 28th January 1986. GPS operation was fully declared on the 17th July 1995 with the Block II/IIA satellites in orbit. The GPS satellites launched at an altitude of 20200km 24 in number implies that at any point on the earth's surface a minimum of four satellites can be accessed for positioning. This is true if the site is not obstructed. Throughout a day, mostly 6 to 10 satellites will be visible at a point. The U.S Department of Defence ensures that a constellation of 24 satellites is accessed 70% of the time while 21 satellites are accessed 98% of the time when fixing a point. The GPS satellites being in nearly circular orbits at 20200km from the earth (orbital radius), causes the following as unique to the GPS system:

- The orbital period of each satellite around its orbital path is 11hrs 58mins. This implies the satellite will make two revolutions each day (sidereal day). Where the sidereal day is the period that the earth takes to rotate about its axis with respect to the stars.
- Each satellite will be over the same point over the earth after a sidereal day. This day is 23hrs 56mins.
- Considering the solar day (24hours period), the satellite is in the same spot each day in the sky four minutes earlier.
- The satellite orbiting repeats every day except for some small drift in the western direction. This drift is controlled or mitigated by periodic manoeuvres of the satellite at the control segment.

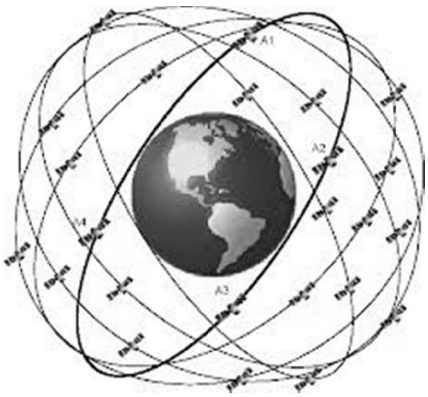

Figure2.6 The GPS Constellation "Birdcage"

- If the satellite is in a very high altitude, it will be viewed longer above the horizon. The satellites with one of the highest altitudes are the geostationary satellites.
- Also the high a satellite is in its orbit, the large area it will cover on the earth. This is because this kind of satellite travels slowly and is viewed from many points on the earth.
- The GPS satellites have a large inclination angle and hence have more northerly orbits.
- There may be a need to simultaneously make observations to more than one satellite from one or more ground stations depending on the positioning technique that one is applying.

The Block II satellites are launched into six (6) orbital planes that are at 60^o interval separation at the equator. Each orbit contains four satellites. These satellites can be moved about their orbits as controlled from the control segment. These manoeuvres help to replace the satellites that have failed. The inclination angle of the orbital plane to the equatorial plane is 55^o. A satellite is above the observer's horizon for 6-7 hours in one pass because the altitude of the satellite is three times the radius of the earth. Even if at some time of day 12 satellites can be simultaneously observed, there are times and points on the earth where the satellite coverage is very degraded (bad). The degraded satellite coverage is normally measured in terms of the DOP factor (Dilution of Precision). If the DOP factor or value is high, this means the satellite geometry is bad. This implies the satellites being observed are collected in only one point of the sky. The reverse is true if the DOP factor is low the satellite geometry is good. This means the satellites being used for the positioning are well spread in the sky from horizon to horizon.

2.4 GPS Signal Components

The GPS signals are based on the L-band carrier signals. The L-band carrier signals are generated by multiplying the fundamental frequency f_o (10.23MHz) by constants 154 and 120. The generated L-band carrier waves L1 and L2 respectively are 1575.42 MHz and 1227.6 MHz. These signals are radio waves that can transmit through the atmosphere over very long distances. These signals however, cannot penetrate solid objects like dense tree canopies and buildings. GPS satellites transmit the same L-band signals (L1 and L2) from all the satellites. This is however different with the GLONASS system where each satellite transmits a signal of different frequency. The L-band carrier waves do not carry any information, they must therefore be modulated. The L-band carrier waves are modulated by the GPS ranging codes below:

- The C/A code is referred to as "clear/access" or "coarse/acquisition" code and at times the "S code".
- The P code also referred to as either the "private" or "precise" code was designed for the military only and some other authorised users.

The L1 carrier wave is modulated by the p and C/A codes. Well as the L2 carrier wave is modulated only by the p code. A new code ("Y code") was created by encrypting the "P code" with the secret "W code". This is what was referred to as Anti-spoofing. This was to limit the

access to the p code to the military only (U.S military) and the other authorised users. The L1 and L2 carrier waves contain the navigation message.

It is by timing the travel of the C/A and P or Y codes that the one-way ranges to the satellites are determined. These codes are binary codes generated by mathematical algorithms and hence are referred to as "pseudo-random-noise" (PRN codes). Each satellite is assigned one C/A code. The PRN code number is normally used as the satellite I.D. Every C/A code is a 1023 chip long binary sequence. The C/A code is generated at a rate of 1.023 million chips per second. This implies the entire C/A code sequence repeats every millisecond. The P code is a more complex binary sequence of 0's and 1's. This code is 267 days long and has a chipping rate at the fundamental frequency of f_o (10.23 MHz). The resolution of the P code is ten times that of the C/A code. The P code is not uniquely assigned to each satellite as the C/A code does. The O code is allocated so that every satellite will transmit only one week portion of the 267 day long PRN sequence. The code sequence is restarted at the end of the week.

The ranging codes should be known by the user's receiver if the one way range is to be measured. If the PRN code being transmitted is known then a receiver can generate a local replica. The P or C/A code generated from the satellite will correlate with the replica of itself when the two codes are aligned.

2.5 GPS Enhancements

GPS accuracy is very important and we will now examine the main factors that influence GPS positioning accuracy:

- Measurement biases and measurement errors.
- Absolute or differential positioning mode.
- Satellite-receiver geometry.
- Processing algorithms, operational mode and other enhancements.

2.5.1 Factors Influencing GPS Accuracy

All GPS measurements; pseudo-range, carrier phase and Doppler frequency are all affected by errors and biases. Errors are due to internal instrument noise or random errors and un modelled or residual biases. Biases are errors that make the measurements to be different from the true ranges by a systematic amount. For example the ranges can be either too short or too long. These biases should be accounted for in the mathematical models if high accuracy is sought in the positioning. There exist different sources of the GPS biases encountered in GPS positioning. Biases may be physically based for example the effects of the atmosphere on signal propagation. However other biases may enter at the data processing stage by the use of imperfect constants, for example the wrong assumption of the satellite coordinates, station coordinates and velocity of light.

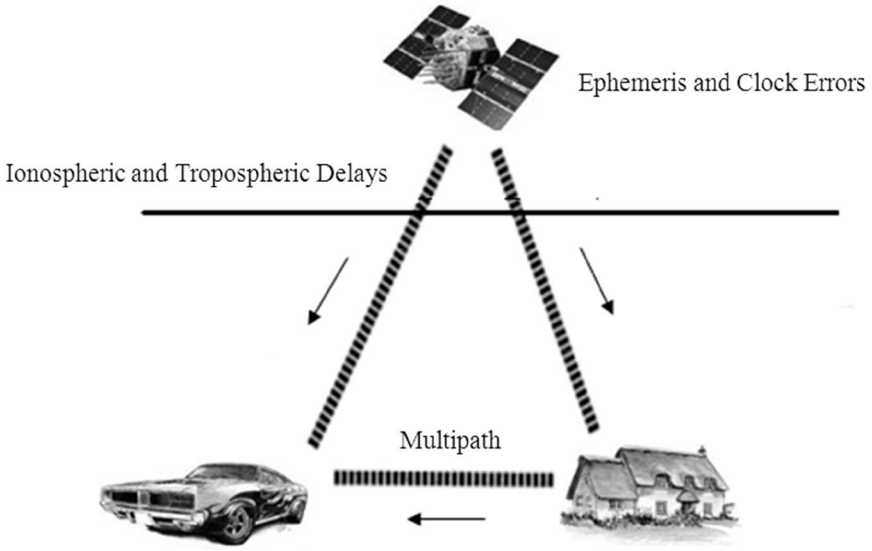

Figure2.7 Some GPS Biases and Errors Affecting Observations

Spatially correlated biases are overcome by using two receivers which are simultaneously tracking the same satellites. This technique of GPS positioning is referred to as Differential Global Positioning System (DGPS). DGPS can be implemented differently but the idea is still the same where the point of interest is fixed relative to another reference receiver.

2.5.2 GPS Measurement Biases and Errors

The C/A code has a resolution of 300 metres and a 3m range precision. The P code has a resolution of 30 metres and a 0.3 range precision. This shows that the P code has a better precision by tenfold.

The carrier phase measurement noise on the other hand is less compared to that of Code measurement noise. The L1 carrier wave has a wave length of 0.19m hence a resolution of approximately 0.19m. L2 carrier wave has a wave length of 0.24m hence a resolution of approximately 0.24m. It can be appreciated that carrier wave resolution is at millimetre accuracy while that of the codes is at metre accuracy.

The level of measurement noise contributes directly to the accuracy with GPS. High accuracy is as a result of low measurement noise. Various strategies exist on how to deal with different GPS measurement biases:

- Estimated as additional parameters.
- Eliminated by differencing if the biases are correlated.
- Direct measurement of the biases.
- Consider the biases known and modelled.
- Ignoring the biases if they are small.

Biases larger than the measurement noise have to be modelled because these will cause the accuracy to fall below the lowest accuracy level fixed. In the case of pseudo-range measurements, the magnitude of most of the biases is below the noise level of the observations and can therefore be simply ignored (they become absorbed into the "error"). However, in the case of carrier phase measurements all biases are potentially a matter of concern. In other words, different GPS applications require different levels of GPS accuracy, hence there is the possibility of a different partitioning of "biases" and "errors". At one extreme, as in the case of GPS pseudo-range absolute positioning, all biases with the exception of the receiver and satellite clock "uncertainty" are treated as errors, their effects ignored and hence these biases would be expected to distort the positioning results. At the other extreme, involving precise GPS position determination for geodesy applications such as crustal motion surveys, all measurement biases are explicitly accounted for in any solution in order that the results are highly accurate and

reliable. Many ITS and mapping applications fall somewhere in between, requiring the elimination of some of the biases, particularly Selective Availability.

Fortunately, differential positioning is the most effective means of accounting for many of the troublesome GPS measurement biases, and hence is the basis for all high precision GPS positioning techniques. Although differential positioning does place additional operational demands (two GPS receivers are required, with a data link between them when DGPS is implemented in real-time), no explicit measurement or modelling of the spatially correlated biases is required. They are simply lumped together and eliminated, to a lesser or greater extent, from the relative position results. In general, the biases can be considered to belong to one of three classes: **satellite-dependent biases**, **receiver-dependent biases**, and **signal propagation biases**.

Satellite-Dependent Biases: The ephemeris information used to calculate the GPS satellite positions is generated from the tracking data collected by the five monitor stations of the Control Segment. The data is processed at the Master Control Station and the satellite navigation message information is uploaded to every satellite, and are available to GPS users at the time of observation. The satellite orbit bias is therefore the discrepancy between the "true" position (and velocity) of a satellite and its broadcast ephemeris. With regard to accuracy, there are (in principle) several distinct effects:

- There is the effect arising from the accuracy of the orbit computation procedure itself. The data used are P code pseudo-ranges, and although the tracking geometry is not strong (most of the tracking stations are in the equatorial belt), accuracies better than 5 metres are achievable.
- There are errors resulting from unpredictable orbital motion during the period since upload. These are essentially the prediction errors. Their magnitude can vary from a few metres (close to the time of navigation message upload) to several tens of metres.
- There is the effect due to Selective Availability (SA), which involves the deliberate degradation of the broadcast ephemeris parameters. The resulting orbit error may be highly variable (the degradation algorithm is classified), but we may assume it could be as high as 100 metres or more. (Though it is unclear whether SA also degrades the orbit information at present.)

What is the effect of the satellite orbit bias on GPS positioning? Expressed another way, if there is no other option than to assume the available orbit data is correct, what is the effect of an error in the satellite orbit? The following comments can be made:

- The height is a weekly determined component because there are no satellites below the horizon. This component is usually of the order of 2 or 3 times less accurate than the horizontal components.
- The effect on single receiver operation is to propagate the orbit error into the position results. A position result error is amplified.
- When two receivers are being positioned, both will be in error by nearly the same amount (the extent to which this is true is a function of the distance between the two receivers-the closer they are, the more similar the error due to orbital bias). Relative positioning is therefore an effective strategy for minimizing the effect of this bias.

One option for overcoming satellite bias error is to use a precise ephemeris as generated by the International GNSS Service (IGS). These ephemerides are accurate to the sub- metre level and are computed after global tracking data is collected from the IGS stations. Hence they are only available "post-mission" (unlike the broadcast ephemerides which are predicted into the future from the computed orbit and which can be used in real-time applications). Plans are underway to generate predicted IGS orbits of sub-metre accuracy.

Although GPS satellites use high quality caesium or rubidium atomic clocks for time-keeping and signal synchronization, there are unavoidable clock errors which change with time. These satellite clock errors cannot be ignored, hence they are a significant bias which are monitored by the control segment during tracking data analysis. The only way they can be accounted for in single receiver positioning is by using the broadcast clock error model defined by the polynomial coefficients. The three polynomial coefficients are known well enough to match the basic pseudo- range accuracy that is to an accuracy of a few metres. However, under the policy of SA the coefficients are no longer able to adequately model satellite clock error. The range error resulting from the residual satellite clock bias (after correcting the range using the broadcast error model) can be more than 30m.

As all observations made at an instant, to a particular satellite, by all GPS receivers, are contaminated by the same satellite clock error, then the possibility exists for eliminating this bias through the principles of differential positioning.

Receiver-Dependent Biases: GPS receivers are equipped with relatively inexpensive quartz crystal oscillators. Although the time defined by individual receiver clocks has essentially arbitrary origins, they can be tied to a well established time scale, such as GPS Time (GPST), in a number of ways. The offset between the receiver clock time and GPST is the receiver clock error that contaminates all satellite-receiver ranges made at that instant by that receiver, and leads to these quantities being referred to as "pseudo-ranges". Typically, the solution to this problem is to treat the clock bias as an additional parameter in the pseudo-range navigation estimation procedure, requiring that four or more pseudo- range measurements are available. An alternative strategy is to take differences between data collected to the different satellites so that the common bias is eliminated. The subsequent time scale defined by the corrected receiver clock is then nominally that of GPST because:

1. The synchronization at some epoch (that is, the process of defining the time origin) is susceptible to error. Generally, it can be carried out only at the few metre level.
2. The stability of the time scale is directly related to the quality of oscillator used, and how often the current clock time is synchronized using GPS pseudo-range observations.

Signal Propagation Biases: The ionosphere is the band of the atmosphere from around 50 to 1000 km above the surface of the earth. In this region, free electrons are released as a result of the gas molecules being excited by solar radiation. When the electromagnetic GPS signals propagate through this medium dispersion occurs, changing the velocity of the propagated signal. The ionospheric propagation delay of the code signals will cause the measured range to be longer than the true range. (On the other hand, the delay to the carrier phase signals is negative, and hence will cause the measured phase-range to be shorter than the true range.)

Ionospheric delay can range from about 50m for signals at the zenith to as much as 150m for observations made at the receiver's horizon. To reduce the ionospheric effect, coefficients of a correction formula are transmitted within the satellite navigation message. The correction can be applied to the measured data. However, the accuracy of the correction is very much dependent

on the reliability of the estimate of Total Electron Content (TEC) along the signal path, which varies as a function of: the latitude of the receiver, the season, the time of day the observation of a satellite's signal is being made, and the level of solar activity at the time of observation.

For example, at night the ionospheric delay is approximately five times less than for day time observations. (Total Electron Content) TEC is a maximum at mid to low latitudes, and is a minimum at the poles. A diurnal cycle for TEC occurs with a maximum occurring two hours after solar noon and is a minimum before dawn. Ionospheric disturbances, which can occur suddenly and be very severe, also affect the value of TEC. As the TEC is difficult to accurately determine, applying the correction formulae cannot effectively remove this effect. It is generally conceded that the broadcast correction model can be used to remove up to about 50% of the ionospheric delay at mid-latitude regions. For single frequency receivers the use of the correction model parameters is often the only option for point positioning. However, the ionospheric bias is spatially correlated (it is approximately the same for receivers up to a few tens of kilometres apart), and effectively is eliminated in differential positioning.

The ionospheric delay on a signal is a function of the signal frequency, hence if dual-frequency receivers are available this factor can be used to remove 99% of the ionospheric effect by making measurements on L1 and L2 signals and combining them in a special linear combination. However, all civilian GPS navigation receivers likely to be installed in vehicles are the single frequency (that is, the L1 tracking) variety.

The troposphere extends from the surface of the earth to about 8 km. GPS signals travelling through this medium will experience a tropospheric refraction delay that is a function of elevation and the altitude of the receiver, and is dependent on the atmospheric pressure, temperature, and water vapour pressure. The bias ranges from approximately 2m for signals at the zenith to about 20m for signals at an elevation angle of 10^{o}. The propagation of GPS signals in this medium is frequency independent (the troposphere is sometimes referred to as the "neutral atmosphere") therefore this effect cannot be removed by combining observations made on two frequencies. There are several options:

- Many models are available for this correction, the commonly used ones are the Hopfield model, the Black model, and the Saastamoinen model. About 90% of the delay stems from the dry gas component of the troposphere which can be modelled accurately without too much difficulty. The remaining 10% owing to the water vapour content is much more difficult to accurately model.
- For high precision applications the residual tropospheric bias has to be parameterised in the final position solution. This is not an option that is exercised for GPS navigation applications.
- Avoid tracking low elevation satellites. Generally satellites below 20^o have much greater problems with the tropospheric delay than high elevation satellites. However, for navigation applications , tracking of satellites down to the horizon is usually necessary.
- As with the ionospheric bias, the fact that the bias is spatially correlated over distances up to several tens of kilometres means that differential positioning is an effective strategy for mitigating the effect of the tropospheric bias on positioning results. However, the correlation times and distances for ionospheric delays and tropospheric delays are different, with tropospheric delays being typically a more local phenomenon.

Another signal propagation bias does not have its origin in the physics of the atmosphere. The satellite to receiver distance, if measured using the carrier wave signal, can be expressed as cycles of the signal wavelength (approximately 19cm for the L1 signal, and 24cm for the L2 signal) plus the fraction of a cycle. For example, a measurement of -1993673.239 L1 cycles is a valid range measurement for while the fractional part of this data (0.239 cycle) is accurately measured, the integer cycle part (-1993673) is only arbitrarily assigned at the beginning of the satellite tracking process. The count of cycles since the beginning are precisely recorded and assuming that there is no loss of signal lock between the beginning of the tracking process t_{oc} (start of tracking) and time t (end of tracking period), the actual distance at time t will be equal to the phase measurement at time t, plus an integer bias. This bias is usually termed the initial carrier phase cycle ambiguity. It has the following characteristics:

- The ambiguity is an integer number (a multiple of the carrier wavelength).
- The ambiguity is different for L1 and L2 phase observations.
- The ambiguity is different for each satellite-receiver pair.

- The ambiguity is a constant for a satellite-receiver pair for all epochs of continuous tracking.

Once this bias is estimated the ambiguous carrier phase measurement can be converted into a standard (unambiguous) range measurement similar to the pseudo-range - it is affected by the same biases mentioned earlier - but with much higher measurement precision (that is, lower measurement noise) and significantly lower multipath error.

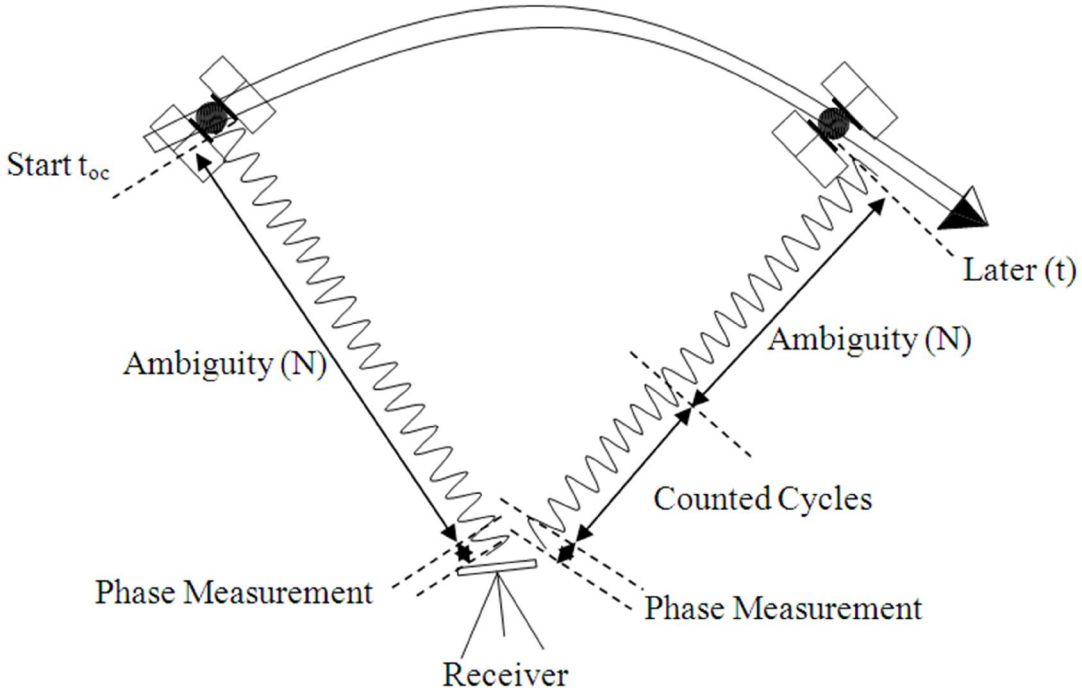

Figure2.8 Geometrical Interpretation of Integer Ambiguity

2.6 GPS Measurement Errors

Apart from the measurement noise and the residual biases referred to earlier there are several other errors. Multipath effects are propagation errors arising from the interference of the direct signal by reflected signals from water and metallic surfaces and nearby buildings. The combined direct and reflected signals will give rise to incorrect pseudo-range or phase measurements. The maximum multipath error that can occur in the case of pseudo-range data is one half the chip length (or resolution) of the code, that is, about 300m for the C/A code measurements, and 30m for P code measurements. This is a very large error which must be guarded against, especially in

land navigation applications where the GPS receiver is located on the metal surface of a vehicle. (Carrier phase multipath on the other hand does not exceed one quarter of the wavelength; that is, 4cm on L1.) Effective ways to reduce this effect include the use of specially designed antennas such as choke ring type and careful antenna mounting (for example, avoiding reflective surfaces-often very difficult in many mapping applications). New receiver technology is being developed to effectively filter out multipath effects using advanced signal processing.

Another important error affects only carrier phase measurements. If satellite signals are obstructed by objects, or interfered by other signals, a loss of lock on the satellite signal will occur. On the resumption of lock to the satellite(s), the accurate fractional part of the phase observable can again be measured, however the integer part will be re-initialised and the initial integer ambiguity will no longer be a valid connection between the ambiguous fractional cycle measurement and the satellite- receiver range. For this reason there is a "jump" in the measurement data just before and immediately after the epoch at which the loss of lock occurred, and all measurements beyond this epoch are shifted by the same integer number of cycles. This "jump" is known as a cycle slip, and can occur independently on L1 and L2. The detection and repair of cycle slips is therefore an important carrier phase data preprocessing step.

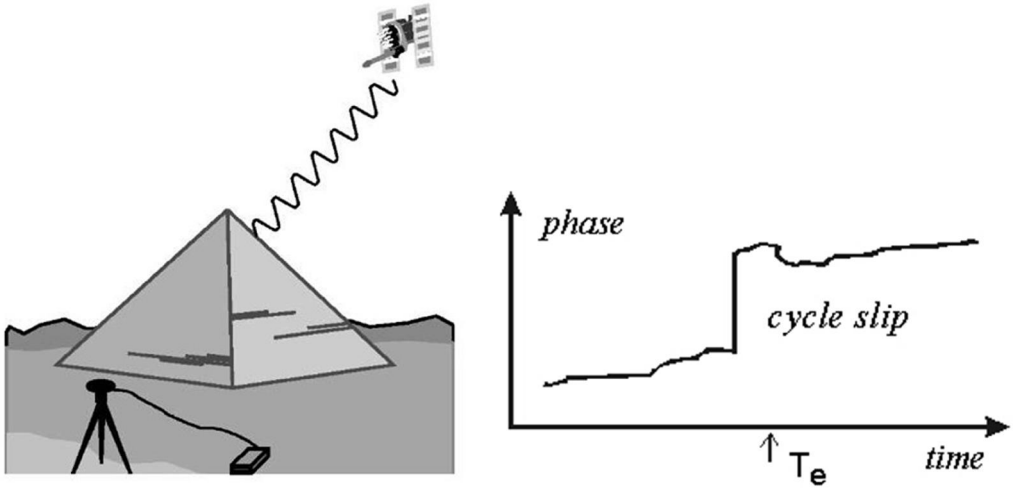

Figure2.9 Occurrence of cycle slips in Global Positioning Systems

2.7 Tropospheric Delay Modelling

In the above section of the chapter two, we have discussed how GPS works slightly touching how the atmosphere (Troposphere) affects the GPS signal. In this section we look at the effect of the Tropospheric delay on the GPS signal in detail. It will include a discussion of the different Tropospheric Delay models, different Mapping Functions and the modelling of the gradient of the satellite-as it affects the signal from the satellite.

The earth's atmosphere can be coarsely subdivided in several concentric layers. The characterization of these layers depends on the purpose for which the subdivision is made. Well-known characteristic features are: temperature, ionization, and propagation (Seeber, 1993). Characterizing the atmosphere by the way radio waves are propagated leads to a subdivision of a troposphere and ionosphere. The ionosphere, the upper part of the atmosphere, is a dispersive medium (the propagation delay is frequency dependent), whereas the troposphere is non dispersive. The troposphere is also referred to as neutral atmosphere to distinguish with its original definition, which is actually based on the characterizing temperature profile.

The Tropospheric delay consist both the wet and the hydrostatic delay. The hydrostatic delay is caused by atmospheric gases that are in hydrostatic equilibrium. This is usually the case for dry gases and part of the water vapour. This part of the delay can very well be modelled based on the surface air pressure. The wet delay is caused by water vapour that is not in hydrostatic equilibrium. We can derive models for this delay based on the partial pressure of water vapour or relative humidity at the surface, but these models have a low accuracy and need empirical constants that may vary widely with location and time of year.

Both the wet and dry delays are usually expressed as the product of the delay in the zenith direction and a mapping function, which depends on the zenith angle of the signal. The wet and dry-delay mapping functions differ because of the thickness of both parts of the troposphere. Water vapour is more concentrated near the surface than dry gases. The thicknesses may vary with time and location, and mapping functions therefore depend on physical parameters like surface temperature, total air pressure or partial pressure of water vapour, or by parameters like height, day of year, and latitude. Because physical parameters such as pressure and temperature

are often not given or measured, they are usually modelled by a standard atmosphere, which gives them as a function of height under mean atmospheric conditions.

The signal propagation on a layer depends on the temperature, the pressure and the water vapour. The factor that describes the variability of the troposphere is the refractive index (n).

If we take the simplified mathematical model for the observable to be one in which the signal is assumed to be propagating in a straight line and at the speed of light in vacuum, the atmospheric delay is defined to be the difference between the true path length and this assumed straight line length. Using this definition, the atmospheric delay is a term to be added to the simplified model.

According to Fermat's principle, the measured range s is defined by

$$s = \int_{user}^{sat} n \, ds \tag{2.1}$$

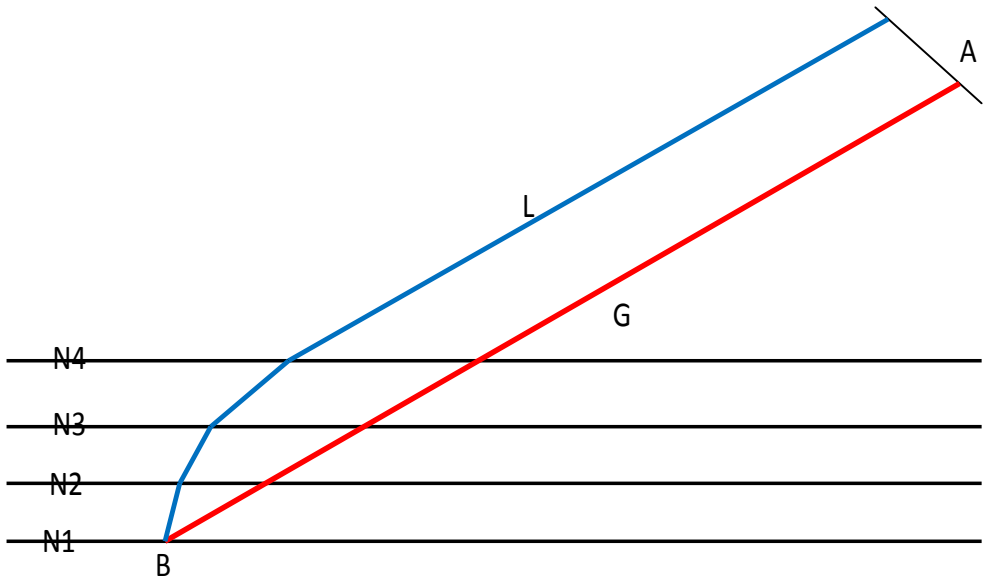

Figure2.10 Tropospheric Delay Propagation

Through a hypothetical horizontally stratified atmosphere with four layers of constant refractivity $N1 > N2 > N3 > N4 > 0$. The red line would be the line of propagation in vacuum.

As the energy travels at the group velocity $v = c/n$ along the path, Eqn. (2.1) can be rewritten as:

$$s = \int_{user}^{sat} n\, ds = \int_{user}^{sat} \frac{c}{v}\, ds = c \int_{user}^{sat} dt \tag{2.2}$$

The quantity L

$$L = \int_{user}^{sat} n\, ds \tag{2.3}$$

is the electromagnetic path length as opposed to the geometric (i.e. straight) path G, the path that would be travelled by the ray in vacuum.

$$G = \int_{user}^{sat} 1 * ds \tag{2.4}$$

On Figure2.10, G would be the red path and L the blue path. The neutral atmospheric delay Δ^{Trop} is defined as the difference between L and G:

$$\Delta^{Trop} = \int_{user}^{sat} n\, ds - \int_{user}^{sat} 1 * ds \tag{2.5}$$

As you can see from Figure 2.10, the two integrals don't integrate along the same path in Eqn. (2.5), therefore:

$$\Delta^{Trop} \neq \int_{user}^{sat} (n-1) ds$$

The quantity Δ^{Trop} can then be written as

$$\Delta^{Trop} = \int_{user}^{sat} (n-1) ds_{\,ray} + \left[\int_{user}^{sat} ds_{ray} - \int_{user}^{sat} ds_{vacuum} \right] \tag{2.6}$$

Where it has been made use of two different integration variables $ds_{\,ray}$ and $ds_{\,vaccum}$ to underline the fact that the first term of Eqn. (2.6) refers to the actual path whereas the second refers to the case when the signal travels in a vacuum. The square bracket expression is purely

geometric and evaluates the geometrical delay (also known as the ray bending), that is, the excess path length travelled when going from satellite to user following the path used by the ray in a real atmosphere compared to the geometrical path. The first term is the delay due to the slower speed of propagation, due to a refractive index greater or equal to unity.

Eqn. (2.6) refers to it as the excess path delay. To summarize, what will be referred to as the "neutral atmosphere delay" or "Tropospheric delay". In general the Tropospheric delays include the two contributions: excess path delay and geometric delay. The bending term is much smaller especially for higher elevation satellite relative to the observer's horizon. For rays oriented along the zenith, and in the absence of horizontal gradients in n, the ray path is straight line and the bending terms vanishes(Herring, T.A. (1992),).

Usually instead of the refractive index, the refractivity

$$N^{Trop} = 10^6(n-1) \tag{2.7}$$

is used so that Eqn. (2.7) becomes

$$\Delta^{Trop} = 10^{-6} \int_{user}^{sat} N^{Trop} ds \tag{2.8}$$

The refractivity is divided in two components; the term N_d is the refractivity due to the gases of air, except the water vapour, and called "dry" or "hydrostatic" refractivity (hydrostatic equilibrium or hydrostatic balance is the condition in fluid mechanics where a volume of a fluid is at rest or at constant velocity. This occurs when compression due to gravity is balanced by a pressure gradient force. For instance, the pressure gradient force prevents gravity from collapsing the Earth's atmosphere into a thin, dense shell, while gravity prevents the pressure gradient force from diffusing the atmosphere into space). The term N_w which is the refractivity due to the water vapour and it is called "wet" refractivity.

Separating the N^{Trop} into dry and wet component

$$N^{Trop} = N_d^{Trop} + N_{wet}^{Trop} \tag{2.9}$$

And

$$\Delta^{Trop} = \Delta_d^{Trop} + \Delta_{wet}^{Trop} \tag{2.10}$$

$$\Delta^{Trop} = 10^{-6} \int_{user}^{sat} N_{\mathrm{d}}^{Trop} ds + 10^{-6} \int_{user}^{sat} N_w^{Trop} ds \tag{2.11}$$

About 90% of the tropospheric refraction arise from the dry and 10% from the wet component (Herring, T.A. (1992),). The wet delay is equal to zero if there is no water vapour present along the path of the signal and it is poorly predicted using measurements of conditions at the site alone. This difficulty is caused by the "unmixed" nature of the atmospheric water vapour, which means that the water vapour is present in "blobs". Because of this condition, models for the wet delay are notoriously inaccurate. Actually, one can attempt to measure the delay caused by water vapour along the line of transmission. Such measurement will probably be necessary if the highest possible accuracy in GPS measurements is to be achieved. The instruments capable of measuring water vapour and water liquid content are called water vapour radiometers (WVR). The WVRs usually operate with two frequencies: near 22GHz to measure water vapour and near 31GHz to measure liquid water. WVRs are very expensive and cannot be used in practical surveying. Alternatively, radiosondes measure pressure, temperature and humidity along their vertical path. Unfortunately, radiosondes drift with varying wind conditions and require considerable logistics to operate. Like WVRs, radiosondes are expensive and are very seldom used in routine GPS surveying

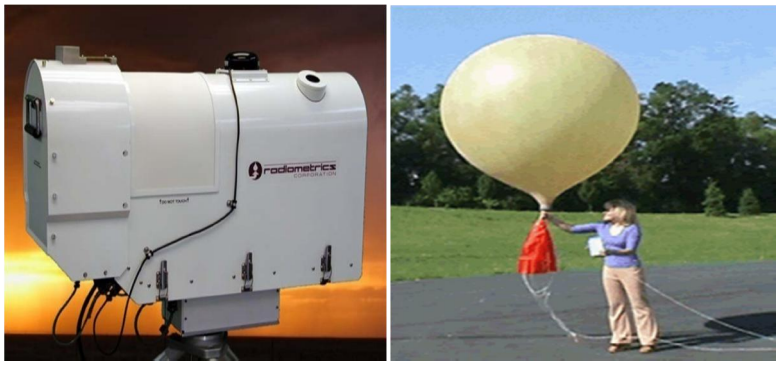

(a) (b)

Figure2.11 A Typical Radiometer (a) and Radiosonde (b)

In practice, there are different models available to calculate the effects of the troposphere delay. Models for dry and wet refractivity at the surface of the earth have been known. The dry component at the surface is given by (Herring, T.A. (1992),).

$$N_{d,0}^{Trop} = b_1 \frac{p}{T}, \quad b_1 = 77.64\ K\ mb^{-1} \tag{2.12}$$

Where p is the atmospheric pressure in millibar (mb) and T is the temperature in Kelvin (K). The wet component is given by

$$N_{w,0}^{Trop} = b_2 \frac{e}{T} + \quad b_3 \frac{e}{T^2} \quad , \quad b_2 = -12.96\ K\ mb^{-1}\ , b_3 = 3.718.10^5\ K^2\ mb^{-1} \tag{2.13}$$

Where e is the partial pressure of the water vapour in mb. The value of b_1, b_2, b_3 are empirically determined and cannot fully represent the local situations in every GPS observation stations. Hence, currently most GPS software estimate the wet zenith delay from the observations.

2.8 Tropospheric Delay Models

This section discusses some of the different Tropospheric Delay Models that are used to model the effect of the Troposphere on the GPS signal as it moves from the satellite to the GPS receiver. The Models discussed are Hopfield, Modified Hopfield and Saastamoinen. Though the model used in this research is Saastamoinen, the others were studied to compare their operation to Saastamoinen so that the strengths or weaknesses of Saastamoinen could be highlighted.

2.8.1 Saastamoinen Model

The Saastamoinen (1973) models the tropospheric delay, expressed in metres:

$$\Delta^{Trop} = \frac{0.002277}{\cos z}\left[p + \left(\frac{1255}{T} + 0.05\right)e - tan^2 z\right] \tag{2.14}$$

as a function of e, p , T, z.

The total tropospheric zenith delay can be separated into two components for Saastamonien models, as dry and wet without including the mapping function, the cosecant of the elevation

angle as in Eqn. (2.14). These two components can be estimated from surface measurements according to Davis (1986):

$$\Delta_d^{Trop} = 0.002277 \frac{P}{1-0.002666\,cos(2\varphi)-0.00028.10^{-3}H} \tag{2.15}$$

and

$$\Delta_w^{Trop} = 0.002277 \left(\frac{1255}{T} + 0.05\right) \frac{e}{1-0.002666\,cos(2\varphi)-0.00028.10^{-3}H} \tag{2.16}$$

Where Δ_d^{Trop} and Δ_w^{Trop} are measured in metres, P and e the total pressure and the partial pressure due to water vapour at the surface, respectively (millibars); T the surface temperature (degrees Kelvin), φ the geodetic latitude of the site and H the height above the geoid (m). The weather data used in the above formulas are:

$$tk = tc + 273.15 \tag{2.17}$$

$$e = rh \times 6.11 \times \left(\frac{tk}{273.15}\right)^{-5.3} e^{(25.2 \times \frac{tc}{tk})} \tag{2.18}$$

Where rh is the relative humidity. In the absence of in situ metrological data, a global numerical weather model (NWM) can be used.

2.8.2 Hopfield Model

Hopfield (1969) has developed a troposphere delay model using real data covering the whole earth. The empirical formula representing the dry refractivity with a function of height h

$$N_d^{Trop} = N_{d,0}^{Trop} \left[\frac{h_d - h}{h_d}\right]^4 \tag{2.19}$$

Under the assumption of a layer with a thickness

$$h_d = 40136 + 148.72(T - 273.16) \quad \text{(m)} \tag{2.20}$$

The integral Eqn. (2.11) can be solved if the troposphere delay is calculated along the vertical direction and the curvature of the signal is neglected. Substituting (2.19) into (2.11) starting from the earth surface at $h = 0$ for the dry part becomes

$$\Delta^{Trop} = 10^{-6} N_{d,0}^{Trop} \frac{1}{h_d^4} \int_{h=0}^{h_d} (h_d - h)^4 dh \tag{2.21}$$

Thus

$$\Delta_d^{Trop} = \frac{10^{-6}}{5} N_{d,0}^{Trop} \, h_d \tag{2.22}$$

is the dry portion of the Tropospheric Zenith Delay. The wet component is much more difficult to model because of strong variability of the water vapour with respect to time and position. Hopfield model also assume the same functional model for both the dry and wet components.

$$\Delta_w^{Trop} = N_{w,0}^{Trop} \left[\frac{h_w - h}{h_w}\right]^4 \tag{2.23}$$

where the mean value $h_w = 11000\ m$

Introducing the same mapping function, $m(E) = {}^{1}/_{sin\sqrt{E^2 + 6.25}}$, the tropospheric delay can be formed as

$$\Delta_{dry}^{Trop} = \frac{10^{-6}}{5} \frac{77.64}{sin\sqrt{E^2+6.25}} \frac{P}{T} [40136 + 148.72(\mathrm{T} - 273.16)] \tag{2.24}$$

$$\Delta_{wet}^{Trop} = \frac{10^{-6}}{5} \frac{(-12.96\,T + 3.718\times10^5)}{sin\sqrt{E^2+6.25}} \frac{e}{T^2} \times 11000 \tag{2.25}$$

Measuring e, T, P at the observation location when you take your GPS measurements and by calculating the elevation angle$E$, the total tropospheric delay is obtained using Eqn. (2.24) and (2.25) for dry and wet components respectively.

2.8.3 Modified Hopfield Model

Eqn. (2.21) can be re-written by introducing lengths of position vectors instead of heights. Denoting the radius of the earth R_E, the corresponding lengths are $r_d = R_E + h_d$ and $r = R_E + h$, see Figure 2.12.

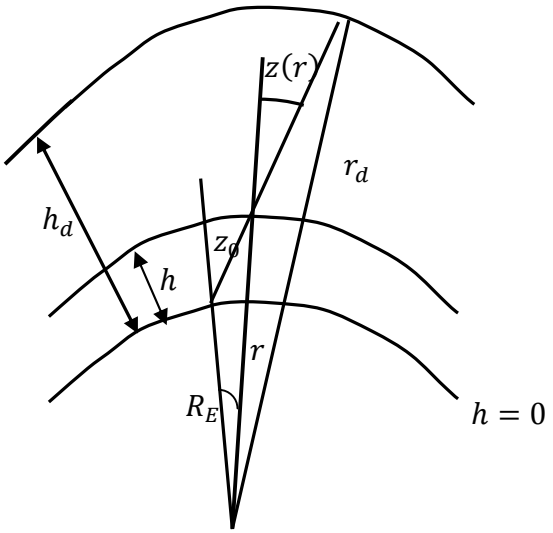

Figure2.12 Geometry for the Tropospheric Path Delay

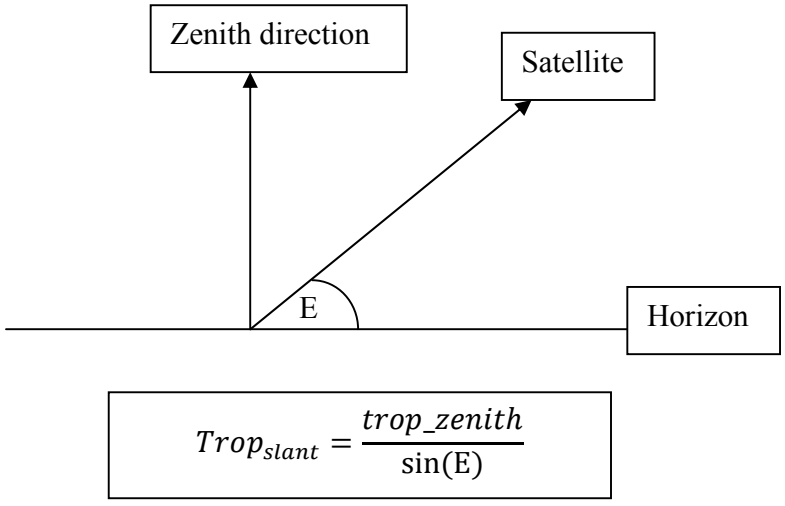

Figure2.13 Relation between Zenith and Slant Direction

Using Eqn. (2.11) and introducing a mapping function for the dry component gives

$$\Delta_d^{Trop} = 10^{-6} \int_{r=R_E}^{r=r_d} N_{d,0}^{Trop} \left[\frac{r_d - r}{r_d - R_E}\right]^4 \frac{1}{\cos z(r)} dr \qquad (2.26)$$

Note that the zenith angle $z(r)$ is variable. Assuming that the zenith angle at the observation site is : z_0, using sine law (see Figure 2.13), we get

$$sin\, z(r) = \frac{R_E}{r} sin\, z_0\ ,\ cos\, z(r) = \frac{1}{r}\sqrt{r^2 - R_E^2 sin^2\, z_0} \tag{2.27}$$

Substituting (2.27) in to (2.26)

$$\Delta_d^{Trop} = \frac{10^{-6} N_{d,0}^{Trop}}{(r_d - R_E)^4} \int_{r=R_E}^{r=r_d} \frac{r(r_d - r)^4}{\sqrt{r^2 - R_E^2 sin^2\, z_0}}\, dr \tag{2.28}$$

The corresponding wet component, assuming the same model as the dry, we get

$$\Delta_w^{Trop} = \frac{10^{-6} N_{w,0}^{Trop}}{(r_w - R_E)^4} \int_{r=R_E}^{r=r_w} \frac{r(r_w - r)^4}{\sqrt{r^2 - R_E^2 sin^2\, z_0}}\, dr \tag{2.29}$$

The above formula can be computed with the following approximations (use elevation angle E instead of zenith ($E = 90 - z$)):

$$r_i = \sqrt{(R_E + h_i)^2 - (R_E\, cos\, E)^2} - R_E sin\, E \tag{2.30}$$

Where E (expressed in degrees) indicates the elevation angle at the observing site.

The Tropospheric Delay in metres is

$$\Delta_i^{Trop} = 10^{-12} N_{i,0}^{Trop} \left[\sum_{k=1}^{9} \frac{\alpha_{k,i}}{k} r_i^k\right] \tag{2.31}$$

Where

$\alpha_{1,i=1}$

$\alpha_{2,i=4a_i}$

$\alpha_{3,i=6a_i^2 + 4b_i}$

$\alpha_{4,i=4a_i\,(a_i^2+3b_i)}$

$\alpha_{5,i=a_i^4+12a_i^2 b_i+ 6b_i^2}$

$\alpha_{6,i=4a_i b_i(a_i^2+3b_i)}$

$\alpha_{7,i=b_i^2(6a_i^2+4b_i)}$

$\alpha_{8,i=4b_i^3 a_i}$

$\alpha_{9,i=b_i^4}$

And

$$a_i = -\frac{\sin E}{h_i} \qquad\qquad b_i = \frac{cos^2(E)}{2h_i R_E}$$

We can replace i by d for dry and w for wet delay in Eqn. (2.31) for each respective components. Thus

$$\Delta_{dry}^{Trop} = 10^{-12} N_{dry,0}^{Trop} \left[\sum_{k=1}^{9} \frac{\alpha_{k,i}}{k} r_i^k\right] = 10^{-12} \times 77.64 \frac{P}{T} \left[\sum_{k=1}^{9} \frac{\alpha_{k,i}}{k} r_i^k\right] \tag{2.32}$$

And for wet

$$\Delta_{wet}^{Trop} = 10^{-12} N_{wet,0}^{Trop} \left[\sum_{k=1}^{9} \frac{\alpha_{k,i}}{k} r_i^k\right] = 10^{-12} \times \left[-12.96 \frac{e}{T} + 3.718 \times 10^5 \frac{e}{T^2}\right] \left[\sum_{k=1}^{9} \frac{\alpha_{k,i}}{k} r_i^k\right] \tag{2.33}$$

2.9 Tropospheric Mapping Functions

The path delay introduced in Eqn. (2.8) corresponds to delay from the satellite to the station in the zenith direction. Because observations are not generally made in zenith direction, the Zenith Path Delay (ZPD) has to be transformed (mapped) into the desired slant direction s. This transformation of the zenith path delay into the slant tropospheric delay is usually called Tropospheric Mapping Functions (MF). Typically the zenith path delay is isotropic, although small planar dependencies, expressed in horizontal gradients in two principal directions (north and east), are usually introduced. The tropospheric mapping represents a major challenge, since even the dominant hydrostatic portion of the atmosphere is also highly variable, in particular with respect to space-geodetic observations taken at low elevation angles. Although the MF is approximately equal to $1/\sin E$ (see, Figure 2.13) for most precise analysis, a better approximation of the mapping function is needed.

$$\Delta SPD = map(E) \times \Delta ZPD \tag{2.34}$$

Different sets of coefficients are necessary for the hydrostatic (dry) and wet parts of the ΔZPD so the required slant delay of Eqn. (2.10) is transformed to

$$\Delta_{Slant}^{Trop} = map_{dry}(E, a_d, b_d, c_d)\Delta_{dry}^{Trop} + map_w(E, a_d, b_d, c_d)\Delta_{wet}^{Trop} \quad (2.35)$$

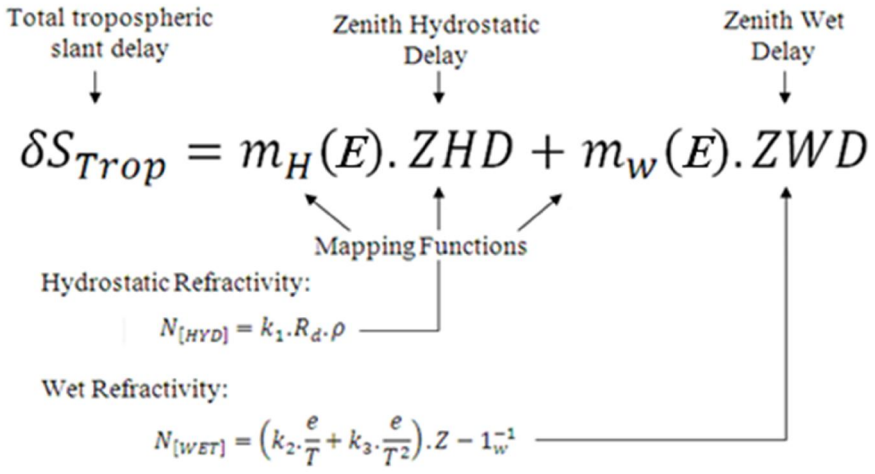

Where $map_{dry}(E)$the mapping function is associated with Δ_{dry}^{Trop} and $map_{wet}(E)$ is the mapping function associated with Δ_w^{Trop} . ΔSPD is the slant path delay, $map(E)$ is the corresponding mapping function, and ΔZPD is the zenith path delay. The dry zenith delay Δ_d^{Trop} is typically obtained from surface meteorological measurements or numerical weather models. The wet delay Δ_{wet}^{Trop} is normally considered unknown parameter and is estimated, in GAMIT-GLOBK GPS software.

For meteorological applications, the ZWD is sometimes expressed in terms of Integrated Water Vapour (Bevis et al., 1992)

2.9.1 MTT Herring Mapping Function

In the Saastamoinen model Eqn. (2.14), the refractivity can be deduced from the gas laws. The Saastamoinen model can be used to find the phase changes due, in particular, to relative humidity, temperature and relative pressure. It is assumed that the atmosphere is divided spatially into columns with a certain average value of the three variables. Because of the

different behaviour of the lower as compared to the higher atmosphere, Herring developed a mapping function based only on the ray tracing of atmospheres at 10 locations in the United States (close to VLBI stations) were temperature and water vapour profiles were obtained from radiosondes (Herring, 1992). They need a single meteorological input: the surface temperature at the site. The model adopted from the mapping function was a normalized three Marini's term (Marini 1972) expansion used for mapping both the hydrostatic and the wet components:

$$map_{\{d,w\}}(E) = \frac{1+\frac{a_{d,w}}{1+\frac{b_{d,w}}{1+c_{d,w}}}}{\sin E+\frac{a_{d,w}}{\sin E+\frac{b_{d,w}}{\sin E+c_{d,w}}}} \tag{2.36}$$

Where the coefficients are defined as

$$a_d = \left[1.2320 + 0.0139cos\varphi - 0.0209\,h + 0.00215(T-10)\right].10^{-3}$$

$$b_d = \left[3.1612 - 0.1600cos\varphi - 0.0331h + 0.00206(T-10)\right].10^{-3}$$

$$c_d = \left[71.244 - 4.293cos\varphi - 0.149h + 0.0021(T-10)\right].10^{-3}$$

Depending on the latitude φ and height h (in km) of the observing station and the temperature T in C^o. For the wet part the mapping function is the same as (2.36) but the corresponding coefficients are different:

$$a_w = \left[0.583 - 0.011cos\varphi - 0.052h + 0.0014(T-10)\right].10^{-3}$$

$$b_w = \left[1.402 - 0.102cos\varphi - 0.101h + 0.002\,(T-10)\right].10^{-3}$$

$$c_w = \left[45.85 - 1.91cos\varphi - 1.29h + 0.015(T-10)\right].10^{-3}$$

Herring reported typical Root Mean Square (RMS) differences between ray traced and mapped delays at 5 degrees to be 30 mm for the hydrostatic and 10 mm for the wet.

2.9.2 Updated Vienna Mapping Function (VMF1)

The Vienna Mapping Function (VMF) was developed by Johannes Boehm at TT-Viens. The coefficients of the extended fraction are derived by ray-tracing through actual meteorological data (the ECMWF global data is used) rather than using best-fitting values to radiosonde data (as per the NMF mapping function) or just some atmospheric parameters (such as the IMF mapping function) (Australian National University, 2005).

IMF and VMF mappings functions have been included in the modified GAMIT software since January 2004(Australian National University, 2005). This component is accessed through the standard release version 10.2 but not many people are aware of this, hence its application in GPS processing (Tropospheric delay modelling) is still moderate. It is used by changing NMFH/NMFW in sittbl. to VMFH/VMFW. It should however be noted that the VMF coefficients for IGS site are only available beyond 31st March 2004 for use in the processing (Australian National University, 2005).

In the period April 2004 to March 2005, 12 months of GPS data have been processed using four, interwoven global sub networks (Australian National University, 2005). The sub networks chosen are those used by Tom Herring for the IGS Analysis performed at MIT. Daily site coordinates were extracted for all sites with more than 100 days of data included in the solutions (Australian National University, 2005).

In the last years, troposphere mapping functions have been developed which are based on data from numerical weather models, e.g. from the European Centre for Medium-Range Weather Forecasts ECMWF (VMF1 Website, 2009). The Vienna Mapping Functions 1 (VMF1) are relying on empirical equations for the "b" and "c" coefficients of the continued fraction form, whereas the "a" coefficients are determined from rigorously ray traced mapping functions at 3 degrees elevation (VMF1 Website, 2009).

The VMF1 mapping function is provided on a global grid of 2.5 x 2.0 degrees. This grid has a resolution of 0.25 degrees for recent data at selected sites. The gridded hydrostatic “a” coefficients are valid for zero heights and the site dependent values of “a” are valid for actual station height (VMF1 Website, 2009). The hydrostatic and wet coefficients “a” are then input

parameters to the Fortran subroutine vmf1.f, which then yields the hydrostatic and wet mapping functions. Thus, for VMF1 given on the grid you need the subroutine vmf1_ht.f, whereas for the site dependent VMF1 you need vmf1.f (VMF1 Website, 2009). Both of these subroutines are implemented in GAMIT/GLOBK software.

The coefficients "a" are given on a global grid with 2.0 degrees sampling from north to south and 2.5 degrees sampling from west to east. For each parameter there are four files per day, i.e. at 0, 6, 12, and 18 UT, and they are stored in yearly directories (VMF1 Website, 2009).

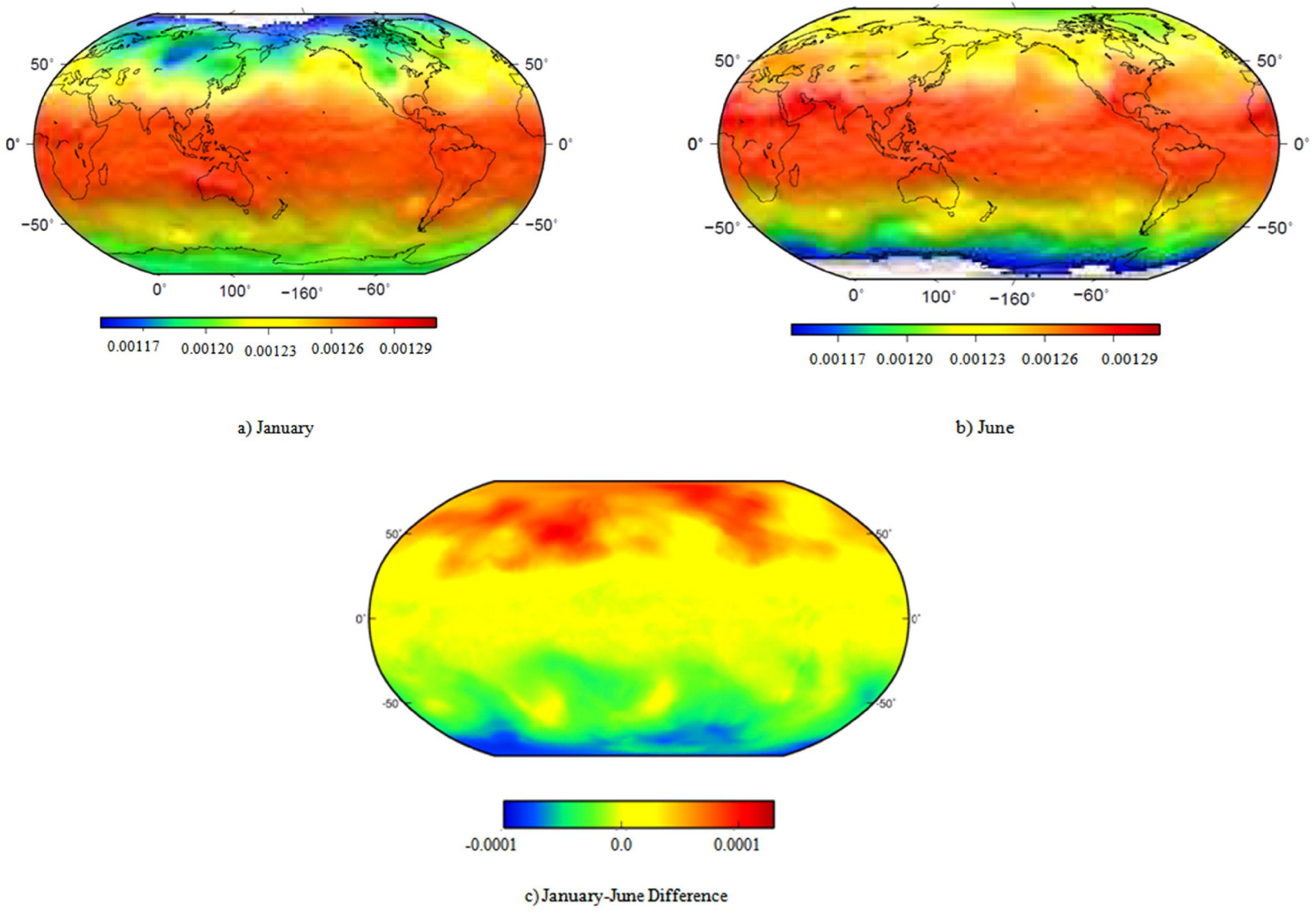

Figure2.14 Global Plots of Hydrostatic "a" Coefficients of the VMF1 Mapping Function at 0UT 2011

Above are global plots of the determined hydrostatic "a" coefficients (*ah*) for VMFG (VMF Grid). The plots were prepared from files VMFG_20110101.H00 (Figure 2.14a) and VMFG_20110531.H00 (Figure2. 14b) files for the months of January and June of the year 2011 at 0UT (Universal Time). These files were obtained from the internet. The website from which they were obtained is http://ggosatm.hg.tuwien.ac.at/DELAY/GRID/VMFG/2010/ . The, *ah*, coefficients vary considerably on the globe. The, ah, coefficients are highest at the equator as shown in the Figures 2.14a and 2.14b. This is because, these are tropics having high temperatures. The VMF grid, *ah*, grid values at the poles are less interchanging during January and June. In January, the, *ah*-coefficients are least at the North Pole increasing towards the equator and reducing again to the South Pole (Figure2.14a).

During summer, *ah*-coefficient is least in the south hemisphere increasing towards the equator and reducing towards the north hemisphere. Basically to some extent it mimics the weather condition. In June, the south hemisphere is winter while it is summer in the northern hemisphere. VMFG covers the whole globe sufficiently as observed for the figures above (Figures 2.14a and 2.14 b). The difference between the, ah-coefficients from January to (summer) June is displayed in Figure 2.14c. In this figure it is seen that from January to June *ah*-coefficients increase in the northern hemisphere while they reduce in the southern hemisphere.

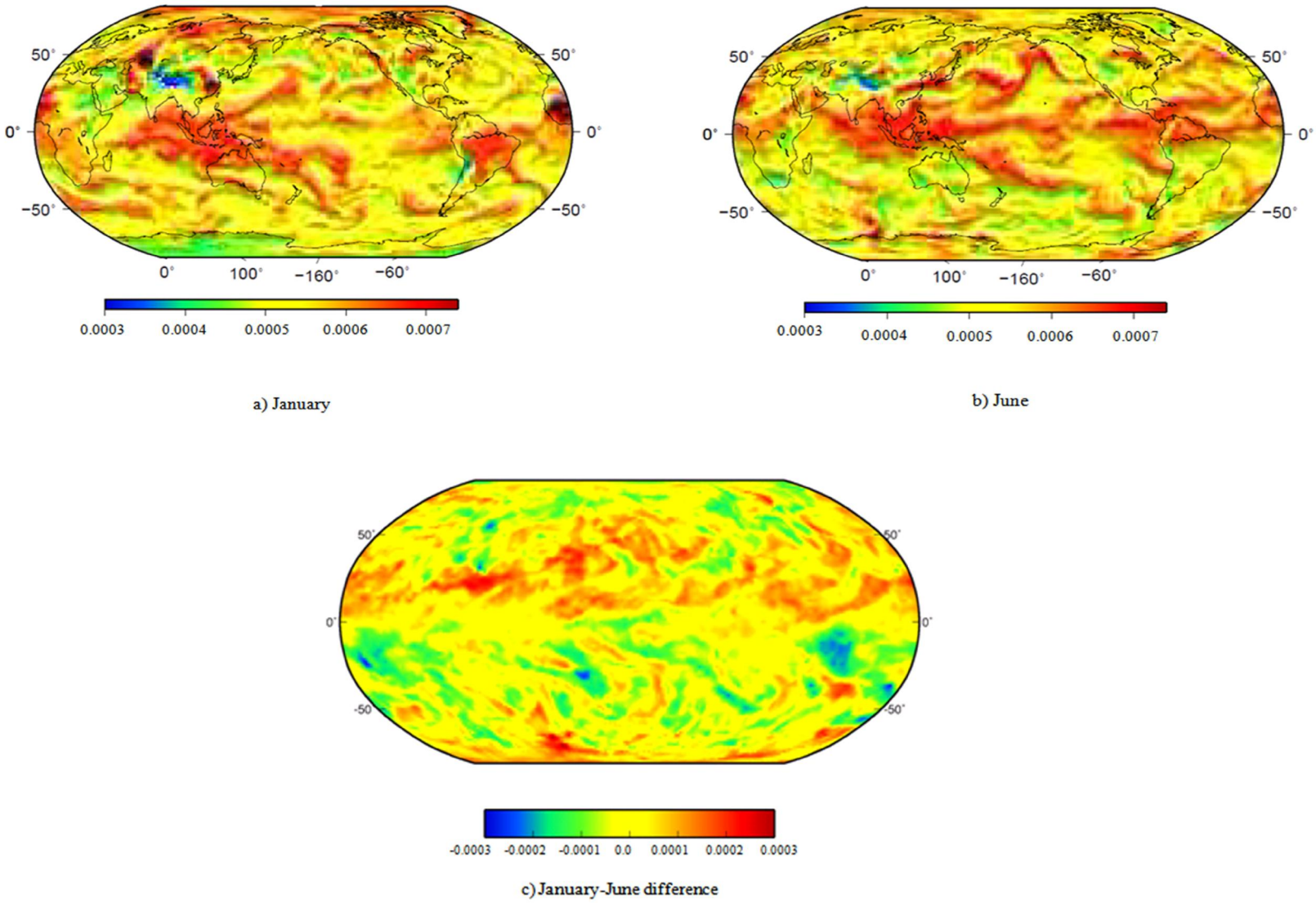

Figure2.15 Global Plots of Wet "a" Coefficients of the VMF1 Mapping Function at 0UT 2011

The *aw*-coefficients are of less magnitude (Figure 2.15a and b) compared to the *ah*-coefficients (Figure 2.14a and b). This is because the effect of the Tropospheric delay due to the water vapour is less compared to the effect due to the hydrostatic part (temperature and atmospheric pressure). The *aw*-coefficients are least at the Himalayas / Karakorum / Hindu Kush (with an altitude of 3862km) both in January and June but the area with minimum values is smaller in June due to the increased temperatures generally. The other dry areas like the rocky mountains of North America located on the western side of North America and Andes of South America have also low values for the *aw*-coefficients. The values of *aw*-coefficients are generally high around the tropical region of the globe. To note is that the high values are parches (Figure 2.15a and 2.15b) compared to those of the *ah*-coefficients (Figure 2.14a and b) that are gradual. The high values of *aw*-coefficients are however more spread around Indonesia as shown in Figure 2.15a and 2.15b. The Antarctica also has low values of the *aw*-coefficients increasing from January to June due to the general temperature increases as shown in Figure 2.15a and 2.15b. The change of the *aw*-coefficients from January to June is not significantly great. The difference in the *aw*-coefficients between winter and summer is displayed in Figure 2.15c. The change in the coefficients is greater in the northern hemisphere than in the southern hemisphere. In the northern hemisphere, we have the *aw*-coefficients increasing while they reduce in the southern hemisphere. The northern region of South America has significant fall in the *aw*-coefficients from January to June Figure2.15c.

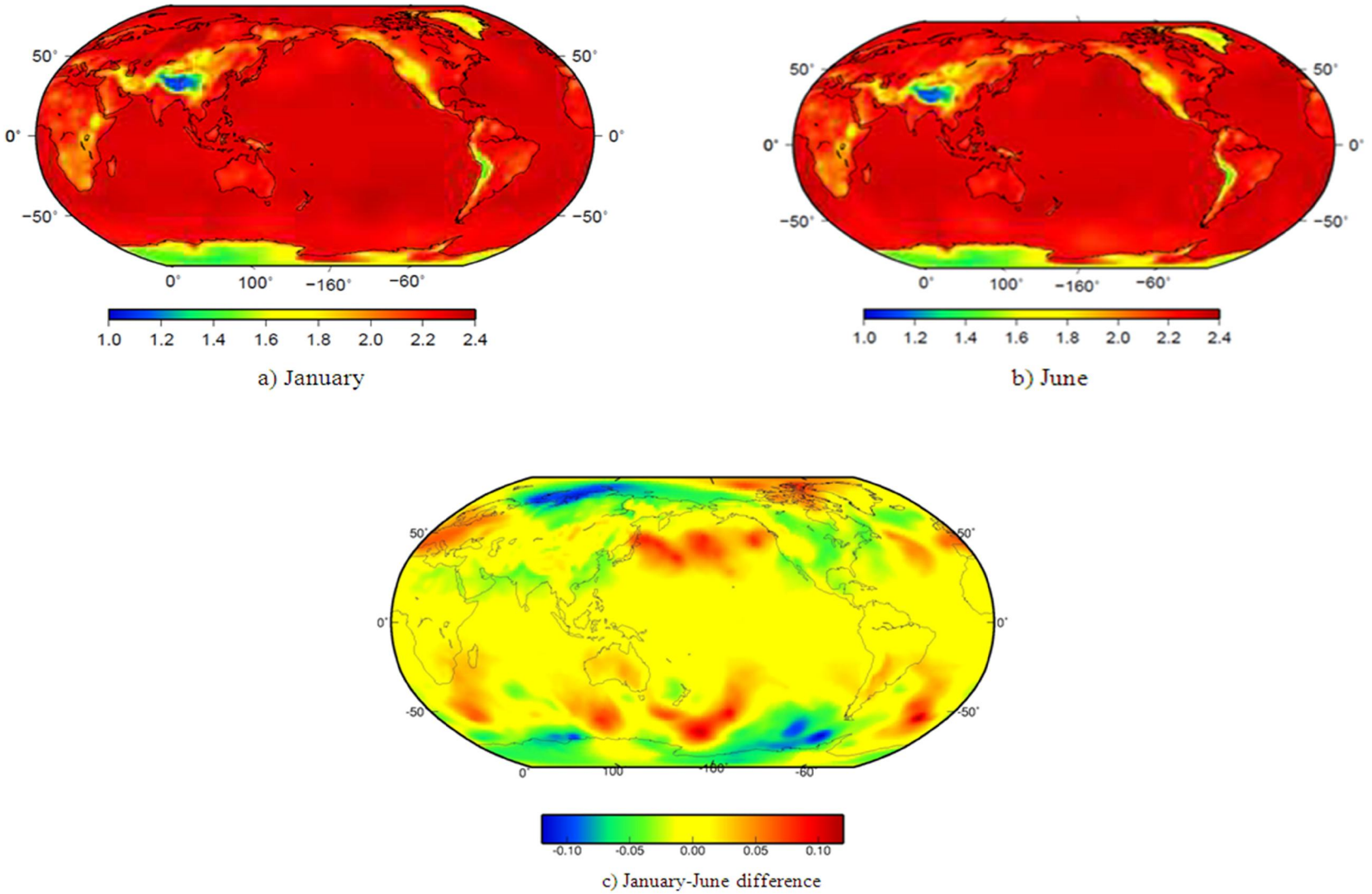

Figure2.16 Global Plots of Zenith Hydrostatic Delay (ZHD) of the VMFG grid at 0UT 2011

Not only are the "a" coefficients provided on the grid but also the hydrostatic and wet zenith delays are also given. Consistent with Boehm et al. (2006a), the approximation of Davies et al. (1985) is used for Z_h in metres in Equation 2.37 Kouba (2009). Their values are in m, and the filenames are starting with "*zh*" and "*zw*", respectively.

$$Z_h(h) = 0.0022768 \frac{p(h)}{(1-0.00266\cos(2\varphi)-0.28x10^{-6}h)} \tag{2.37}$$

And that of Berg (1948) for the pressure lapse rate (in hpa):

$$p(h) = 1013.25(1 - 0.0000226h)^{5.225} \tag{2.38}$$

Where h is the height in metres. Using the Equation 2.37 it implies that if the pressure of a station at latitude φ and height h is known then the hydrostatic delay $Z_h(h)$ can be computed as shown in the Figures 2.16 a and b above Kouba (2009).

The *ZHD* (Zenith Hydrostatic Delay) value attains a maximum at about 2.4 metres at zenith angle at sea level. The values of the *ZHD* are pretty much the same every especially over the ocean as you can obverse in the Figure 2.16a and 2.16b. The *ZHD* attains approximately a minimum value of 1.0 metres at zenith angle at Himalayas / Karakoram / Hindu Kush. This is true for the VMF grid of January and June (summer). This is because *ZHD* is basically a pressure at a very good approximation. In mountainous countries like Ethiopia, in the Andes (South America) and in Himalayas including the Antarctica the *ZHD* value gets smaller reflecting that pressure reduces at high altitudes hence reduction in the zenith hydrostatic delay. The change in the zenith hydrostatic delay from January to June is again minimal. The difference in the *ZHD* values between January and June is shown in Figure2.16c. As it can be observed in Figure 2.16c, generally the values of *ZHD* remain the same. This is because *ZHD* is basically a pressure and pressure of points does not significantly change over time. Some points have a significant reduction in the *ZHD* value from January to June (regions at the North Pole (longitude 100^0) and some parts near the Antarctica). There are also pockets of regions both in the northern and southern hemisphere where we have significant rise in the *ZHD* values.

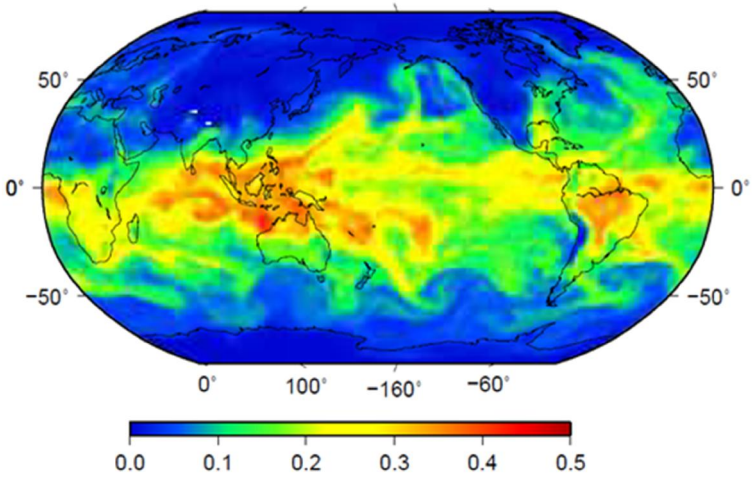

a) January

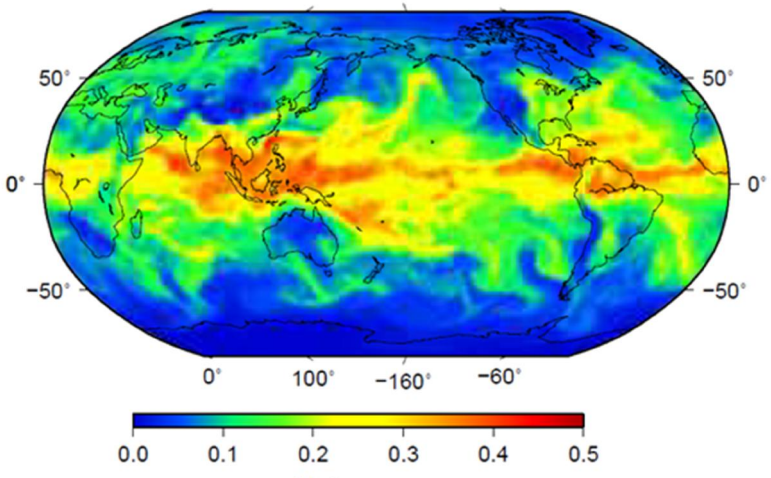

b) June

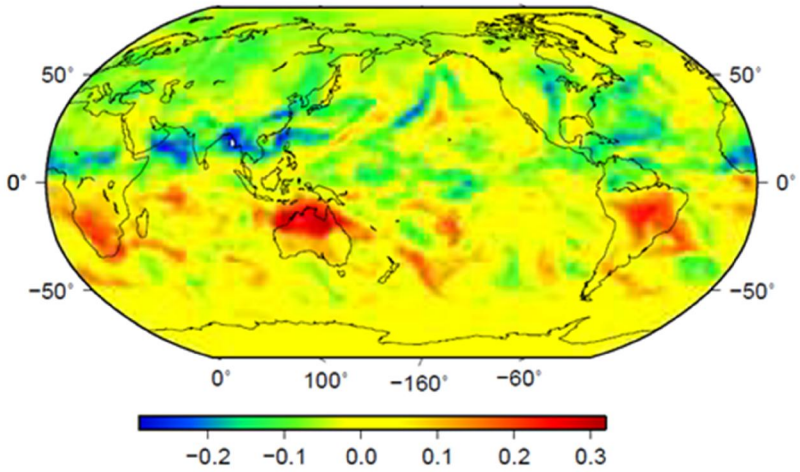

c) January-June difference

Figure2.17 Global Plots of Zenith Wet Delay (ZWD) of the VMFG grid at 0UT 2011

The *ZWD* is least at the north and south extremes of the globe (areas near the north and South Pole). The *ZWD* is greatest again around the tropical region, great in January around Indonesia and South America and great around Indonesia and Central America in June (Figure 2.17a and Figure 2.17b). This is due to the high humidity in these areas caused by the significant temperatures. The difference in the *ZWD* values from January to June is shown in Figure 2.17c. There is a general fall in these values in the northern hemisphere while the *ZWD* values remain constant in the southern hemisphere. There is also a significant rise in the *ZWD* values for southern Africa, part of Indonesia and central part of South America (Brazil) Figure2.17c. Modelling the path delays due to the neutral atmosphere for microwave signals emitted by satellites or radio sources is one of the major error sources in the analyses of Global Positioning System (GPS) and Very Long Baseline Interferometry (VLBI) observations. The concept is based on the separation of the path delays, ΔL, into a hydrostatic and a wet part (e.g., Davis et al., 1985).

$$\Delta L(E) = \Delta L_h^z . mf_h(e) + \Delta L_w^z . mf_w(e) \tag{2.39}$$

In Eqn. 2.39, the total delays ΔL(E) at an elevation angle **E** are made up of a hydrostatic (index h) and a wet (index w) part, and each of these terms is the product of the zenith delay (ΔL_h^z or ΔL_w^z) and the corresponding mapping function mf_h or mf_w. These mapping functions, which are independent of the azimuth of the observation, have been determined for the hydrostatic and the wet part separately by fitting the coefficients a, b, and c of a continued fraction form (Marini, 1972) to standard atmospheres (e.g., Chao, 1974), to radiosonde data (Niell, 1996), or recently to numerical weather models (NWMs) (e.g., Niell, 2000; Boehm and Schuh, 2004).

$$mf(e) = \frac{1+\frac{a}{1+\frac{b}{1+c}}}{sine+\frac{a}{sine+\frac{b}{sine+c}}} \tag{2.40}$$

Whereas the hydrostatic zenith delays, ΔL_h^z(m), which can be determined from the total pressure p in hPa and the station coordinates (latitude ϕ and height h in m) at a site (Saastamoinen, 1973) (Eqn. 2.40), and the hydrostatic and wet mapping functions are assumed to be known, the wet zenith delays, ΔL_w^z, are estimated within the least-squares adjustment of the GPS or VLBI analyses.

$$\Delta L_h^z = 0.0022768.\frac{p}{1-0.00266.cos(2\varphi)-0.28.10^{-6}.h} \quad (2.41)$$

However, there might be errors in the hydrostatic zenith delays or the mapping functions, and their influence on station heights is well described with a rule of thumb by Niell et al. (2001) The error in the station height is approximately one third of the delay error at the lowest elevation angle included in the analysis. Following a refinement of this rule of thumb by Boehm (2004), the factor is rather 1/5 than 1/3 for a minimum elevation angle of 5°, which is also close to the value 0.22 found by MacMillan and Ma (1994). The following two examples illustrate this rule of thumb, which holds for both GPS and VLBI, but which depends on the actual distribution of elevations and on whether elevation-dependent weighting is used: The hydrostatic and wet zenith delays are taken to be 2000 mm and 200 mm, respectively, the minimum elevation angle is 5°, and the corresponding values for the hydrostatic and wet mapping functions are 10.15 ($mf_h(5°)$) and 10.75 ($mf_w(5°)$). (1) We assume an error in the total pressure measured at the station of 10 hPa: 10 hPa correspond to ~20 mm hydrostatic zenith delay (compare Eqn. 2.22), which is then mapped down with the wrong mapping function (factor 0.6 = 10.75 −10.15). At 5° elevation the mapping function error is 12 mm, and one fifth of it, i.e. 2.4 mm, would be the resulting station height error. (2) We consider an error in the wet mapping function of 0.01 ($mf_w(5°)$ = 10.76 instead of 10.75) or in the hydrostatic mapping function of 0.001 ($mf_h(5°)$ = 10.151 instead of 10.15). The error at 5° elevation in both cases is 20 mm, i.e. the error in the station height would be approximately 4 mm.

The Vienna Mapping Functions (VMF) introduced by Boehm and Schuh (2004) depend only on elevation angle and not on azimuth, i.e. they assume that the troposphere is symmetric around the stations. For the b and c coefficients (see Eqn. 2.40) the best values available at that time were taken from the Isobaric Mapping Functions (IMF) (Niell and Petrov, 2003) for the hydrostatic part and from the Niell Mapping Functions (NMF) at 45° latitude (Niell, 1996) for the wet part. Later, an updated version for the VMF (Boehm and Schuh, 2004) is developed, which is based on new b and c coefficients for the hydrostatic mapping functions and which will be called VMF1 hereafter. For VMF1, the c coefficients from raytracing are fit to a function of latitude and day of year to remove systematic errors.

This is important for geophysical applications of geodesy, for instance, to determine the correct seasonal and latitude dependence of hydrology. An alternative approach to the traditional

separation into wet and hydrostatic mapping functions is the introduction of the 'Total' Vienna Mapping Function' (VMF1-T) for mapping down the total delays, which uses the total refractivity instead of its hydrostatic and wet components. Different procedures are described for calculating a priori zenith delays that can be used for GPS and VLBI analyses, including their determination from the operational analysis pressure level dataset of the ECMWF (European Centre for Medium-Range Weather Forecasts).

At the ECMWF, the ERA-40 (ECMWF Re-Analysis 40-years) data are stored as expansions of spherical harmonics with a horizontal resolution corresponding to about 125 km (Simmons and Gibson, 2000). From these data, monthly mean profiles for the year 2001 (for the epochs 0, 6, 12, and 18 UT) were downloaded on a global grid (30° in longitude by 15° in latitude). These profiles consist of 23 levels from 1000 hPa to 1 hPa (1000, 925, 850, 775, 700, 600, 500, 400, 300, 250, 200, 150, 100, 70, 50, 30, 20, 10, 7, 5, 3, 2, 1), and they comprise values for height, total pressure, temperature, and water vapour pressure for each level.

In a first step, for all 7488 profiles (156 grid points times 12 months times 4 epochs per day) the total and hydrostatic mapping functions as well as the vacuum elevation angles **E** are determined for 10 different initial elevation angles e0 (3.2°, 5°, 7°, 10°, 15°, 20°, 30°, 50°, 70°, 90°) (compare Boehm, 2004). The vacuum elevation is the asymptotic final elevation angle of the outgoing ray and corresponds to the direction expected for the target observed, either the GPS satellite or the VLBI radio source. The geometric bending effect ΔL_{bend} (see, Davies et al., 1985) is added to the hydrostatic and to the total mapping functions.

$$mf_h(E) = \frac{\Delta L_h(E) + \Delta L_{bend}(E)}{\Delta L_h^z} \tag{2.42}$$

$$mf_t(E) = \frac{\Delta L_h(E) + \Delta L_w(E) + \Delta L_{bend}(E)}{\Delta L_h^z + \Delta L_w^z} \tag{2.43}$$

Then, the three coefficients a, b, and c of the total and hydrostatic mapping functions are fitted to the ten discrete mapping function values of each profile by a least-squares adjustment. The residuals of their fit are usually smaller than 0.5 mm. These 7488 mapping functions will be used as 'rigorous' reference for evaluations. The mean value of all b coefficients for both the total (index t) and hydrostatic (index h) mapping functions is found to be

$$b_t = b_h = 0.0029 \tag{2.44}$$

and is kept fixed in all further analyses. In the next step the least-squares adjustment is repeated, but only the coefficients a and c are estimated for all profiles, while the coefficient b for the hydrostatic and total mapping functions is kept fixed to the value given in Eqn. 2.44. The coefficients c then show a clear variability depending on season and latitude, but unlike former mapping functions, the coefficients c are not symmetric with respect to the equator (apart from the phase offset for the two hemispheres). For example, the coefficient c at the North pole in January is significantly smaller than c at the South pole in July (Figure 2.18).

Therefore, Eqn. 2.45 is used to model the coefficient c, when doy is the day of the year and 28 January has been adopted as the reference epoch (Niell, 1996), ϕ is the latitude, and ψ specifies the northern or southern hemisphere (see the last columns of Table 2.1 and 2.2).

$$c = c_0 + \left[\left(\left(\frac{Doy-28}{365}2\pi + \Psi\right) + 1\right)\frac{c_{11}}{2} + c_{10}\right](1 - cos\,\phi) \tag{2.45}$$

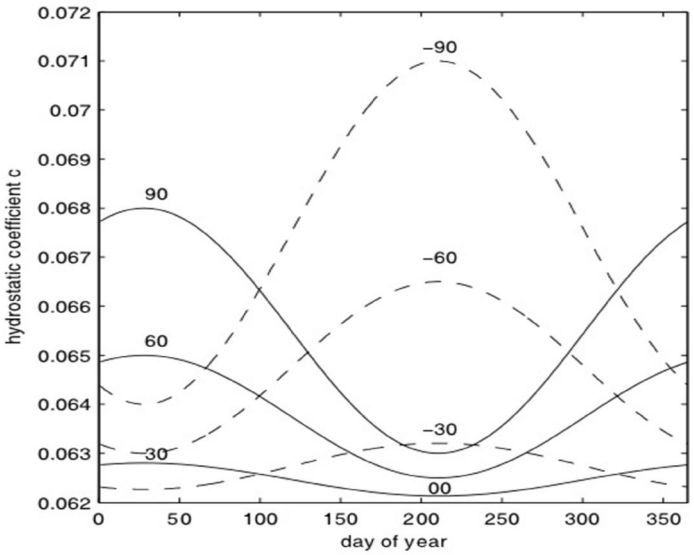

(Courtesy of Boehm et al, 2006a)

Figure2.18 Hydrostatic coefficients c for 0°, ±30°, ±60°, and ±90° latitude

Table 2.1 and Table 2.2 contain the parameters of Eqn. (2.45), which are obtained for the hydrostatic and total mapping functions. As an example, the coefficient c in January 2001 is plotted in Figure 2.18 for different latitudes.

Table2.1: Parameters c0, c10, c11, and ψ needed for computing the coefficient c of the Hydrostatic Mapping Function.

Hemisphere	c_0	c_{10}	c_{11}	Ψ
Northern	0.062	0.001	0.005	0
Southern	0.062	0.002	0.007	π

Table 2.2: Parameters c0, c10, c11, and ψ needed for computing the coefficient c of the Total Mapping Function.

Hemisphere	c_0	c_{10}	c_{11}	Ψ
Northern	0.063	0.000	0.004	0
Southern	0.063	0.001	0.006	π

The b and c coefficients of the wet mapping functions do not have to be changed because the wet zenith delays are smaller by a factor of ~10 than the hydrostatic zenith delays and the effect of variations in b and c is not significant. The b and c coefficients of the wet mapping function are still fixed to those of NMF (Niell, 1996) at 45° latitude and the coefficient a is estimated for each profile, i.e., the recommended wet mapping function is still VMF(wet).

The 'fast' approach (in which the parameter a is estimated from a single ray trace at initial elevation angle E_θ = 3.3°) can be compared with the 'rigorous' approach that determines all three coefficients in a least-squares adjustment using ten different initial elevation angles. The maximum differences are encountered at 5° elevation because the 'fast' mapping functions (VMF1) are 'tuned' for elevations of ~3°, i.e. there is no error at ~3°, while at elevation angles considerably higher than 5° the differences between the rigorous and the fast approach are also vanishing. With the new b and c coefficients (Eqn. 2.45 and Tables 2.1 and 2.2), the deviation from the rigorous approach at 5° elevation is always smaller than 8 mm, which means that the corresponding error in the station height is always smaller than 1.6 mm. This holds for all months in 2001 and for all latitudes and longitudes (see, Table 2.3).

Table2.3 Mean biases and standard deviations of hydrostatic delay differences at 5° elevation for NMF, VMF, and VMF1 with respect to the hydrostatic mapping functions derived from the numerical weather model for a global grid and 12 months in 2001.

	Mean bias (mm)	Standard deviation (mm)
NMF	21.8(4.4)	35.0(7.0)
VMF	3.3(0.7)	11.2(2.2)
VMF1	2.3(0.5)	2.0(0.4)

The principle of VMF1 (which is the principle of VMF(fast) in (Boehm and Schuh, 2004)) is to use the best coefficients b and c available, determine the values of the mapping functions at E_0 = 3.3° initial elevation angle from the NWM, and derive the coefficient a by simply inverting the continued fraction form (Eqn. 2.36). In our study, the values of the mapping functions for the VLBI and GPS stations are determined from the ECMWF operational pressure level data. No horizontal interpolation for the sites has to be done between grid points because the latitudes and longitudes of the stations are input parameters to the expansion of spherical harmonics of the operational pressure level data corresponding to a horizontal resolution of about 0.3°. With VMF1 no height correction is necessary (compare, Niell (1996)), since the ray tracing starts at the actual station height. To get the meteorological parameters at the position of each site, the temperature is interpolated linearly between the pressure levels, and the total and water vapour pressure are interpolated exponentially applying the hypsometric equation (see, (Boehm, 2004)). Figure 2.19 shows the differences of the hydrostatic delays at 5° elevation between VMF (Boehm and Schuh, 2004) and VMF1 for 213 IGS (International GNSS Service) stations for the day 28 in 2005 (January) and the day 210 in 2004 (July) (at 0, 6, 12, and 18 UT). It can be seen that the two hydrostatic mapping functions agree best at mid-latitudes, but that there are systematic differences closer to the equator and near the winter poles which are caused by deficiencies of the c coefficients in VMF (Boehm and Schuh, 2004). These systematic errors of VMF were not detected by Boehm and Schuh (2004), since they made their checks only for the

CONT02 stations which are situated mostly at mid-latitudes where the 'fast' VMF agrees well with the 'rigorous' approach.

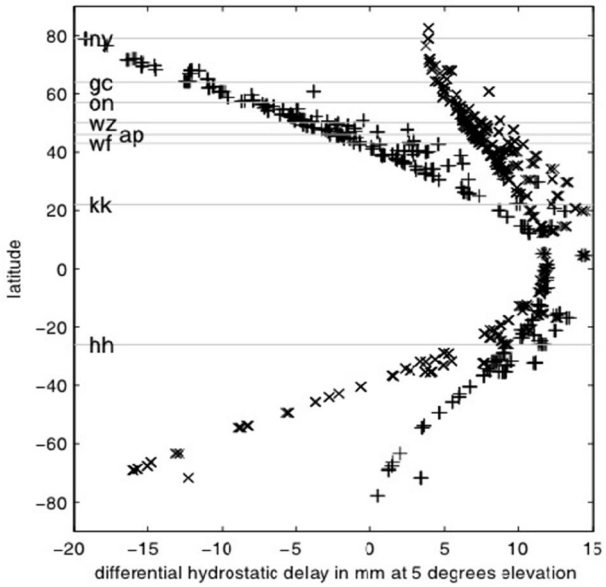

(Courtesy of Boehm et al, 2006a)

Figure2.19 Hydrostatic delay differences (in mm) VMF minus VMF1 on day of year 28 in 2005 (+) and on day of year 210 in 2004 (x) at 5° elevation for 213 IGS stations. Additionally, the latitudes of the eight CONT02 stations are marked by thin horizontal lines.

For the VMF (Boehm and Schuh, 2004), the hydrostatic b and c coefficients were taken from the Isobaric Mapping Functions IMF (Niell and Petrov, 2003), but it has to be mentioned that the development of IMF was based on radiosonde data which were taken mainly at mid-latitudes where the agreement between VMF and VMF1 is very good. In our work here, a global distribution was used to derive functions for the b and c coefficients, and this allowed detection of deficiencies at the winter poles and near the equator of earlier hydrostatic mapping functions.
Table 2.3 shows the mean biases and standard deviations of the hydrostatic delays at 5° elevation (assuming 2000 mm hydrostatic zenith delay) between reference values determined from ray tracing through the numerical weather model at all grid points described at the beginning and

those from NMF, VMF, and VMF1, respectively. The minor standard deviation of 2mm between the ray traced mapping function at 5° elevation and VMF1 justifies the exclusive determination of the coefficient a instead of all three coefficients a, b, and c. Contrarily, there are significant delay errors with NMF which are equivalent to station height errors of 4 mm (bias) and 7 mm (standard deviation), respectively. Niell (2005, personal communication), has compared VMF1 with mapping functions derived from radiosonde data, and he found equivalent station height errors of less than 2 mm, which is similar to the values reported by MacMillan and Ma (1998) for differences between mapping functions from radiosonde data and numerical weather models at four selected sites.

Vienna Total Mapping Function (VMF1-T): Instead of separating the delays into a hydrostatic and a wet part, an alternative concept of total delays has also been investigated for tropospheric modelling, that is the use of a single Total Mapping Function mf_t (Eqn. 2.43) for mapping down the a priori total zenith delays $\Delta Lz_{t,0}$ and as partial derivative for the estimation of the residual total delays ΔLzt,res (Eqn. 2.46 and 2.47).

$$\Delta L_t^z = \Delta L_h^z + \Delta L_w^z = \Delta L_{t,0}^z + \Delta L_{t,res}^z \tag{2.46}$$

$$\Delta L(E) = \Delta L_{t,0}^z . mf_t(E) + \Delta L_{t,res}^z . mf_t(E) \tag{2.47}$$

A benefit of the numerical weather models is that they enable the determination of not only the total mapping functions but also of the a priori total zenith delays. Although for the analysis of VLBI sessions a priori total zenith delays are used, a priori hydrostatic zenith delays could have been applied, too, because the mapping function for the a priori zenith delays is the same as for the residual zenith delays.

With the classical separation into a hydrostatic and a wet part, errors of the hydrostatic zenith delays cannot be fully compensated for by estimating the remaining wet part, because the hydrostatic and wet mapping functions are significantly different, especially at low elevations. The advantage of this concept is that it cannot be affected by poor a priori hydrostatic zenith delays. On the other hand, the total mapping function is close in value to the hydrostatic mapping function, which allows estimation of the residual hydrostatic delays properly only if a) the wet zenith delays have been accurately calculated from the ECMWF, and b) they do not differ from the linear interpolation between 6-hour values that is used to construct the a priori total delay.

A limitation to the concept of the total mapping function is that it is affected by bad a priori information about the wet part in the atmosphere from the numerical weather models. Snajdrova et al. (2005) show that the wet zenith delays determined from pressure level data of the ECMWF and the wet zenith delays estimated in the VLBI analysis for CONT02 agree at the 1 cm level in terms of bias and up to the 2 cm level (for stations with high humidity like Kokee Park) in terms of scatter. While a bias of 1 cm is not that critical (corresponds to a bias of 1.2 mm in station height), a noise of about 3 mm is added to the vertical scatter at humid sites. But even if the information about the hydrostatic and wet part provided by the numerical weather models at the 6-hour time epochs was accurate at the mm level, the total mapping function would not be able to perfectly model the path delays since the variation - especially in the wet part - is more rapid than can be modelled with 6-hour time intervals. This again adds noise to the station heights and baseline lengths, because the total mapping function, which is close to the hydrostatic mapping function, is not appropriate to estimate these rapid variations of the wet zenith delays.

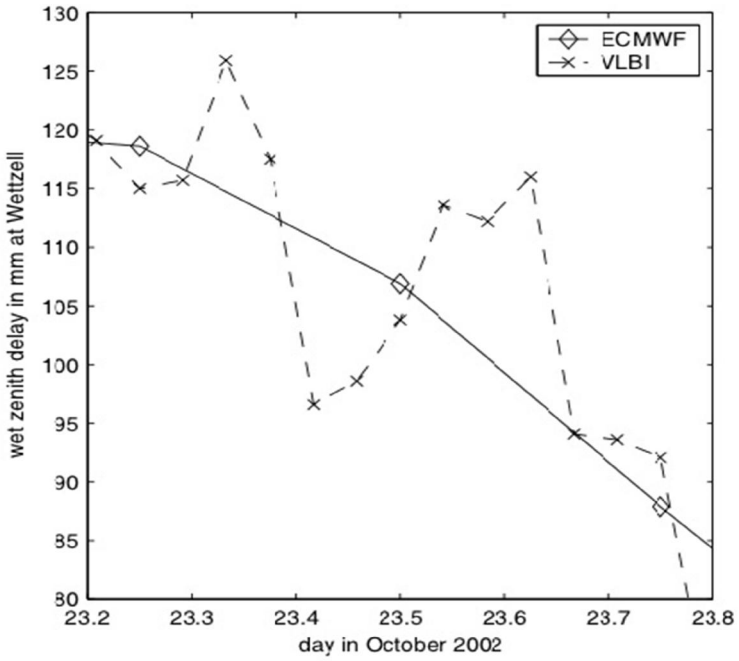

Figure2.20 Wet zenith delays in mm at station Wettzell on 23 October 2002. It shows that there is more variation in the wet zenith delays than can be modelled with 6-hour data from the ECMWF.

2.9.3 Niell Mapping Function (NMF)

A mapping function that does not require surface meteorology measurements, but provides comparable accuracy and precision to others that requires such data is presented in (Niell,1996). This mapping only uses the receiver geographic location and measurement time as inputs.
The Niell's mapping involves two different obliquity factors, for the dry and wet components, which are computed from the Eqns. (2.48) to (2.49), where (E) is the elevation of ray and (H) is the receiver height, in kilometres:

Hydrostatic mapping function:

$$M_{dry}(E,H) = m(E,a_d\ ,b_d\ ,c_d) + \Delta m(E,H)$$

With

$$\Delta m(E,H) = \left[\frac{1}{sinE} - m(E,a_{ht}\ ,b_{ht}\ ,c_{ht})\right].H \tag{2.48}$$

Wet Mapping Function:

$$M_{wet}(E) = m(E,a_w\ ,b_w\ ,c_w) \tag{2.49}$$

Where, m (E,a,b,c) is the (Marini, 1972) mapping normalized to unity at zenith:

$$\mathrm{m}(E,a,b,c) = \frac{1+\frac{a}{1+\frac{b}{1+c}}}{sin\,E+\frac{a}{sin\,E+\frac{b}{sin\,E+c}}} \tag{2.50}$$

The Hydrostatic parameters a_d, b_d, c_d are time (t) and latitude (Φ) dependent parameters given by:

$$\xi(\phi,t) = \xi_{avg}(\phi) - \xi_{amp}(\phi)cos\left(2\pi\frac{t-T_o}{365.25}\right) \tag{2.51}$$

Where, t is the time from January 0.0, in days, and T_0 is taken as DOY 28 (i.e., $T_0 = 28$). The parameters
$\xi_{avg}(\phi_i)$ and $\xi_{amp}(\phi_i)$ are linearly interpolated from Table2.4 between the nearest $\xi(\Phi_i)$. The a_{ht}, b_{ht}, c_{ht} are taken directly from the same Table 2.4.

Table2.4 Coefficients of the Hydrostatic Mapping Function

Coefficient ξ	Latitude (ϕ)				
	15^0	30^0	45^0	60^0	75^0
	Average				
A	1.2769934e-3	1.2683230e-3	1.2465397e-3	1.2196049e-3	1.2045996e-3
b	2.9153695e-3	2.9152299e-3	2.9288445e-3	2.9022565e-3	2.9024912e-3
c	62.610505e-3	62.837393e-3	63.721774e-3	63.824265e-3	64.258455e-3
	Amplitude				
A	0.0	1.2709626e-5	2.6523662e-5	3.4000452e-5	4.1202191e-5
b	0.0	2.1414979e-5	3.0160779e-5	7.2562722e-5	11.723375e-5
c	0.0	9.0128400e-5	4.3497037e-5	84.795348e-5	170.37206e-5
	Height Correction				
a_{ht}	2.53e-5				
b_{ht}	5.49e-3				
c_{ht}	1.14e-3				

Table2.5 Coefficients of the Wet Mapping Function.

Coefficient ξ	Latitude (ϕ)				
	15^0	30^0	45^0	60^0	75^0
A	5.8021897e-4	5.6794847e-4	5.8118019e-4	5.9727542e-4	6.1641693e-4
b	1.4275268e-3	1.5138625e-3	1.4572752e-3	1.5007428e-3	1.7599082e-3
c	4.3472961e-2	4.6729510e-2	4.3908931e-2	4.4626982e-2	5.4736038e-2

The Niell Mapping Function (NMF) was built on one year of radiosonde profiles from the northern hemisphere (Niell, 1996); the spatial and temporal variability of the mapping function is accounted for with only a latitude and seasonal dependence. This empirical approach considerably simplifies the estimation process since no external data are required. However, following the development of NMF, two deficiencies became evident: a) latitude- dependent biases, which are largest in high southern latitudes, and b) the lack of sensitivity to the longitude of a site, what causes systematic distortions of estimated positions in some areas, for example over northeast China and Japan. The simple temporal and latitudinal functions of the NMF do not provide the resolution to capture the higher variability in space and time that are seen in mapping functions based on NWM data (Boehm and Schuh, 2004; Boehm et al., 2006).

In conclusion: NMF sets its coefficients by applying ray-tracing to nine elevation angles from 3± to 90± on Radiosonde data, which had been collected for one year between 1987 and 1988 (Niell 1996). The coefficients are provided only at four latitudes; 15, 30, 45, and 60±N. Thus, for a site not located at those four latitudes, the coefficients should be determined by linear interpolation. The coefficients of the wet mapping function are defined as a constant by latitude, and those of the hydrostatic mapping function are defined as a function of latitude and observation time as follows (Niell 1996):

$$a_h(\phi, t) = a_{avg}(\phi) - a_{amp}(\phi) cos\left(2\pi \frac{DOY-28}{365.25}\right) \quad (2.52)$$

In the Eqn. (2.52), ϕ is the site latitude and Day-of-Year (DOY) is the date based on UT (Universal Time). a_{avg} and a_{amp} stand for the mean value and an amplitude, respectively; and they are given as constants.

The hydrostatic mapping function of NMF needs correction terms to make up for the height difference of observation site. Therefore, the hydrostatic mapping function of NMF should be redefined as Eqn. (2.53) with correction terms:

$$m_h(E) = f(E, a_h, b_h, c_h) - \left(\frac{1}{sine} - f(E, a_{ht}, b_{ht}, c_{ht})\right) xH \quad (2.53)$$

In the equation, H is the height of the site (km), and the coefficients of correction terms a_{ht}; b_{ht}, and c_{ht} are given as constants (Niell 1996).

2.9.4 Global Mapping Function (GMF)

Determination of the Global Mapping Function: Using 15^0 x 15^0 global grids of monthly mean profiles for pressure, temperature, and humidity from the ECMWF (European Centre for Medium-Range Weather Forecasts) 40 years reanalysis data, the coefficients a_h and a_w were determined for the period September 1999 to August 2002 applying the same strategy which was used for VMF1. Taking empirical equations for b and c (from VMF1) the parameters a, were derived by a single raytrace at 3.3_ initial elevation angle (Boehm et al., 2006).

Thus, at each of the 312 grid points, 36 monthly values were obtained for the hydrostatic and wet a, parameters. The hydrostatic coefficients were reduced to mean sea level by applying the height correction given by Niell (1996). The mean values, a_0, and the annual amplitudes A of a sinusoidal function (Eqn. (2.54)) were fitted to the time series of the, a parameters at each grid point, with the phases referred to January 28, corresponding to the NMF. The standard deviations of the monthly values at the single grid points with respect to Eqn. (2.54) increase toward higher latitude from the equator, with a maximum value of 8 mm (equivalent station height error) in Siberia. For the wet component, the standard deviations are smaller with maximum values of about 3 mm at the equator.

$$a = a_0 + A.cos\left(\frac{doy-28}{365}.2\pi\right) \tag{2.54}$$

$$a_0 = \sum_{n=0}^{9}\sum_{m=0}^{n} p_{nm}(sin\varphi).[A_{nm}.cos(m.\lambda) + B_{nm}.sin(m.\lambda)] \tag{2.55}$$

Then, the global grid of the mean values a_0 and that of the amplitudes A for both the hydrostatic and wet coefficients of the continued fraction form were expanded into spatial spherical harmonic coefficients up to degree and order 9 (according to equation (2.55) for a_0) in a least-squares adjustment. The residuals of the global grid of a_0 and A values to the spherical harmonics are in the sub-millimetre range (in terms of station height). The hydrostatic and wet coefficients a, for any site coordinates and day of year can then be determined using Eqn. (2.54).

In conclusion: VMF1 has a weakness that it has to directly apply ray-tracing by using a NWM in order to calculate the coefficients a_h and a_w, or has to download coefficients from a web site. To make up for this limitation, GMF defined the coefficients a_h and a_w as mathematical formulae. GMF applied ray-tracing to the monthly average values out of ERA40 from 1999 to 2002, and set the coefficients a_h and a_w by calculating ray-traced values for 36 months at 312 grid points around the world.

In Eqn. (2.56), the coefficient a is defined as a function of DOY (Boehm et al. 2006a). In the equation, a_0 indicates the mean, and A is the amplitude about a_0. In both the hydrostatic and wet mapping function, a_0 and A were expanded into spherical harmonics up to degree and order nine (Boehm et al. 2006a).

$$a = a_0 - Acos\left(2\pi \frac{DOY-28}{365.25}\right) \tag{2.56}$$

2.10 Azimuthal asymmetry and gradient parameters

The atmosphere has mostly been considered to be horizontally layered and azimuthally symmetric during the modelling of the troposphere. Even if this assumption about the troposphere is appropriate for some geodetic works of lesser precision, significant errors will be introduced if the atmosphere is assumed azimuthally symmetric for high precision work (i.e. deformation monitoring of very large structures of significant importance as Dams, Historic buildings and Bridges). Some of the first publications about the effect of horizontal refractivity gradients were (Gardner, 1977) and (Iyer and Bufton, 1977). The asymmetry is modelled by assuming a tilted atmosphere as shown in Figure 2.21. The refractivity N as a function of height h and the horizontal position $\vec{x}$ is given by the formula below.

$$N(\vec{x}, h) = N(0, h) + \nabla\vec{N}.\vec{x} \tag{2.57}$$

The gradient vector is given by::

$$\nabla\vec{N} \doteq \frac{\partial N}{\partial \vec{x}}\Big| \vec{x} = 0 \tag{2.58}$$

Where zero if it is has to satisfy refractivity due to asymmetry of the atmospheric model.
The dot in Eqn. (2.57) denotes an inner product. The sum of the delay in a symmetric atmosphere and the correction due to the azimuthal asymmetry gives the Tropospheric delay in an azimuthally asymmetric atmosphere.

$$D_{asym}(\alpha, z) = D_{sym}(z) + D_{az}(\alpha, z) \tag{2.59}$$

The correction term follows from Eqn. (2.60) as:

$$D_{az} \approx M(z)\, tan\, z\, \vec{\gamma}.\vec{e} \tag{2.60}$$

Where $\vec{e} \doteq [cos\alpha; sin\alpha]$ is a unit vector in the direction of $\vec{x}$, and

$$\vec{\gamma} \doteq 10^{-6} \int_{h_0}^{\infty} \nabla\vec{N}\, h\, dh \tag{2.61}$$

is the gradient vector in the opposite direction of the projected normal with components

$\vec{\gamma} \doteq [\gamma N, \gamma E]$. The first part of Eqn. (2.60), $M(z)\, tan\, z$ is the mapping function of the zenith angle. The second part is the azimuth (α) dependent gradient part:

$$\gamma(\alpha) \doteq \vec{\gamma}.\vec{e} = \gamma N\, cos\alpha + \gamma E\, sin\alpha \tag{2.62}$$

The gradient delay is thus composed of a north and an east parameter describing the azimuth dependence. The combined model (2.60) and (2.62) was given in (Macmillan,1995) and (Macmillan and Ma,1997). Using the above given definition, a slant gradient delay is a product of a gradient mapping function $M_{az}(z)$ and gradient delay $\gamma(\alpha)$:

$$D_{az}(\alpha, z) = M_{az}(z)\gamma(\alpha) \tag{2.63}$$

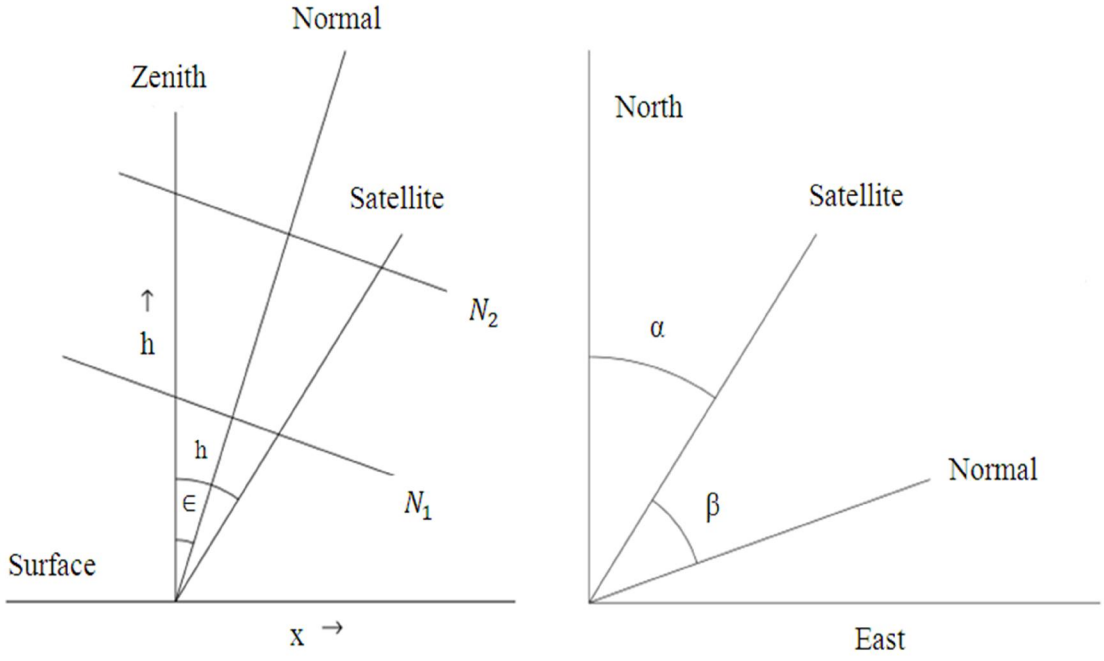

Figure2.21 Tilted atmosphere with lines of equal refractivity N_1and N_2

In analogy to the symmetric case, the 'asymmetric' delay in the slant direction is also a product of a mapping function and, in this case, the delay in the direction of the normal $D^n \approx D^z$ (De Munck, 1991).

$$D_{asym} = M(z - \epsilon cos\beta)D^n \approx (M(z) - \frac{dM(z)}{dz}\epsilon cos\beta)D^z \quad (2.64)$$

Where β is the angle between the projected normal and the projected slant direction. The approximation is however because $\epsilon cos\beta$ is small. From Eqn. (2.59) and (2.64) now follows:

$$D_{az} \approx -\frac{\mathrm{d}M(z)}{dz} D^z \epsilon cos\beta. \quad (2.65)$$

So, if a radio signal received is from the direction of the normal, the total delay is the least due to the passage through a shorter atmosphere. Because the mapping function is approximately M(z) ≈ sec z , and so $dM(z)/dz \approx sec\, z\, tan\, z$, from Eqns. (2.60), (2.62), and (2.65) can be seen that $\vec{\gamma}.\vec{e} = |\vec{\gamma}|.1.cos\beta \approx -D^z \epsilon cos\beta.$ so the length of the gradient vector is about $|\vec{\gamma}| \approx D^z|\epsilon|$,
which is an upper bound of the gradient delay for a particular azimuth.

In (Chen and Herring, 1997) an azimuthal mapping function is given as:

$$M_{az}(z) = \frac{1}{cosz\, cotz} + \frac{C_1}{cosz\, cotz} + \frac{C_2}{cosz\, cotz} + \cdots \quad (2.66)$$

In fact, this mapping function was truncated after the first constant:

$$M_{az}(z) = \frac{1}{cosz\, cotz} + \mathrm{C}' \quad (2.67)$$

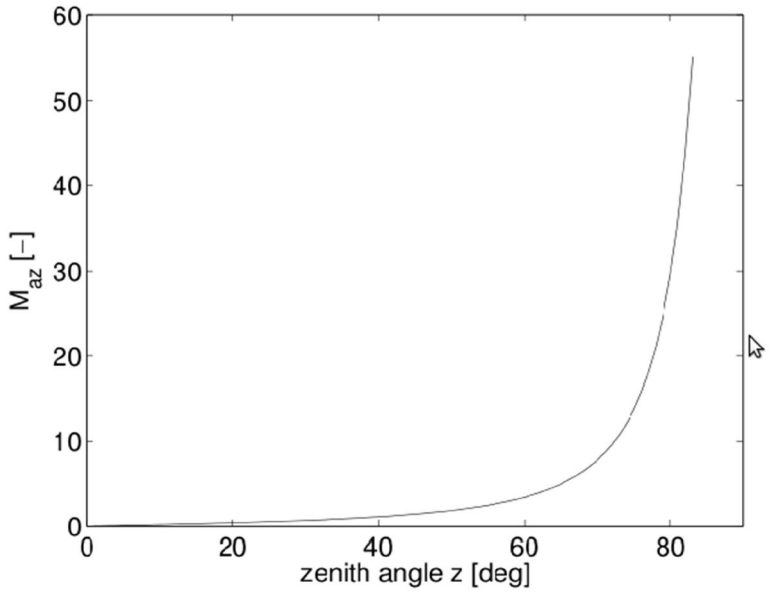

Figure2.22 Gradient mapping function of Chen and Herring

where C = 0.0032. The same type of mapping function could have been found by truncating $M(z)\ tanz$ after the first constant. In (Bar-Sever et al., 1998), $M(z)\ tanz$ was chosen as a mapping function. They stated that essentially no different results were found in GPS Precise Point Positioning with M(z) the wet or hydrostatic mapping function.

Hydrostatic gradients produced by pressure or dry temperature gradients have a large spatial scale of about 100km and a temporal scale of days. Wet atmosphere gradients have a smaller spatial scale(<10km) and can vary more rapidly on time scales of hours or less and are a function of water vapour content and temperature (MacMillan, 1995). GPS or VLBI estimates of gradient delays cannot be separated into a wet and a hydrostatic component. With WVRs however, estimates of only wet gradients can be derived. In (Davis et al., 1993), average values were found of approximately 1 mm for $|\vec{\gamma}|$ in Onsala. The largest value was approximately 8 mm. Bar-Sever et al. (1998) report hydrostatic gradients of about 0.6 mm from GPS estimates by comparing total gradients with wet gradients obtained by WVR-based estimates.

The model of (Davis et al., 1993) was slightly more complicated. They recognized that symmetric mapping functions are evaluated at un refracted zenith angles, where in fact tan z depends on the refracted zenith angle. They used an approximation for the bending:

$$\tau \approx -tanz\,\Delta n = -\tan z\,.10^{-6}N_0 \tag{2.68}$$

The tangent of the refracted zenith angle then is:

$$tan(z+\tau) = tanz + sec^2 z.\tau = tanz[1 - 10^{-6}N_0 sec^2 z]. \tag{2.69}$$

Therefore, instead of the mapping function $M(z)\,tan\,z$, they used the function $M_{az}tanz[1 - 10^{-6}N_0 sec^2 z]$. As can be seen from Figure 2.22, gradients become increasingly influential at lower elevation angles.

2.11 Computing Residuals

Station position estimates (at epoch t_i) are combined using a position x_{to}, at a common arbitrary reference epoch (t_0) and a linear velocity for each station $\dot{x}$ (Davies and Blewitt, 2000):

$$x_{t_i} = x_{t_0} + (t_i - t_0)\dot{x} \tag{2.70}$$

Where:

$$x = \begin{Bmatrix} x \\ y \\ z \end{Bmatrix} \qquad \dot{x} = \begin{Bmatrix} \dot{x} \\ \dot{y} \\ \dot{z} \end{Bmatrix} \tag{2.71}$$

(Davies and Blewitt, 2000).

A weekly global coordinate estimate (from now on referred to as an epoch solution) y_{t_i} at epoch t_i consists of n station Cartesian coordinate triplets x:

$$y_{t_i} = \begin{Bmatrix} x_{1,t_i} \\ x_{2,t_i} \\ \cdot \\ \cdot \\ x_{n,t_i} \end{Bmatrix} \tag{2.72}$$

For m included stations there are m 3x1 position parameters at epoch t_0 and m 3x1 velocities giving the model parameter vector:

$$y_{t_0} = \begin{Bmatrix} x_{1,t_0} \\ x_{2,t_0} \\ . \\ x_{m,t_0} \\ \cdots\cdots \\ \dot{x}_1 \\ \dot{x}_2 \\ . \\ \dot{x}_m \end{Bmatrix} \tag{2.73}$$

The elements of the 3n x 6m linear design matrix A_i in $y_{t_i} = A_i y_{t_0}$ are simply a 3 x 3 identity matrix **I** for each station position triplet and a 3 x 3 identity matrix scaled by the time factor $(t_i - t_o)$ for each velocity triplet. If a station estimate is not available in an epoch solution these matrices are zero, e.g. for an identical station parameter list and epoch solution:

$$A_i = \begin{bmatrix} \boldsymbol{I} & 0 & \ldots & 0 & \vdots & \boldsymbol{I}(t_i - t_0) & 0 & \ldots & 0 \\ 0 & \boldsymbol{I} & \ldots & 0 & \vdots & 0 & \boldsymbol{I}(t_i - t_0) & \ldots & 0 \\ \vdots & \vdots & \ddots & 0 & \vdots & \vdots & \vdots & \ddots & 0 \\ 0 & 0 & 0 & \boldsymbol{I} & \vdots & 0 & 0 & 0 & \boldsymbol{I}(t_i - t_0) \end{bmatrix} \tag{2.74}$$

The system is solved by sequential LS (e.g. Cross, 1992), summing normal equation components for k epoch solutions:

$$\mathrm{N} = \sum_{\mathrm{i}=1}^{\mathrm{k}} \mathrm{A}_\mathrm{i}^\mathrm{T} \mathrm{W}_\mathrm{i} \mathrm{A}_\mathrm{i} \qquad \mathrm{p} = \sum_{\mathrm{i}=1}^{\mathrm{k}} \mathrm{A}_\mathrm{i}^\mathrm{T} \mathrm{W}_\mathrm{i} \mathrm{y}_{\mathrm{t_i}} \tag{2.75}$$

Where W_i is the inverse of the weekly estimate covariance matrix C_i for y_{t_i}. The final estimate and variance-covariance matrices are given by:

$$\hat{\mathrm{y}}_{\mathrm{t_0}} = \mathrm{C}_{\hat{\mathrm{y}}} \mathrm{P} \qquad \mathrm{C}_{\hat{\mathrm{y}}} = \mathrm{N}^{-1} \tag{2.76}$$

Residuals to a free-network estimated using (Eqn. 2.70) - (Eqn. 2.76) cannot be directly computed since each of the epoch free-networks is in a slightly different frame. The frame difference at each epoch is removed by mapping the kinematic solution $\hat{y}_{t_0}$ and covariance matrix $C_{\hat{y}}$ to an epoch estimate at each weekly epoch using:

$$y_{i(mapped)} = A_i \hat{y}_{t_0} \qquad C_{i(mapped)} = A_i C_{\hat{y}} A_i^T \tag{2.77}$$

Where A_i is the same design matrix used at each epoch in the estimation (Eqn. 2.74). The frame difference between the mapped epoch solution and the epoch solution can then be removed by estimating a 6 parameter (no scale) Helmert transformation. Solving for a weekly translation of the network as well as rotation about the axes is necessary to avoid absorbing any weekly translation into the orientation parameters giving an erroneous transformation (Blewitt, 1993). The residuals to the Helmert transformation are the kinematic residuals at each epoch and are free from any reference frame definition.

Residuals computed above are a means by which the quality of a least squares adjustment (i.e. in GPS processing) is assessed where large residuals imply a good least squares adjustment and the reverse is true. This is done using an overall model test where the Root Mean Square (RMS) of the stations and their residual plots are examined directly. The problems in the estimation process can only be identified in detail through direct examination and use of alternative models. Sufficient time is needed to iron out systematic errors from the position time series. The importance of this is very paramount in GPS positioning.

RMS-The most commonly used measures of observation scatter for individual site velocity estimates are the repeatability or Root Mean Square (RMS) of residuals and the weighted repeatability (WRMS) (Dixon, 1991). The RMS statistic is defined by:

$$RMS = \sqrt{\sum_{i=1}^{m} \frac{v_i^2}{m}} \tag{2.78}$$

for m residuals v to the station velocity component in question. An alternative is the WRMS; this takes into account individual variances σ_i^2, the diagonal elements of the estimated residuals covariance matrix (Dixon, 1991). The WRMS is given by:

$$\mathrm{WRMS} = \sqrt{\frac{\left(\frac{m}{m-1}\right)\sum_{i=1}^{m}\frac{v_i^2}{\sigma_i^2}}{\sum_{i=1}^{m}\frac{1}{\sigma_i^2}}} \tag{2.79}$$

CHAPTER 3

3.1 Methodology

This research is based on GPS data collection over continuous points and non continuous points. The continuous points included two sets; the one in North America, near Nevada and Europe. The non continuous GPS points were located in Uganda and data was collected over these points for three consecutive days. The continuous GPS points of Europe and North America had GPS data of four years starting from 2008 to 2011 downloaded from the IGS station website. However due to the data combinations that I did, only the year of 2011 data was used because the amount of data would be very large for processing using only a personal laptop if all four year data was used.

The GAMIT/GLOBK software was used in the processing of the collected GPS data. This software is Linux based and free. The only challenge is to learn how to use it and the Linux command language. GAMIT was used to process the GPS day data while GLOBK was used to process the repeatability of the fixed points. During the modelling of the Tropospheric Delay, Saastamoinen was the Tropospheric Delay Model used together with the VMF1 (Vienna Mapping Function), NMF (Niell Mapping Function) and GMF (Global Mapping Function). These mapping functions were used with the UFL (U-file) and GPT 50 (Global Pressure Temperature Humidity (50)) a priori constraints to investigate the variance of the Tropospheric Delay modelling.

As it can be seen in the flow chart below, the above combinations were done with two gradients estimated per day to determine the optimum combination while using the Saastamoinen, VMF1 and UFL, gradients 0, 1, 2 and 3 were estimated. During the modelling, Ocean Loading, Atmospheric Loading and 2^{nd} and 3^{rd} Ionospheric effects on GPS positioning were included.

This research models the dependence of the Tropospheric delay on azimuth using GAMIT/GLOBK and the Vienna Mapping Function and the different a priori constraints. Three case studies were investigated; Uganda, Europe and North America. The modelled Tropospheric Delay in Europe and North America is regional while for Uganda, it is local. This determined the

variance of the Tropospheric effect on GPS measurements over different points on the earth's surface.

The IGS stations monitored in Europe were BRUS, PTBB, VILL, ONSA, MATE, FFMJ and ZIMM whose location relative to each other is shown in chapter one in the case study description. The IGS stations monitored in North America were BLYT, BRAN, CIT1, WSLN and JPLM. These were particularly used because they are located in a dry part of North America (Nevada). This would determine the effect of the Tropospheric Delay on the GPS points in dry conditions. This would thus show results of how the Tropospheric Delay changes with the change in humidity of an area.

GAMIT (GPS Analysis at Massachusetts Institute of Technology) and GLOBK are GPS analysis software packages that have been developed at MIT (Massachusetts Institute of Technology) in the Department of Earth Atmospheric and Planetary Sciences.

GAMIT, GLOBK, and TRACK form a comprehensive suite of programs for analyzing GPS measurements primarily to study crustal deformation. The software has been developed by MIT, Scripps Institution of Oceanography, and Harvard University with support from the National Science Foundation.

GAMIT is collection of programs to process phase data to estimate three-dimensional relative positions of ground stations and satellite orbits, atmospheric zenith delays, and earth orientation parameters. The software is designed to run under any UNIX operating system.

GLOBK is a Kalman filter whose primary purpose is to combine various geodetic solutions such as GPS, VLBI (Very Long Baseline Interferometry), and SLR (Satellite Laser Ranging) experiments. It accepts as data, or "quasi-observations" the estimates and covariance matricies for station coordinates, earth-orientation parameters, orbital parameters, and source positions generated from the analysis of the primary observations. The input solutions are generally performed with loose a priori uncertainties assigned to all global parameters, so that constraints can be uniformly applied in the combined solution. The current release is 10.40 (November 2010).

3.1.1 Ionospheric Delay Models

The first-order effect of the ionosphere on microwave observations can be written

$$l1 = -\frac{40.3 \int N_e dL}{f_1^2} \tag{3.1}$$

Where N_e is electron density, f is the signal frequency, and L is the path length. This effect can introduce tens of metres to the signal path but cancels in the linear combination (LC) of L1 and L2 used in GAMIT for baselines greater than a few km. Hence, we do not attempt to model the first-order effect except in applying an ionospheric constraint to resolve wide- lane phase ambiguities when precise pseudorange is not available (LC_HELP option, used for data prior to ~1995). However, second and third order terms do not cancel in the LC observable and can add up 15 mm of path delay under high ionospheric conditions. Models for these terms have been added to GAMIT by Elizabeth Petrie of Newcastle University with Release 10.4 (Petrie et al., 2010).

The second order term is affected by both ionospheric electron content and the geomagnetic field, while the third order term is not affected by the geomagnetic field and is much smaller in magnitude. The terms can be written as follows:

$$l2 = -\frac{1.1284x10^{12} \int N_e B cos\theta dL}{f_1^3} \; and \; l3 = \frac{812.47 \int N_e^2 dL}{f_1^4} \tag{3.2}$$

Where B is magnetic field strength and θ is the angle between the magnetic field and the GPS signal. The terms are applied in GAMIT using the approximations for the integrals method described in Fritsche et al. (2005). For the I_2 term, the magnetic field is taken outside the integral and evaluated at a fixed height of 450km. For the I_3 term, the integral of N_e^2 is approximated using a shape factor, and becomes:

$$\eta N_m \int_0^{h_s} N_e dh \, , where \; \eta = \frac{\int_0^{h_s} N_e^2 dh}{N_m \int_0^{h_s} N_e dh} \tag{3.3}$$

And is generally taken as 0.66. N_e is the peak electron density along the profile, and is estimated using the interpolation suggested by Fritsche et al. (2005).

$$N_m = \frac{(20-6)x10^{12}}{(4.55-1.38)x10^{18}} x(TEC - 4.55x10^{18}) + 20x10^{12} \quad (3.4)$$

Though this version is corrected from that printed in the paper (pers. comm. Fritsche 2007), TEC is Total Electron Content in electrons/m^2 and in this approximation assumed to be vertical (VTEC) rather than path-dependent.

The recommended magnetic field option is IGRF11, which is the latest release of the International Geomagnetic Reference Field. The IGRF consists of spherical harmonic coefficients, representing the Earth's main field and its secular variation. Each release incorporates predicted coefficients for five years of secular variation which are then revised to definitive coefficients as measurements are incorporated.

It should be noted that the IGRF models only the part of the magnetic field that originates from the Earth's core. This is often known as the 'main field' and represents the vast majority of the magnetic field intensity. The IGRF estimates were added using code from the Geomag software, courtesy of the International Association of Geomagnetism and Aeronomy (IAGA).

The software provides a vector magnetic field (in nano Tesla) when supplied with date, geocentric latitude, geocentric longitude and height. The other models coded are the previous IGRF release, IGRF10, and a simple dipole model, (co-centric with the centre of the Earth, and tilted to best align the dipole with the observed field) called using Mag field = DIPOLE.

The ionospheric electron content along the signal path (STEC) is obtained using vertical total electron content and a mapping function. The current GAMIT implementation is coded to obtain vertical total electron content (VTEC) to be obtained from daily IONEX files from the Centre for Orbit Determination in Europe (CODE).

IONEX files are global ionospheric maps of VTEC in the IONEX format (Schaer et al., 1998). The files are created using a single layer assumption and a mapping function to map STEC to

VTEC. Different IGS analysis centres create their own IONEX files which are combined to form an IGS product (Feltens, 2003; Hernandez-Pajares et al., 2008). However, the code in GAMIT is currently set up for the mapping functions used by the CODE IONEX files, so the IGS files should not be used.

Currently both the IGS IONEX files and those created by the individual IGS analysis centres are daily files with 13 maps spaced two hours apart. The files have a resolution of five degrees longitude and two and a half degrees latitude between -87.5 and 87.5 degrees latitude. The combined IGS IONEX files are only available for day of year 152, 1998 onwards. IONEX files for the period back to 1995 are available from the Centre for Orbit Determination in Europe (CODE), though there is only one map per day before DOY 087 1998. For some years, there were 12 maps per day, the first at 0100 hrs and the last at 2300 hrs, with a 2 hr spacing.

The values of VTEC in the file are interpolated for latitude, longitude and time to obtain a value at the 'pierce point' where the GPS signal crosses the single layer. Suggested interpolation strategies are provided by Schaer et al (1998). Essentially, the interpolation used interpolates linearly between maps, but also rotates the maps with time to follow the Sun. Where only one map per day is available, or for the first and last hours of the day when there are 12 maps, rotation is used. For the very few points outside the latitude range of the IONEX file (-87.5 and 87.5 degrees) the values at the maximum extent are used. To convert the ionospheric information from VTEC to STEC a mapping function must be used, preferably the mapping function used to convert the original data to VTEC during the file production. Typically the mapping function used is the single layer or thin shell mapping function:

$$F(z) = \frac{1}{cosz'} \; with \; sinz' = \frac{R_E}{R_E + h_i} sin(z) \tag{3.5}$$

Where z is the zenith angle of the signal at the receiver, R_E is the mean Earth radius (~6371 km), h_i is the height of the thin shell above the Earth's surface and z' is then the zenith angle at h_i. For the IGS IONEX files, h_i is set as 450 km. However, for the CODE IONEX files, h_i is 450 km after DOY 087 1998, but 400 km on and before DOY 086 (Schaer, 1997) so these values are

used to calculate the pierce point coordinates. However, the magnetic field evaluation height was kept at 450km for consistency, as magnetic field strength changes with height.
After DOY 251 in 2001, the CODE IONEX files change from the single layer mapping function to use the Modified Single-Layer Model Mapping Function:

$$F(z) = \frac{1}{cosz'} \; with \; sinz' = \frac{R_E}{R_E+H} sin(\alpha z) \tag{3.6}$$

with values of RE = 6371 km, H = 580.1 km and α = 0.9782 which best approximate the JPL extended slab model mapping function, assuming a maximum zenith distance of 80 degrees (CODE, 2007). In order to reverse the original mapping to VTEC as closely as possible, the mapping function and shell height used to create the original IONEX files should be used to convert back from VTEC to STEC.

Further details of modelling higher order ionospheric terms and their effects have been discussed elsewhere (see e.g. (Hernandez-Pajares et al., 2007; Bassiri and Hajj, 1993; Hoque and Jakowski, 2008), with an excellent summary of derivations in Datta-Barua et al. (2006). Finally, a review paper on higher order ionospheric effects is now available (Petrie et al., in press) which includes an assessment of methods of modelling the terms and discussion of potential errors.

Using the second and third order terms thus requires downloading daily IONEX files containing total electron content (TEC) at 2-hr intervals from CODE into the (expt)/ionex directory and linking these into the day directory using '-ion' in the sh_gamit command file (i.e. add –ion to the list of calling options when running sh_gamit). To apply the effects in processing, set 'Ion model = GMAP' and 'Mag field = ITRF11' in the sestbl. Due to the limited resolution of the IONEX files pre 1998, caution is suggested when interpreting the effects of the applied terms in this period.

3.1.2 Atmospheric Loading

Positions fixed using GPS are affected by atmospheric loading. Atmospheric loading is the pressure that the atmosphere exerts on the earth due to its constituents. The atmosphere contains gases, water vapour, smoke, dust, just to mention a few. These are in different proportions over the earth's surface, this is the reason that atmospheric loading is spatially correlated. The Atmospheric loading effect is also a function of the thickness of the atmosphere above the ground. The points that are at low elevation will greatly be affected. This effect is also dependant on the humidity of an area. Areas with high humid levels have high loading effect compared to the dry areas for example the deserts. Though it affects GPS observations as a whole, it has a great effect on the height of a point. This implies greater emphasis has to given to atmospheric loading in Deformation monitoring. This effect has to therefore be modelled in GPS data analysis. In GAMIT processing, the models used are atmdisp_ce.yyr, atmdisp_cf.yyr and atmdisp_cm.yyr where these are calculated towards the earth centre, earth fixed and centre of mass of the earth respectively. The models are computed for each year and hence the one that correspond to the time of GPS data collection should be used. In this research atmdisp_cm.yyr was used. This model was copied to the gg/tables directory and linked so that it is used.

3.1.3 Ocean Loading

Oceans are large connecting bodies of salt water that take up three-fourth of the earth's surface. The Arctic, Atlantic, Indian, and Pacific Oceans are the largest oceans, but one smaller ocean, the Southern, has just been named. The weight of the water held by the ocean exerts force beneath points close to the oceans. This force varies with time as the force varies with the weight of water held by the oceans. The change in water held by the oceans is due to the change in weather which is closely linked to the melting of ice or evaporation of water from the oceans. In this research, the ocean loading model used was otl_FES2004.grid. This model was formed in 2004 but is still useable as these models are not released annually as the atmospheric loading models.

3.1.4 A priori Zenith Delay Constraints

GAMIT uses initial Temperature, Pressure and Humidity values to approximate the A priori Zenith delay. This is the value used to model the final Tropospheric Delay of the GPS signal. The accuracy of this modelling is based on the file that is used. The files used in this research included, U-Files (UFL) and GPT50 (Global Pressure Temperature). The meteorological files (RNX or Met File) can also be used, however they were not used in this research because not all the IGS stations have the capability to collect their own Met Files. If used then, it would limit the number of IGS stations to use in the GPS data analysis which would reduce the overall accuracy of fixing the points.

Global Pressure Temperature 50 (GPT50) is the file that contains Pressure, Temperature of points globally and allocates the points humidity of 50. The empirical model GPT is based on spherical harmonics up to degree and order nine. It provides pressure and temperature at any site in the vicinity of the Earth's surface. It can be used for geodetic applications such as the determination of a priori Hydrostatic Zenith Delays (ZHD) and reference pressure values for atmospheric loading. The input parameters of GPT are the station coordinates and the day of the year, thus allowing one to model the annual variations of the parameters. As an improvement compared to previous models, it reproduces the large pressure anomaly over Antarctica, which can cause station height errors in the analysis of space geodetic data of up to one centimetre if not considered properly in troposphere modelling. First tests at selected geodetic observing stations show that the pressure biases considerably decrease when using GPT instead of very simple approaches applied in various Global Navigation Satellite Systems (GNSS) software packages so far. GPT also provides an appropriate model of annual variability of global temperature.

It frequently happens in space-geodetic techniques data analyses that neither observed (recorded) pressure values nor values from a NWM are available to determine the Hydrostatic Zenith Delays. In those cases GPT can be used for Tropospheric modelling in GNSS or VLBI analyses. This model however has the following limitations. GPT derived a priori constant Z_h perform well for only low and mid latitude stations. Due to the actual variations not being accounted for by the

seasonal GPT Model, GPS height solutions errors can sometimes exceed 10mm particularly in polar regions or where elevation cut off angles are less than 10 degrees.

The collection of the data from the field was as follows: The local data collected in Uganda was done for four local stations over three days. The points were located at Mbarara (MBRA) in western Uganda, Jinja (JINJ) in eastern Uganda, Kiboga (KIBO) in central Uganda and Rhino camp (RHIN) in Northern Uganda. During the processing of the local data, other IGS stations located closest to these sites were used. The IGS stations are ADIS in Addis Ababa (Ethiopia) HARB in Central Africa, NKLG also in Central Africa and ZAMB in Zambia.

The GPS data analysis for all the case studies was by double differencing technique. The points were chosen to have baseline lengths not very long to necessitate rotation for baseline adjustment. Since this research modelled the Tropospheric Delay and it is known that the Tropospheric delay depends on the heights of the GPS points, the points in the network were chosen to have considerable height differences at least above 900metres. This would make the findings from the research sufficiently significant.

FLOW CHART

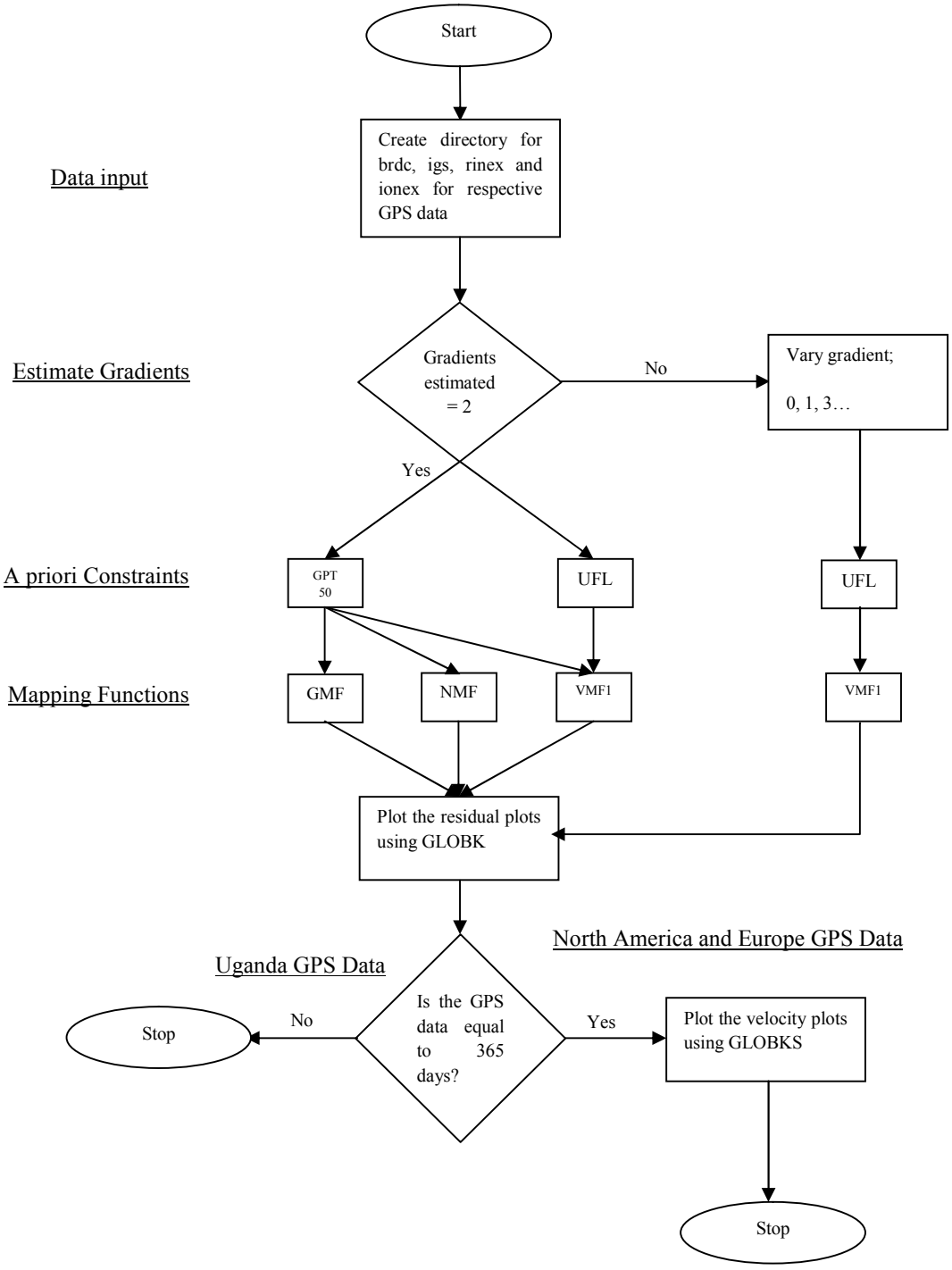

Figure3.1 Flow Chart showing the research methodology

The GPS data collected from the field and that downloaded from the different IGS ftp sites was arranged in different directories; brdc, igs, rinex and ionex. These contained the navigations files, satellite coordinates, site observation data and the ionex files respectively. These files were copied to a newly created directory in the linux (Ubuntu) environment on which the GAMIT/GLOBK GPS software was installed.

Using the default number of estimated gradients (2) with different mapping function a priori constraint combination; GMF, NMF, VMF1 and each with UFL and GPT 50 the Tropospheric delay was modelled. The accuracy or how well the Tropospheric delay was modelled was investigated by plotting residual plots using GLOBK. This was to determine the application of the Vienna Mapping Function in GAMIT/GLOBK GPS data processing.

Velocity plots were also prepared but these were prepared for GPS data for Europe and North America stations only which had data for a year collected. This was not done for Uganda data because of the limited data collected which was only for three days.

The Tropospheric delay was also modelled with the combination of VMF1 mapping function and UFL (U-FILE) a priori zenith delay constraint for different gradients estimated per day and when no gradient is estimated at all. This was to determine the dependence of the Tropospheric delay on the azimuth of the GPS satellites.

a b

Figure3.2 Trimble R7 GNSS Receiver and Accessories

The GPS Receiver used to collect GPS data for the local case in Uganda was; Trimble R7 GNSS 5033147569 version 4.2 and the antenna is TRM41249.00 as shown in figure 3.2a and b. This version was preferred because it is stable in harsh conditions and can be fixed on Tripod stands high enough to minimize the effect of multipath. The data collected using this equipment was analyzed together with the GPS data collected by the other IGS stations shown in the Figures3.3a, b, c and d below.

JPL Mesa

Hartebeesthock

Frankfurt

Onsla

Figure3.3 The Different IGS Stations used in this Research

These are some of the continuous monitoring stations that were used in this research. The stations JPLM, HARB, FFMJ, and ONSA respectively are found in North America (JPL Mesa), Africa (Hartebeesthock), Europe (Frankfurt) and Onsla respectively.

CHAPTER 4

4.1 Results and Discussions

4.1.1 Introduction

In this chapter we discussed the main research contributions of this thesis. The results are discussed in three parts, the results from the local data collected from Uganda, IGS stations in Europe and IGS station from North America around the dry areas of Nevada. The results are displayed in graphs drawn using Gnuplot and tables using values (Weighted Root Mean Squares) from the repeatability graphs obtained from GLOBK as shown in the Appendix at the end of the Report. This analysis is done noting that for the North offset and East offset the Weighted Root Mean Square should not exceed 2mm (millimetres). The allowable Weighted Root Mean Square for the Up offset is 10mm.Using the Tables (4.1 to 4.6), the deviation of the Weighted Root Mean Square (WRM) of the other gradients is computed with reference to the gradient 2. This is because GAMIT uses gradient 2 as the default when processing GPS data. The different mapping function and a priori constraint combinations are also compared with the VMF1-U-FILE combination because this is one of the new Mapping Functions which are presumed to model the Tropospheric delay more effectively, thus the truth of this is also investigated in this research.

4.1.2 Uganda's GPS data

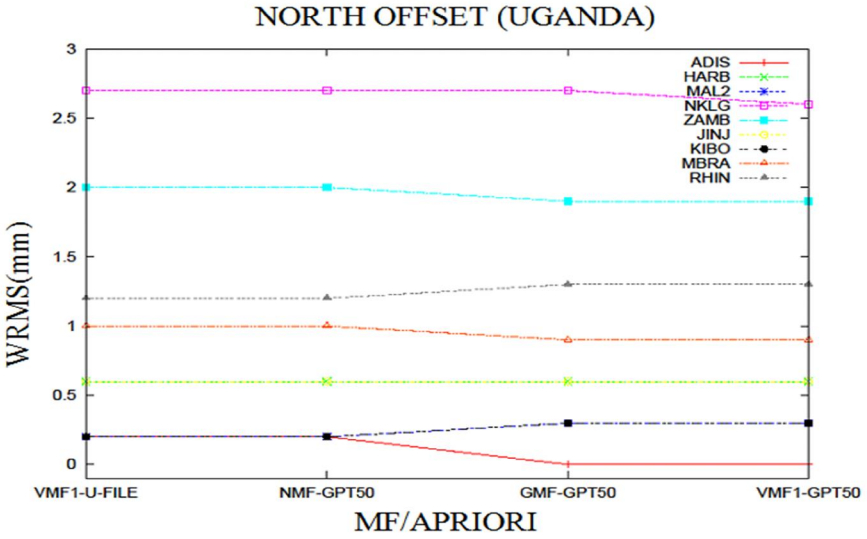

a)

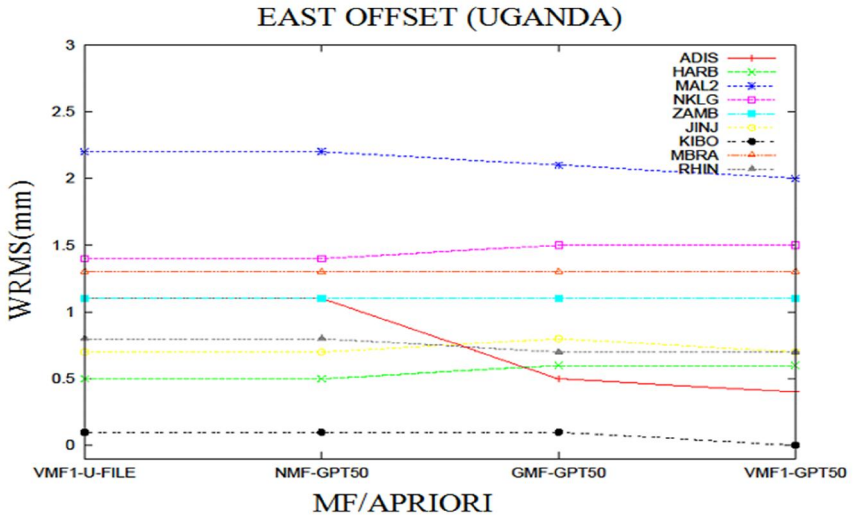

b)

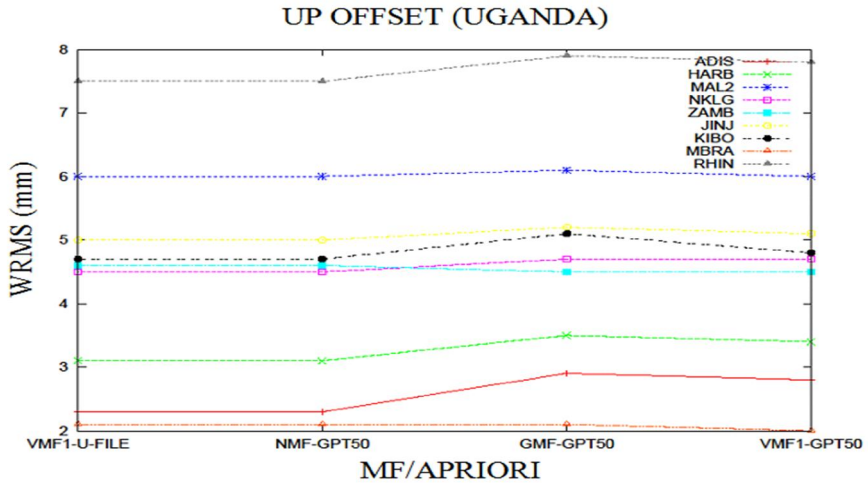

c)

Figure4.1 Different mapping function and a priori constraint combination (Uganda)

Table 4.1 Different mapping function and A priori constraints combinations compared to Vmf1-U-File (Uganda)

GPS STATIONS	VMF1-U-FILE	NMF-GPT50	Vmf1-U-File - Nmf-Gpt50	GMF-GPT50	Vmf1-U-File - Gmf-Gpt50	VMF1-GPT50	Vmf1-U-File - Vmf1-Gpt50
ADIS	0.2	0.2	0	0	0.2	0	0.2
HARB	0.6	0.6	0	0.6	0	0.6	0
MAL2	0.2	0.2	0	0.3	-0.1	0.3	-0.1
NKLG	2.7	2.7	0	2.7	0	2.6	0.1
ZAMB	2	2	0	1.9	0.1	1.9	0.1
JINJ	0.6	0.6	0	0.6	0	0.6	0
KIBO	0.2	0.2	0	0.3	-0.1	0.3	-0.1
MBRA	1	1	0	0.9	0.1	0.9	0.1
RHIN	1.2	1.2	0	1.3	-0.1	1.3	-0.1

a) North Offset

GPS STATIONS	VMF1-U-FILE	NMF-GPT50	Vmf1-U-File - Nmf-Gpt50	GMF-GPT50	Vmf1-U-File - Gmf-Gpt50	VMF1-GPT50	Vmf1-U-File - Vmf1-Gpt50
ADIS	1.1	1.1	0	0.5	0.6	0.4	0.7
HARB	0.5	0.5	0	0.6	-0.1	0.6	-0.1
MAL2	2.2	2.2	0	2.1	0.1	2	0.2
NKLG	1.4	1.4	0	1.5	-0.1	1.5	-0.1
ZAMB	1.1	1.1	0	1.1	0	1.1	0
JINJ	0.7	0.7	0	0.8	-0.1	0.7	0
KIBO	0.1	0.1	0	0.1	0	0	0.1
MBRA	1.3	1.3	0	1.3	0	1.3	0
RHIN	0.8	0.8	0	0.7	0.1	0.7	0.1

b) East Offset

GPS STATIONS	Vmf1-U-File	Nmf-Gpt50	Vmf1-U-File - Nmf-Gpt50	Gmf-Gpt50	Vmf1-U-File - Gmf-Gpt50	Vmf1-Gpt50	Vmf1-U-File-Vmf1-Gpt50
ADIS	2.3	2.3	0	2.9	-0.6	2.8	-0.5
HARB	3.1	3.1	0	3.5	-0.4	3.4	-0.3
MAL2	6	6	0	6.1	-0.1	6	0
NKLG	4.5	4.5	0	4.7	-0.2	4.7	-0.2
ZAMB	4.6	4.6	0	4.5	0.1	4.5	0.1
JINJ	5	5	0	5.2	-0.2	5.1	-0.1
KIBO	4.7	4.7	0	5.1	-0.4	4.8	-0.1
MBRA	2.1	2.1	0	2.1	0	2	0.1
RHIN	7.5	7.5	0	7.9	-0.4	7.8	-0.3

c) Up Offset

The graphs above show the plots of the Weighted Root Mean Square (WRMS) against different Mapping Functions (MF) and a priori zenith delay constraints (APRIORI) for the GPS data collected in Uganda. It can be observed that the accuracy with which the points were fixed is acceptable according to the standards that are specified in the GAMIT/GLOBK manual. This manual specifies that the WRMs of the North and East offset should at least be below 2mm and that of the Up offset below 10mm. However values of less than 5mm were also used in this research with caution after justification of the reason for the anomaly.

As shown in Figures 4.1a, b, c and Tables 4.1a, b and c, VMF1/UFL (U File) and NMF/GPT50 obtain the same WRMS generally just as GMF/GPT50 and VMF1/GPT50. This implies that these combinations can be used interchangeably for the local Troposphere. The WRMs obtained by VMF1/UFL and NMF/GPT50 is the same because NMF works well for the latitudes that Uganda is located and GPT50 provides good a priori information at these latitudes. The WRMS values of the North offset of HARB station is not sensitive to the property of different mapping functions used to correct for the Troposphere effect on the GPS signal propagation because possibly no great lateral variation of pressure, temperature and pressure is experienced at the station.

VMF1/GPT50 attains less WRMS compared to VMF1/UFL for the East and North offsets as shown in Table 4.1a, and b. This implies that the GPT 50 a priori zenith constraints when used the effect of the troposphere on the East and North offsets is modelled well compared to using VMF1/UFL. However VMF1/UFL attains the least WRMS compared to VMF1/GPT50 for the Up offset which implies UFL constraints model well the components of the Tropospheric delay that affect or contribute to the error in the height of the points.

GMF/GPT50 and VMF1/GPT50 attain the least WRMs for the North offset but high value for the WRMS for the East and Up offset. This implies these combinations model well the troposphere effects that propagate into the North offset compared to those that propagate to the East and up offset.

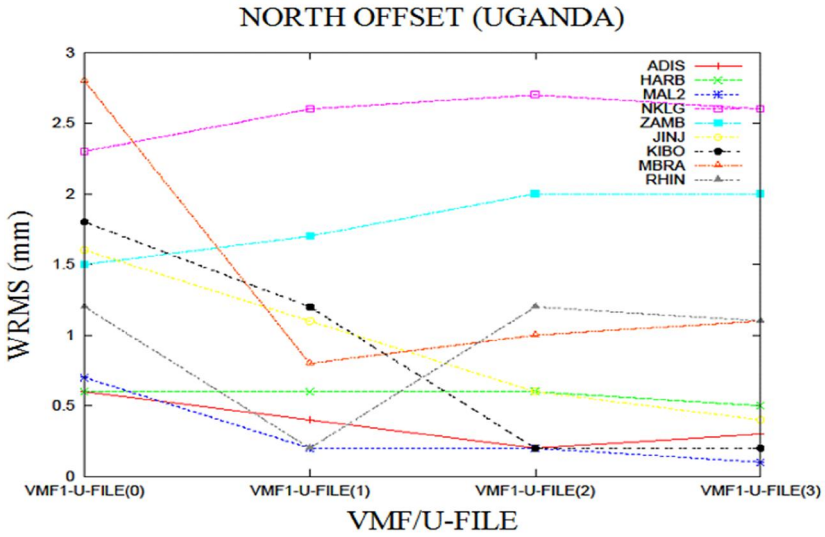

a)

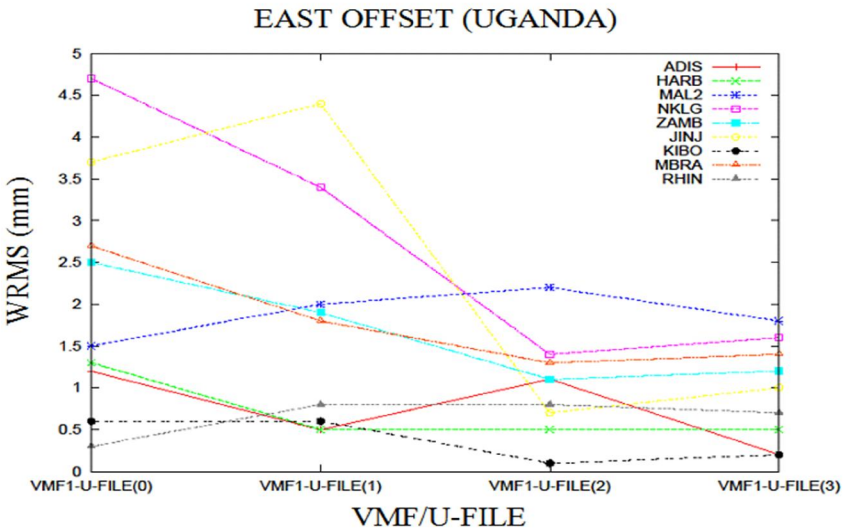

b)

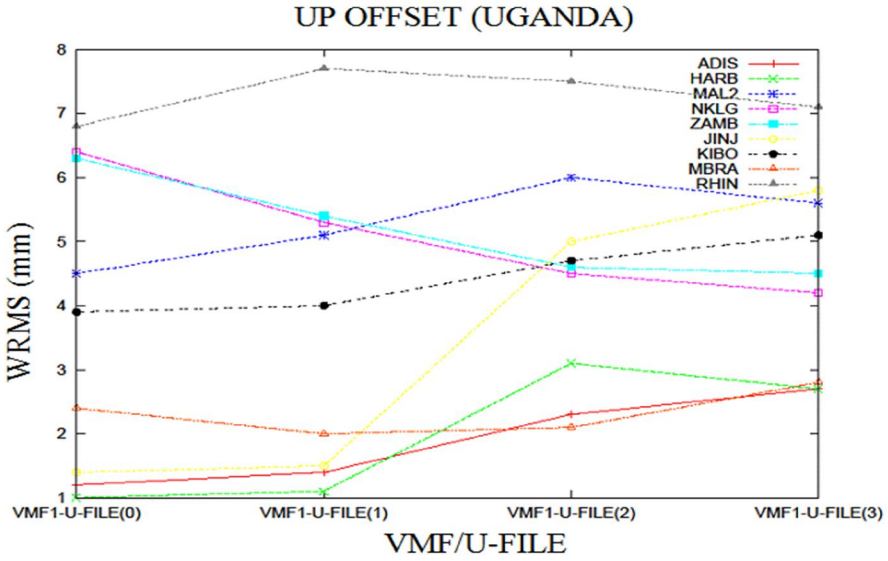

c)

Figure4.2 Different VMF1 and U-File combinations for different gradients (Uganda)

Table 4.2 Different VMF1 and U-File combinations for different gradients compared to Vmf1-U-File (2) (Uganda)

IGS STATIONS	VMF1-U-FILE (2)	VMF1-U-FILE (0)	VMF1-U-FILE (2) - VMF1-U-FILE (0)	VMF1-U-FILE (1)	VMF1-U-FILE (2) - VMF1-U-FILE (1)	VMF1-U-FILE (3)	VMF1-U-FILE (2) - VMF1-U-FILE (3)
ADIS	0.2	0.6	-0.4	0.4	-0.2	0.3	-0.1
HARB	0.6	0.6	0	0.6	0	0.5	0.1
MAL2	0.2	0.7	-0.5	0.2	0	0.1	0.1
NKLG	2.7	2.3	0.4	2.6	0.1	2.6	0.1
ZAMB	2	1.5	0.5	1.7	0.3	2	0
JINJ	0.6	1.6	-1	1.1	-0.5	0.4	0.2
KIBO	0.2	1.8	-1.6	1.2	-1	0.2	0
MBRA	1	2.8	-1.8	0.8	0.2	1.1	-0.1
RHIN	1.2	1.2	0	0.2	1	1.1	0.1

a) North Offset

IGS STATIONS	VMF1-U-FILE (2)	VMF1-U-FILE (0)	VMF1-U-FILE (2) - VMF1-U-FILE (0)	VMF1-U-FILE (1)	VMF1-U-FILE (2) - VMF1-U-FILE (1)	VMF1-U-FILE (3)	VMF1-U-FILE (2) - VMF1-U-FILE (3)
ADIS	1.1	1.2	-0.1	0.5	0.6	0.2	0.9
HARB	0.5	1.3	-0.8	0.5	0	0.5	0
MAL2	2.2	1.5	0.7	2	0.2	1.8	0.4
NKLG	1.4	4.7	-3.3	3.4	-2	1.6	-0.2
ZAMB	1.1	2.5	-1.4	1.9	-0.8	1.2	-0.1
JINJ	0.7	3.7	-3	4.4	-3.7	1	-0.3
KIBO	0.1	0.6	-0.5	0.6	-0.5	0.2	-0.1
MBRA	1.3	2.7	-1.4	1.8	-0.5	1.4	-0.1
RHIN	0.8	0.3	0.5	0.8	0	0.7	0.1

b) East Offset

IGS STATIONS	VMF1-U-FILE (2)	VMF1-U-FILE (0)	VMF1-U-FILE (2) - VMF1-U-FILE (0)	VMF1-U-FILE (1)	VMF1-U-FILE (2) - VMF1-U-FILE (1)	VMF1-U-FILE (3)	VMF1-U-FILE (2) - VMF1-U-FILE (3)
ADIS	2.3	1.2	1.1	1.4	0.9	2.7	-0.4
HARB	3.1	1	2.1	1.1	2	2.7	0.4
MAL2	6	4.5	1.5	5.1	0.9	5.6	0.4
NKLG	4.5	6.4	-1.9	5.3	-0.8	4.2	0.3
ZAMB	4.6	6.3	-1.7	5.4	-0.8	4.5	0.1
JINJ	5	1.4	3.6	1.5	3.5	5.8	-0.8
KIBO	4.7	3.9	0.8	4	0.7	5.1	-0.4
MBRA	2.1	2.4	-0.3	2	0.1	2.8	-0.7
RHIN	7.5	6.8	0.7	7.7	-0.2	7.1	0.4

c) Up Offset

VMF1/UFL was also varied with, first, not modelling the gradients at all and then modelling one, two and three gradients per day to study the effect of the gradients on the accuracy of fixing GPS points Figures 4.2a, b, and c. It is shown in Tables 4.2a, b and c that when the gradients are modelled, there is a reduction in the WRMs in the North and East offsets this implies there is an increase in the accuracy at which these components of the points are fixed. This means errors of considering the atmosphere to be horizontally layered and symmetric will propagate into the East and North offset as shown in Figures 4.2a, b and c. There is however an anomaly for stations NKLG, ZAMB, MAL2 and RHIN which may be explained by the poor data collected at these stations during the GPS data collection. The trend of the reduction of the WRMS with the increase in the gradients estimated per day for the East and North offsets can however be observed from the behaviour of the other stations.

However for the Up offset, the increase in the number of gradients estimated per day leads to the increase in the WRMS from the residual plots. This may possibly mean modelling of more gradients for little GPS data collected may bias the data as noise or using another MF/APRIORI should be conducted in the future to investigate this hypothesis.

4.1.3 Europe's GPS data

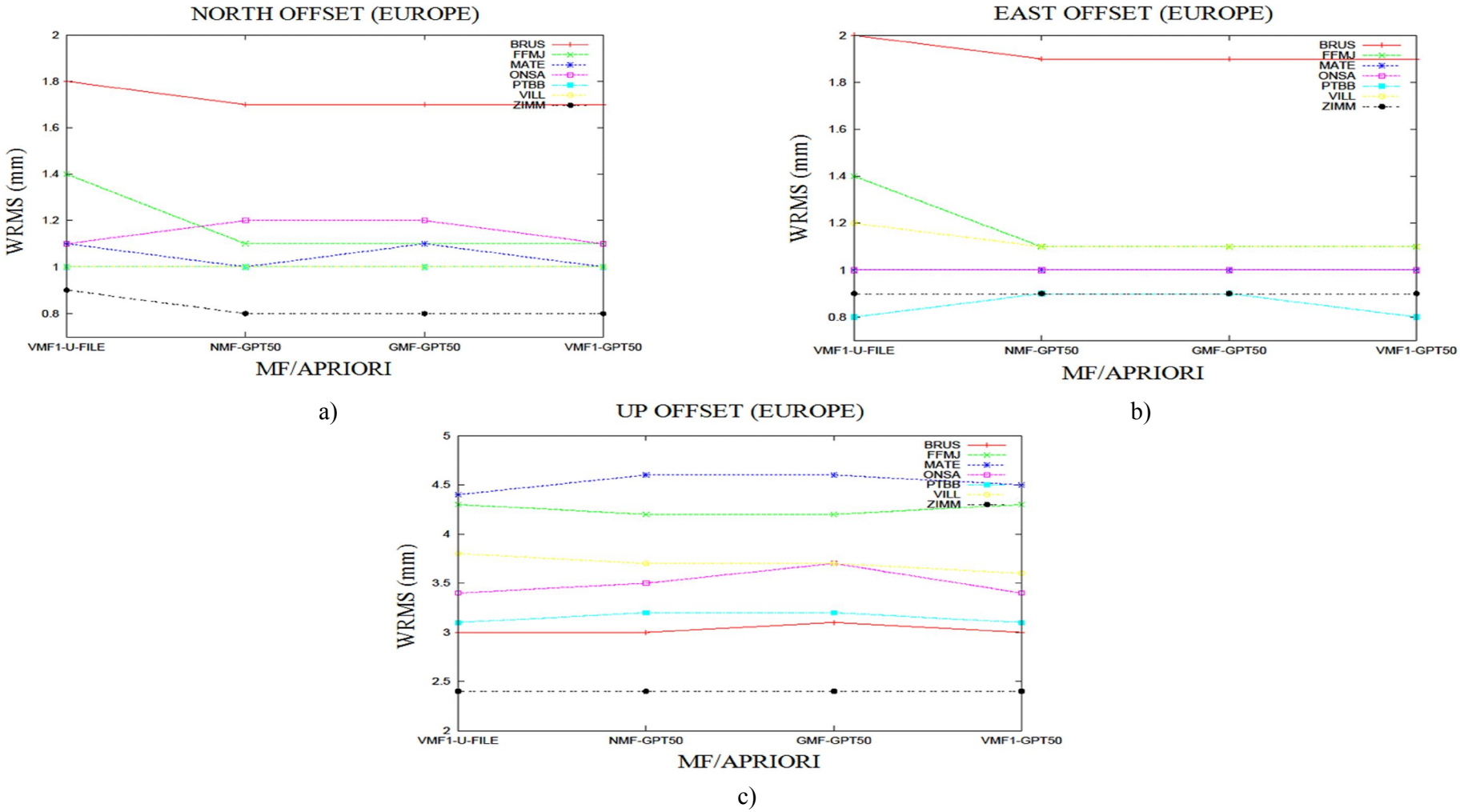

Figure4.3 Different mapping function and a priori constraint combination (Europe)

Table 4.3 Different mapping function and A priori constraints combinations compared to Vmf1-U-File (Europe)

IGS STATIONS	VMF1-U-FILE	NMF-GPT50	VMF1-U-FILE - NMF-GPT50	GMF-GPT50	VMF1-U-FILE - GMF-GPT50	VMF1-GPT50	VMF1-U-FILE - VMF1-GPT50
BRUS	1.8	1.7	0.1	1.7	0.1	1.7	0.1
FFMJ	1.4	1.1	0.3	1.1	0.3	1.1	0.3
MATE	1.1	1	0.1	1.1	0	1	0.1
ONSA	1.1	1.2	-0.1	1.2	-0.1	1.1	0
PTBB	1	1	0	1	0	1	0
VILL	1	1	0	1	0	1	0
ZIMM	0.9	0.8	0.1	0.8	0.1	0.8	0.1

a) North Offset

IGS STATIONS	VMF1-U-FILE	NMF-GPT50	VMF1-U-FILE - NMF-GPT50	GMF-GPT50	VMF1-U-FILE - GMF-GPT50	VMF1-GPT50	VMF1-U-FILE - VMF1-GPT50
BRUS	2	1.9	0.1	1.9	0.1	1.9	0.1
FFMJ	1.4	1.1	0.3	1.1	0.3	1.1	0.3
MATE	1	1	0	1	0	1	0
ONSA	1	1	0	1	0	1	0
PTBB	0.8	0.9	-0.1	0.9	-0.1	0.8	0
VILL	1.2	1.1	0.1	1.1	0.1	1.1	0.1
ZIMM	0.9	0.9	0	0.9	0	0.9	0

b) East Offset

IGS STATIONS	VMF1-U-FILE	NMF-GPT50	VMF1-U-FILE - NMF-GPT50	GMF-GPT50	VMF1-U-FILE - GMF-GPT50	VMF1-GPT50	VMF1-U-FILE - VMF1-GPT50
BRUS	3	3	0	3.1	-0.1	3	0
FFMJ	4.3	4.2	0.1	4.2	0.1	4.3	0
MATE	4.4	4.6	-0.2	4.6	-0.2	4.5	-0.1
ONSA	3.4	3.5	-0.1	3.7	-0.3	3.4	0
PTBB	3.1	3.2	-0.1	3.2	-0.1	3.1	0
VILL	3.8	3.7	0.1	3.7	0.1	3.6	0.2
ZIMM	2.4	2.4	0	2.4	0	2.4	0

c) Up Offset

VMF1/GPT 50 attains the least WRMS for the East and North Offsets for the GPS data collected from the IGS stations of Europe. Which implies that this MF/APRIORI combination models well the Troposphere effects that spill over to the East and North offsets Figure4.3a, b and c and Table4.3a, b and c. VMF1/UFL and VMF1/GPT50 obtain the least WRMS for the Up offset of the collected Europe data. It is clear that VMF1/UFL attains least WRMS for the Up offset again just as for the local Troposphere modelled in Uganda. This is because of the better approximation of the coefficients (*aw* and *ah*) in the UFL files, the four files of the a priori constraints available each day (good frequency to model the temporal variation of the humidity, temperature and pressure) and the 2.5 x 2.0 grid that can be used to accurately interpolate for the pressure at a point (modelling the lateral variation of the humidity, temperature and pressure well).

The accuracy obtained by VMF1/GPT50 for the Up offset improves in the case of the GPS data collected from Europe. This may pose the idea that the VMF1/GPT50 combination's accuracy improves with increase in the number of GPS data collected.

NMF/GPT50 and GMF/GPT50 give better accuracy compared to VMF1/UFL for the East and North offsets. This may be due the high accuracy of the NMF model at these latitudes (the coefficients used are provided only at four latitudes 15, 30, 45 and 60 in the northern hemisphere). The largest latitude dependent biases for the mapping function are largest in southern latitudes but very minimal in the northern hemisphere because the data that this model is based on is was collected from the northern latitudes. GMF is also has good data from this region as it is 15^0 x 15^0 global grid of monthly profiles for pressure, temperature and humidity from the European Centre for Medium-Range Weather Forecast (ECMWF). This is why these combinations model well the Tropospheric delay that propagates into the North and East offset.

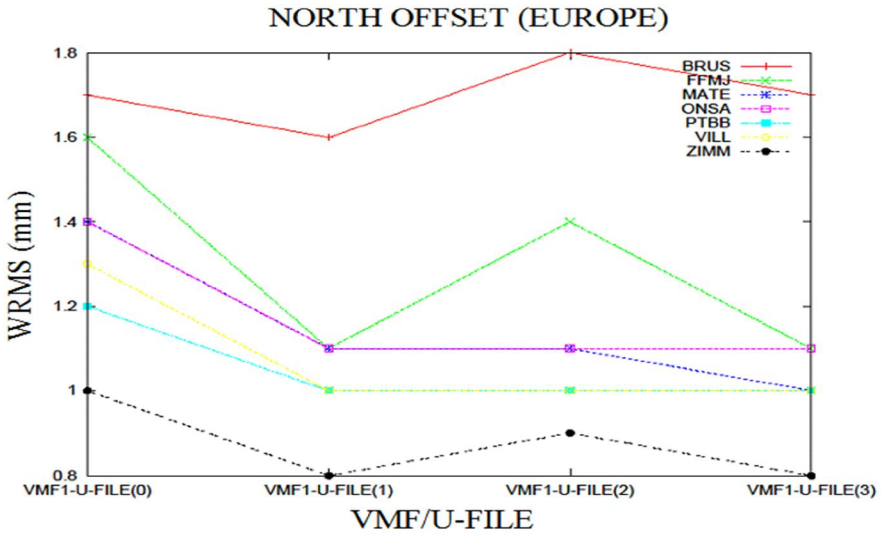

a)

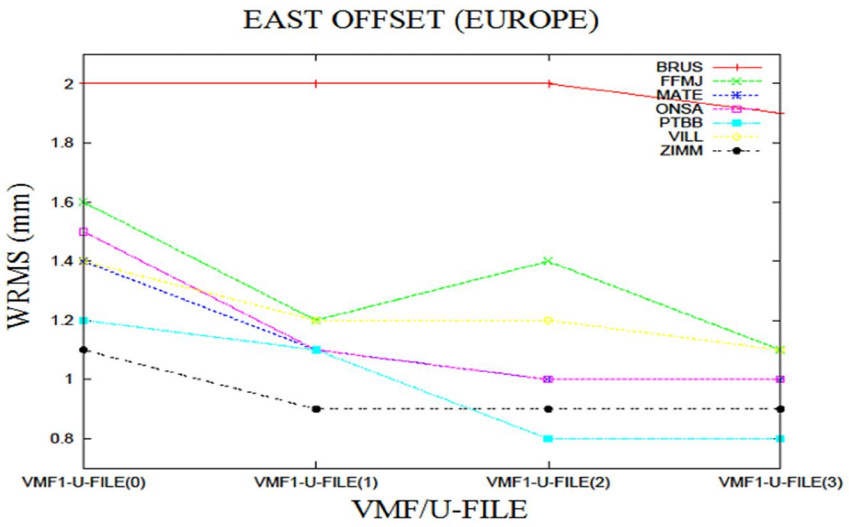

b)

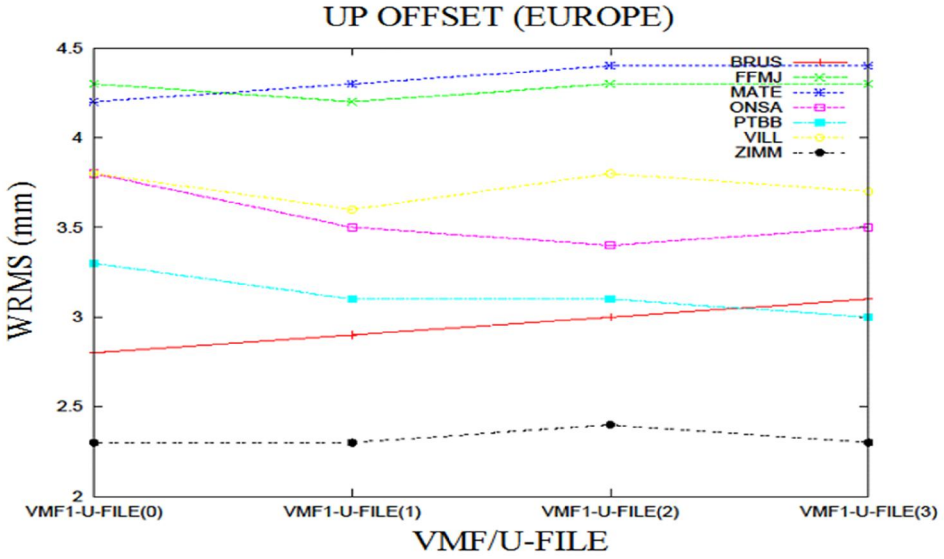

c)

Figure4.4 Different VMF1 and U-File combinations for different gradients (Europe)

Table 4.4 Different VMF1 and U-File combinations for different gradients compared to Vmf1-U-File (2) (Europe)

IGS STATIONS	VMF1-U-FILE (2)	VMF1-U-FILE (0)	VMF1-U-FILE (2) - VMF1-U-FILE (0)	VMF1-U-FILE (1)	VMF1-U-FILE (2) - VMF1-U-FILE (1)	VMF1-U-FILE (3)	VMF1-U-FILE (2) - VMF1-U-FILE (3)
BRUS	1.8	1.7	0.1	1.6	0.2	1.7	0.1
FFMJ	1.4	1.6	-0.2	1.1	0.3	1.1	0.3
MATE	1.1	1.4	-0.3	1.1	0	1	0.1
ONSA	1.1	1.4	-0.3	1.1	0	1.1	0
PTBB	1	1.2	-0.2	1	0	1	0
VILL	1	1.3	-0.3	1	0	1	0
ZIMM	0.9	1	-0.1	0.8	0.1	0.8	0.1

a) North Offset

IGS STATIONS	VMF1-U-FILE (2)	VMF1-U-FILE (0)	VMF1-U-FILE (2) - VMF1-U-FILE (0)	VMF1-U-FILE (1)	VMF1-U-FILE (2) - VMF1-U-FILE (1)	VMF1-U-FILE (3)	VMF1-U-FILE (2) - VMF1-U-FILE (3)
BRUS	2	2	0	2	0	1.9	0.1
FFMJ	1.4	1.6	-0.2	1.2	0.2	1.1	0.3
MATE	1	1.4	-0.4	1.1	-0.1	1	0
ONSA	1	1.5	-0.5	1.1	-0.1	1	0
PTBB	0.8	1.2	-0.4	1.1	-0.3	0.8	0
VILL	1.2	1.4	-0.2	1.2	0	1.1	0.1
ZIMM	0.9	1.1	-0.2	0.9	0	0.9	0

b) East Offset

IGS STATIONS	VMF1-U-FILE (2)	VMF1-U-FILE (0)	VMF1-U-FILE (2) - VMF1-U-FILE (0)	VMF1-U-FILE (1)	VMF1-U-FILE (2) - VMF1-U-FILE (1)	VMF1-U-FILE (3)	VMF1-U-FILE (2) - VMF1-U-FILE (3)
BRUS	3	2.8	0.2	2.9	0.1	3.1	-0.1
FFMJ	4.3	4.3	0	4.2	0.1	4.3	0
MATE	4.4	4.2	0.2	4.3	0.1	4.4	0
ONSA	3.4	3.8	-0.4	3.5	-0.1	3.5	-0.1
PTBB	3.1	3.3	-0.2	3.1	0	3	0.1
VILL	3.8	3.8	0	3.6	0.2	3.7	0.1
ZIMM	2.4	2.3	0.1	2.3	0.1	2.3	0.1

c) Up Offset

When the gradients are estimated as we model the Troposphere, the accuracy of fixing the East and North offset is improved with the Europe GPS data. However the improvement in the accuracy from estimating one gradient per day to three gradients per day is minimal apart from what is observed at stations BRUS and FFMJ these stations had some days of bad data. This was observed during GAMIT/GLOBK processing where these stations had more outliers compared to other stations and theses outliers were eliminated to improve the WRMS. But this reduced on the GPS points that contributed to the overall WRMS hence the stations have high WRMS compared to the other Europe IGS stations Figure 4.4a, b and c and Table 4.4a, b and c. In the East and North offset, it is also noticed that modelling only two gradients per day is sufficient in Tropospheric delay modelling provided that there is no storm surge at the GPS points Figures 4.4a, b and c and Tables 4.4a, b and c.

In the Up Offset, modelling the gradients improved the accuracy of all the stations except BRUS and MATE. Implying that stations BRUS and MATE could be unstable in the vertical compared to the other IGS stations of Europe. The effect of increasing the gradients estimated per day insignificantly increases for some stations while reduces for the others, this may be due to the difference in the accuracy of the data collected at the different IGS stations and absence of a storm surge hence the Tropospheric effect is minimal in this case. Modelling only two gradients is however not the optimal result for the Up offset where modelling three gradients per day improves on the accuracy slightly better than modelling only two gradients.

4.1.4 North America's GPS data

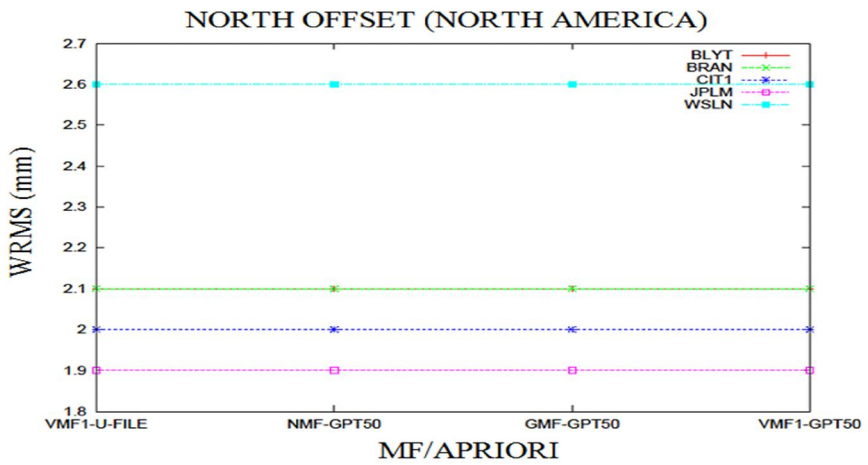

a)

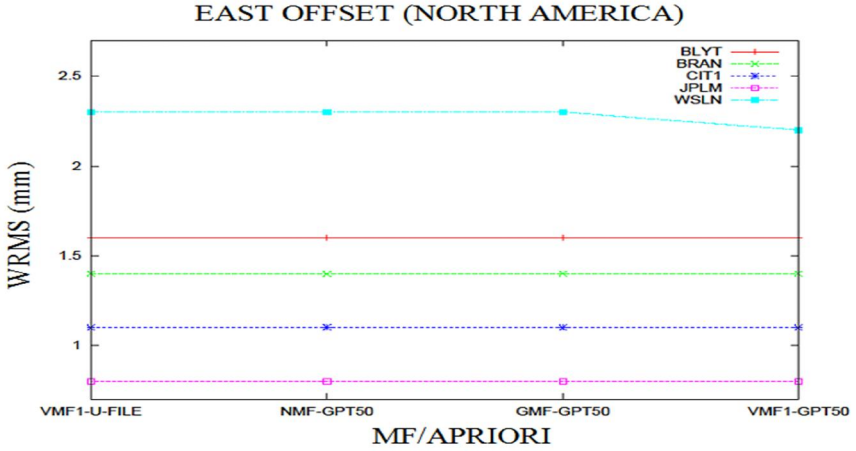

b)

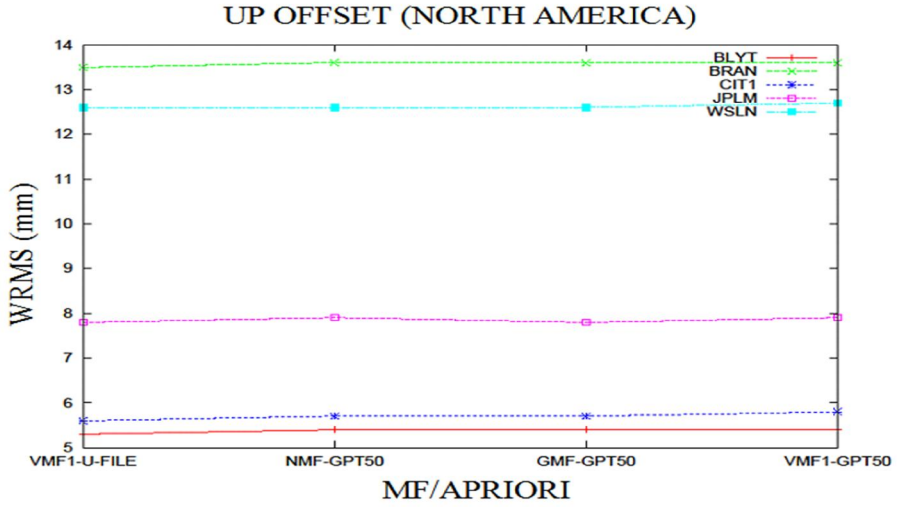

c)

Figure4.5 Different Mapping function and a priori constraint combinations (North America)

Table 4.5 Different Mapping function and a priori constraints combinations compared to Vmf1-U-File (North America)

IGS STATIONS	VMF1-U-FILE	NMF-GPT50	VMF1-U-FILE - NMF-GPT50	GMF-GPT50	VMF1-U-FILE - GMF-GPT50	VMF1-GPT50	VMF1-U-FILE - VMF1-GPT50
BLYT	2.1	2.1	0	2.1	0	2.1	0
BRAN	2.1	2.1	0	2.1	0	2.1	0
CIT1	2	2	0	2	0	2	0
JPLM	1.9	1.9	0	1.9	0	1.9	0
WSLN	2.6	2.6	0	2.6	0	2.6	0

a) North Offset

IGS STATIONS	VMF1-U-FILE	NMF-GPT50	VMF1-U-FILE - NMF-GPT50	GMF-GPT50	VMF1-U-FILE - GMF-GPT50	VMF1-GPT50	VMF1-U-FILE - VMF1-GPT50
BLYT	1.6	1.6	0	1.6	0	1.6	0
BRAN	1.4	1.4	0	1.4	0	1.4	0
CIT1	1.1	1.1	0	1.1	0	1.1	0
JPLM	0.8	0.8	0	0.8	0	0.8	0
WSLN	2.3	2.3	0	2.3	0	2.2	0.1

b) East Offset

IGS STATIONS	VMF1-U-FILE	NMF-GPT50	VMF1-U-FILE - NMF-GPT50	GMF-GPT50	VMF1-U-FILE - GMF-GPT50	VMF1-GPT50	VMF1-U-FILE - VMF1-GPT50
BLYT	5.3	5.4	-0.1	5.4	-0.1	5.4	-0.1
BRAN	13.5	13.6	-0.1	13.6	-0.1	13.6	-0.1
CIT1	5.6	5.7	-0.1	5.7	-0.1	5.8	-0.2
JPLM	7.8	7.9	-0.1	7.8	0	7.9	-0.1
WSLN	12.6	12.6	0	12.6	0	12.7	-0.1

c) Up Offset

From Figures 4.5a, b and c and Tables4.5a, b and c it is shown that WRMS of the stations most especially the Up offset for Stations in North America is high compared to those obtained in Uganda and Europe yet the IGS stations found in North America are in a dry environment and the modelling of the WZD should be easier than the other two places where the weather is very dynamic and variable in space and time. This would mean the WRMS for the stations in North America should be the least of all the case study areas used in this research work.

The justification for this is, of all the other case study areas, the Stations in North America are located on a seismically active region compared to the other places this means the stations are not as stable as the other IGS stations. In consequence to this, a local earth quake file has to be used in GAMIT/GLOBK when processing the GPS data collected over these points. This was done in this research but it seems it was not very effective as it should have been.

Stations WSLN and BRAN have very high WRMS especially for the Up offset this is due to the unstable nature of these IGS stations. Being the reason that they are even not included in ITRF2008 (International Terrestrial Reference Frame realised in 2008). Well as the station WSLN is unstable in the East, North and Up offset, BRAN is only unstable in the Up offset.

The different MF/APRIORI combinations for the case of North America IGS stations achieve similar WRMS for the East and North offsets except WSLN for the East offset. This may be due to the unstable nature of this station. This shows that when the atmosphere is dry (minimal temporal and lateral variation of the temperature, pressure and humidity), the different MF/APRIORI combinations attain the same WRMS. This is because the effect of the troposphere on the GPS measurements in this kind of region in minimal.

The above case is however not the same for the Up offsets. VMF1/UFL obtains the least WRMS for the Up offset. Meaning this combination models well the part of the Tropospheric delay that affects greatly the height of a point compared to VMF1/GPT 50. This also shows us that even if the change in the weather of an environment is minimal, the effect of the troposphere on the height is slightly still detectable (present) and is well modelled using VMF1/UFL.

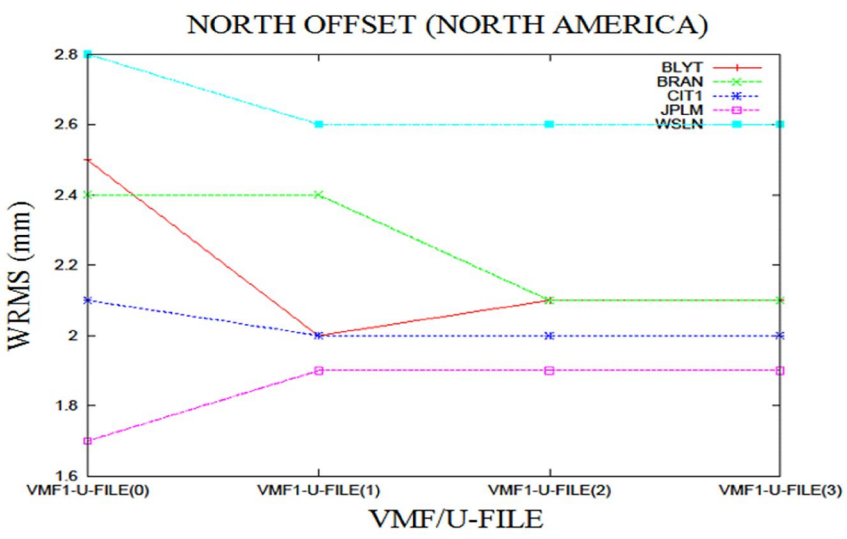

a)

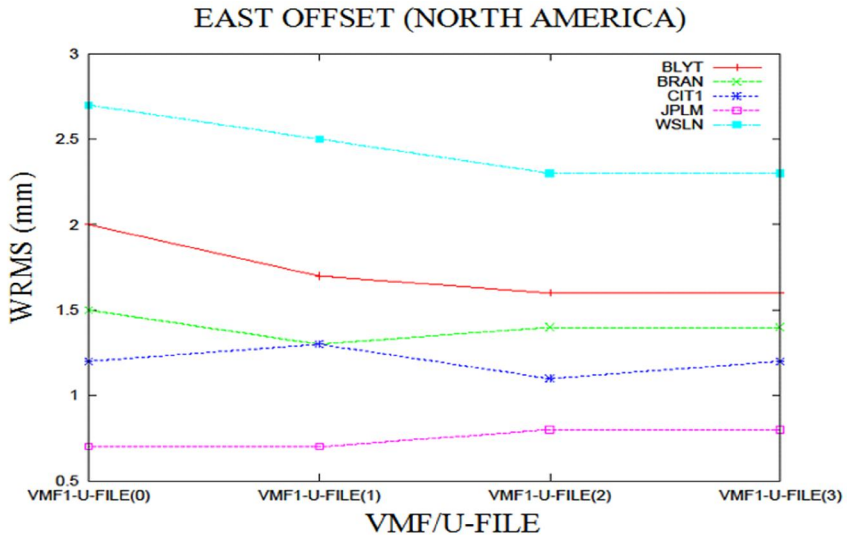

b)

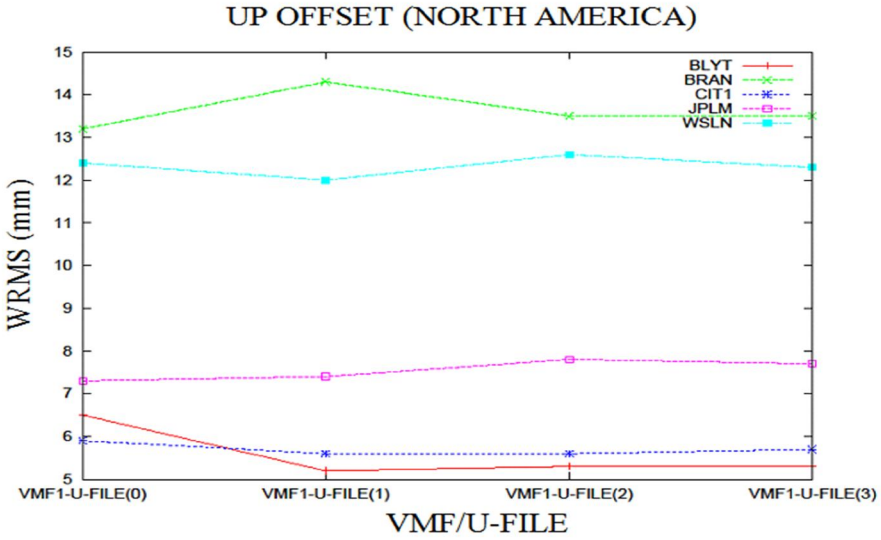

c)

Figure4.6 Different VMF1 and U-File combinations for different gradients (North America)

Table 4.6 Different VMF1 and U-File combinations for different gradients to Vmf1-U-File (2) (North America)

IGS STATIONS	VMF1-U-FILE (2)	VMF1-U-FILE (0)	VMF1-U-FILE (2) - VMF1-U-FILE (0)	VMF1-U-FILE (1)	VMF1-U-FILE (2) - VMF1-U-FILE (1)	VMF1-U-FILE (3)	VMF1-U-FILE (2) - VMF1-U-FILE (3)
BLYT	2.1	2.5	-0.4	2	0.1	2.1	0
BRAN	2.1	2.4	-0.3	2.4	-0.3	2.1	0
CIT1	2	2.1	-0.1	2	0	2	0
JPLM	1.9	1.7	0.2	1.9	0	1.9	0
WSLN	2.6	2.8	-0.2	2.6	0	2.6	0

a) North Offset

IGS STATIONS	VMF1-U-FILE (2)	VMF1-U-FILE (0)	VMF1-U-FILE (2) - VMF1-U-FILE (0)	VMF1-U-FILE (1)	VMF1-U-FILE (2) - VMF1-U-FILE (1)	VMF1-U-FILE (3)	VMF1-U-FILE (2) - VMF1-U-FILE (3)
BLYT	1.6	2	-0.4	1.7	-0.1	1.6	0
BRAN	1.4	1.5	-0.1	1.3	0.1	1.4	0
CIT1	1.1	1.2	-0.1	1.3	-0.2	1.2	-0.1
JPLM	0.8	0.7	0.1	0.7	0.1	0.8	0
WSLN	2.3	2.7	-0.4	2.5	-0.2	2.3	0

b) East Offset

IGS STATIONS	VMF1-U-FILE (2)	VMF1-U-FILE (0)	VMF1-U-FILE (2) - VMF1-U-FILE (0)	VMF1-U-FILE (1)	VMF1-U-FILE (2) - VMF1-U-FILE (1)	VMF1-U-FILE (3)	VMF1-U-FILE (2) - VMF1-U-FILE (3)
BLYT	5.3	6.5	-1.2	5.2	0.1	5.3	0
BRAN	13.5	13.2	0.3	14.3	-0.8	13.5	0
CIT1	5.6	5.9	-0.3	5.6	0	5.7	-0.1
JPLM	7.8	7.3	0.5	7.4	0.4	7.7	0.1
WSLN	12.6	12.4	0.2	12	0.6	12.3	0.3

c) Up Offset

When the gradients are estimated for the East and North offset, the accuracy of the fixed points increases. Apart from JPLM station for the North offset and East offset. The accuracy slightly increases when more gradients (1, 2 and 3) are estimated but more change is observed in the East offsets. This implies even when the change in the weather is minimal, modelling of gradients affects the accuracy of estimating the East and North offsets as shown in Figures4.6a, b and c and Tables4.6a, b and c.

It is observed again that in the Up offset, estimating more gradients per day increases accuracy of fixing some stations BLYT, CIT1, and WSLN but slight increment in the WRMS is seen for stations BRAN and JPLM. JPLM may pose data quality problems because of its very low antenna height which will make the data collected from it more susceptible to effects of multipath.

CHAPTER 5

5.1 Conclusions and Recommendations

5.1.1 Conclusions

- The use of VMF1 increases the accuracy of the fixed point coordinates. The use of VMF1/GPT50 is good for fixing the East and North offsets well as the VMF1/UFL is good for fixing the Up offsets of points. It should however be noted that the accuracy of the GPS height is still not accurate because of the physical limitation of the GPS system. This limitation is that, the receiver cannot track satellites below its horizon, hence symmetrical errors in the heights of the GPS points do not cancel out as does the symmetrical errors in the horizontal coordinates fixed by GPS because a receiver can track satellites from horizon to horizon.

- Modeling more gradients increases accuracy of the points for the East and North offset well and Up offset slightly. Increasing gradients estimated per day from one to three slightly increases the accuracy of the East and North offsets and at some stations it is constant implying that estimating two gradients is sufficient in this case. Also if the WRMS for when one, two and three gradients are estimated per day when modeling the Troposphere is averaged it gives the WRMS obtained when two gradients are estimated per day. This is not the case with the Up offset where the increase in gradients increases the bias in the results for the modeled local Troposphere and accuracy slightly increases and reduces for some stations basing on their stability in the height for long GPS data sessions (Europe and North America). This could be due to the fact that we did not have a serious storm surge when the data used is this research was collected. Estimating two gradients when fixing the Up offset is not sufficient, the more gradients the better the height is fixed.

- In dry and flat regions different MF/APRIORI combinations obtain the same accuracy for the East and North offsets. Implying that for such situations as in the northern part of Africa any MF/APRIORI combination will attain the required accuracy since there is no

drastic change in the weather spatially and temporally. However VMF1/UFL estimates the Up Offset best. This implies that even when there is no lateral or temporal variation in temperature, pressure and humidity in an area the effect of the troposphere may be minimal on the East and North Offset but it will be still significant in the Up offset.

5.1.2 Recommendations

- If there is a serious storm surge over the GPS points that one is fixing, then gradients more than three should be modelled. This is because in such cases the increase in the gradients will capture well the lateral azimuthal variation of temperature, pressure and humidity in the areas. This will produce millimetre accuracy in such bad weather conditions.

- Gradients should also be varied using different MF/APRIORI combinations. This is because in this research, VMF1/UFL was the combination used to study the effect of changing the number of gradients estimated per day on the Tropospheric delay and accuracy of the GPS coordinates fixed. This combination was used because it is one of the newest mapping functions released just in 2004, but with the creation of new mapping functions and luck of knowledge on the effect of increasing gradients on the other MF/APRIORI combinations. Research should be done in this area.

- The Tropospheric delay should also be modelled using the Meteorological Rinex files (RNX) as the a priori zenith constraints. This is anticipated to improve greatly on the accuracy of modelling the Troposphere and improve the accuracy of the fixed GPS points. This is because, the a priori files based on the grid, even if their resolution has greatly improved to 0.25m for VMF1 at some points on the earth's surface. The *ah*-coefficients, *aw*-coefficients, Zenith Hydrostatic and Wet delays are not precisely the ones representing the IGS stations or GPS points environments, it is because the parameters at the stations are derived by interpolation but for the RNX, the parameters will be unique to the stations and will describe the situation at the IGS station or GPS point accurately as the parameters to be included in the files are measured at site. For the

local data, the pressure, temperature and humidity will be observed and measured by the team at site. This will capture well the lateral and temporal variation of the weather around the GPS stations. In this research, these files were not used because still few IGS stations today collect their own RNX files and also pressure, temperature and humidity was not measured at the local stations in Uganda during the GPS data collection. Say, out of eight IGS stations in a network, three or four would have their own RNX files. But in the future this will be no problem as teams maintaining the IGS stations today are incorporating components that measure pressure, temperature and humidity to prepare their own RNX files.

REFERENCES

Bar-Sever, Y. E. , (1998), P. M. Kroger, and J. A. Borjesson, Estimating horizontal gradients of tropospheric path delay with a single GPS receiver, J. Geo-phys. Res., 103, 5019– 5035.

Berg H (1948) Allgemeine Meteorologie. Dümmlers Verlag, Bonn

Blewitt, G., Heflin, M.B., Vigue, Y., Zumberge, J.F., Jefferson, D. and Webb, F.H.,(1993), The Earth viewed as a deforming polyhedron: Method and results. Proceedings of the 1993 IGS Workshop, 25-26 March 1993, Astronomical Institute University of Berne.

Boehm J,Niell A, Tregoning P, Schuh,H (2006a), GlobalMapping Function(GMF): a newempirical mapping function based on numerical weather model data. Geophys Res Lett 33:L07304. doi:10.1029/2005GL025546

Boehm, J., and H. Schuh, (2004), Vienna Mapping Functions in VLBI analyses , Geophys. Res. Lett., 31, L01603, doi:10.1029/2003GL018984.

Chao, C.C.,(1974), The troposphere calibration model for Mariner Mars, JPL Technical Report 32-1587, NASA JPL, Pasadena CA.

Chen, G., and T.A. Herring (1997), Effects of atmospheric azimuthal asymmetry on the analysis of space geodetic data, Journal of Geophysical Research (B).

Chris, Rizos. (1999),.Introduction to GPS. University of New South Wales

Cross, P. A., (1992), Working Paper 6: Advanced least squares applied to position fixing, 2nd edition, Polytechnic of East London Department of Land Surveying.

Datta-Barua, S., Walter, T., Blanch, J., and Enge, P.(2008), Bounding higher order ionosphere errors for the dual-frequency GPS user, Radio Sci., 43, RS5010, doi:10.1029/2007RS003772.

Davies, P., and G. Blewitt (2000), Methodology for global geodetic time series estimation: A new tool for geodynamics, Journal of Geophysical Research, 105, No. B5, 11,083-11, 100,. 102, 20489–20502.

Davis, J.L., T.A. Herring, I.I. Shapiro, A.E.E. Rogers, and G. Elgered (1985), Geodesy by radio interferometry: Effects of atmospheric modelling errors on estimates of baseline length, Radio Science, 20, 1593–1607.

Davis, J.L., G. Elgered, A.E. Niell, and C.E. Kuehn (1993), Ground-based measurements of gradients in the "wet" radio refractivity of air, Radio Science, 28, 1003–1018.

Fritsche, M., R. Dietrich, C. Knofel, A. Rulke, S. Vey, M. Rothacher and P.Steigenberger, (2005), Impact of higher-order ionospheric terms on GPS estimates, Geophys.Res. Lett., 32, L23311, doi:10.1029/2005GL02434223.

Hernandez-Pajares, M., J. M. Juan, J. Sanz and R. Ors,(2007), Second-order ionospheric term in GPS: mplementation and impact on geodetic estimates, J. Geophys. Res.,112, B08417,doi:10.1029/2006JB004707.

Herring, T.A. (1992), Modelling atmospheric delays in the analysis of space geodetic data, in Refraction of trans atmospheric signals in geodesy, pp. 157–164.

Iyer, R.S., and J.L. Bufton (1977), Corrections for atmospheric refractivity in satellite laser ranging, Applied Optics, 16, 1997–2003.

J.Kouba (2009), Testing of Global Pressure / Temperature (GPT) model and Global Mapping Function (GMF) in GPS analyses, Springer – Verlag,. 83:199-208 DOI : 10.1007/s00190-008-0229-6

MacMillan, D.S., and C. Ma,(1998), Using Meteorological Data Assimilation Models in Computing Tropospheric Delays at Microwave Frequencies, Phys. Chem. Earth, Vol. 23, No. 1, pp. 97-102,

MacMillan, D.S., and C. Ma,(1997), Atmospheric gradients and the VLBI terrestrial and celestial reference frames, Geophysical Research Letters, 24, 453–456.

MacMillan, D.S. (1995), Atmospheric gradients from very long baseline interferometry observations, Geophysical Research Letters, 22, 1041-1044.

MacMillan, D.S., and C. Ma,(1994), Evaluation of very long baseline interferometry atmospheric modelling improvements, J. Geophys. Res., 99, B1, pp. 637-651.

Marini, J.W., (1972) Correction of satellite tracking data for an arbitrary tropospheric profile, Radio Science, Vol. 7, No. 2, pp. 223-231.

Munck, J.C. de, (1991),Tropospheric effects on baseline measurements by using (GPS) satellites, Tech. rep. 91-3, DUT, Faculty of Geodetic Engineering.

Niell, A.E., and L. Petrov, (2003), Using a Numerical Weather Model to Improve Geodesy, in Proceedings: The State of GPS Vertical Positioning Precision: Separation of Earth Processes by Space Geodesy, April 2-4, 2003, Luxembourg.

Niell, A.E., A.J. Coster, F.S. Solheim, V.B. Mendes, P.C. Toor, R.B. Langley, and C.A. Upham, (2001), Comparison of Measurements of Atmospheric Wet Delay by Radiosonde, Water Vapor Radiometre, GPS and VLBI, Journal of Atmospheric and Oceanic Technology, 18, pp. 830-850.

Niell, A.E.,(2000), Improved atmospheric mapping functions for VLBI and GPS, Earth Planets Space, 52, pp. 699-702.

Niell, A.E.,(1996), Global mapping functions for the atmosphere delay at radio wavelengths, J. Geophys. Res., 101, B2, pp. 3227-3246.

Saastamoinen, J. (1973), Contributions to the Theory of Atmospheric Refraction, Part II, Bulletin Geodesique, Vol. 107, pp. 13-34.

Seeber, G. (1993), Satellite Geodesy, Foundations, Methods, and Applications, Walter de Gruyter, Berlin.

Spilker Jr., J.J.,(1980), GPS signal structure and performance characteristics. In: Global Positioning System, papers published in **Navigation,** reprinted by the (U.S.) Inst. of Navigation,Vol.1, 29-54.

Simmons, A.J., and J.K. Gibson (editors),(2000), The ERA-40 Project Plan, ERA-40 Project Report Series No. 1, http://www.ecmwf.int.

APPENDIX 1

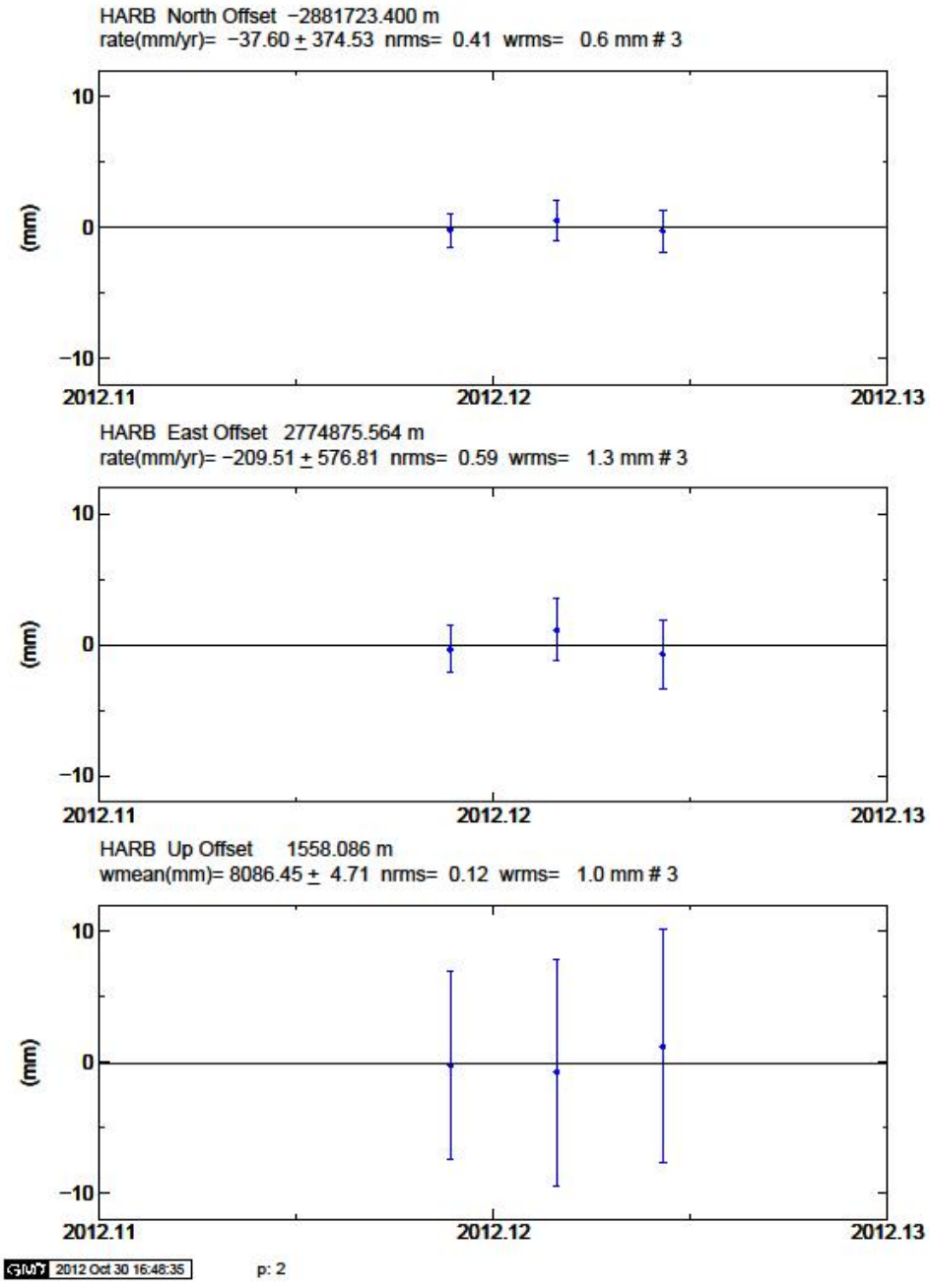

WRMs Residual Plot for VMF1-U-FILE Combination gradient 0 for HARB station (Uganda)

APPENDIX 2

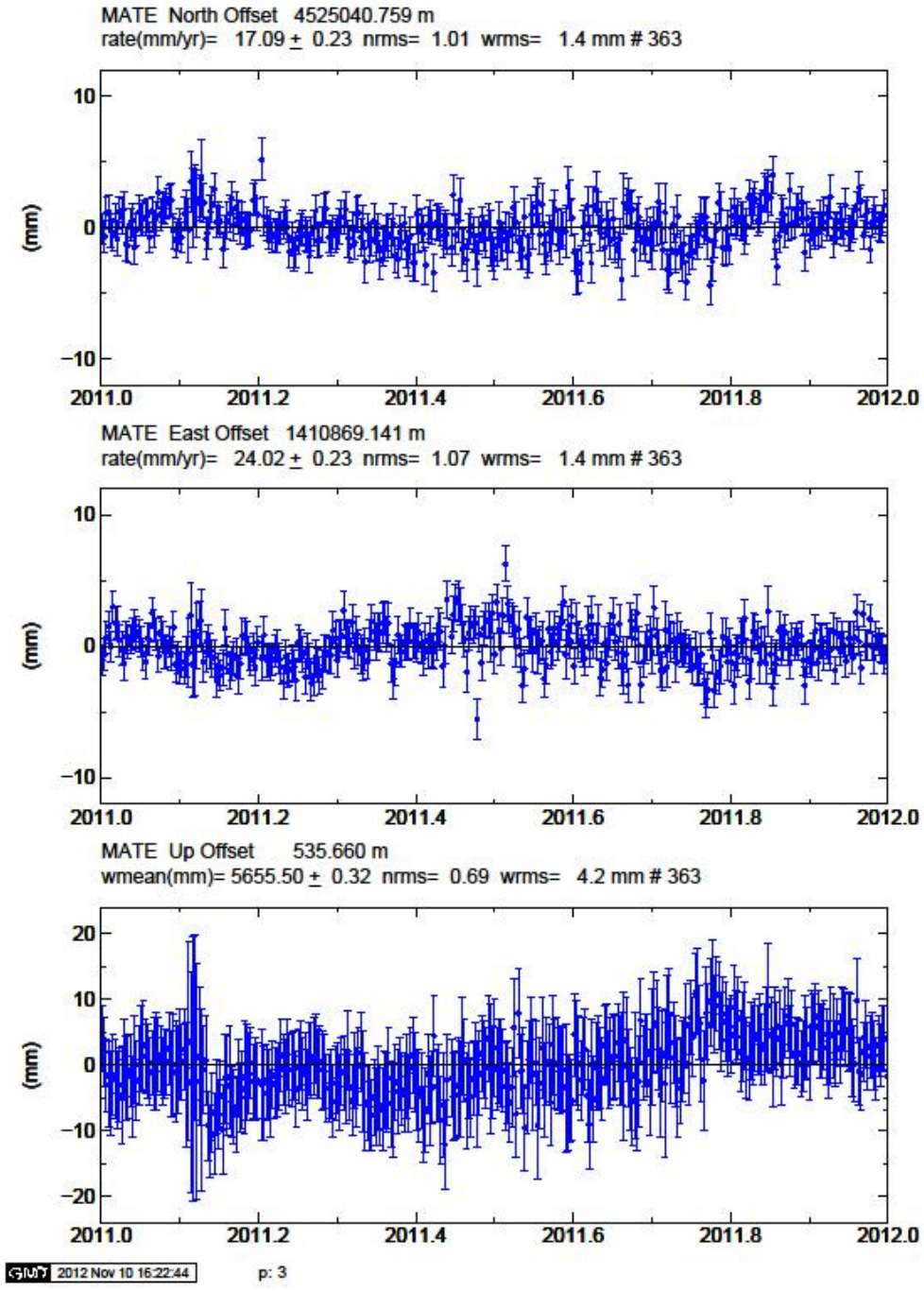

WRMs Residual Plot for VMF1-U-FILE Combination gradient 0 for MATE station (Europe)

APPENDIX 3

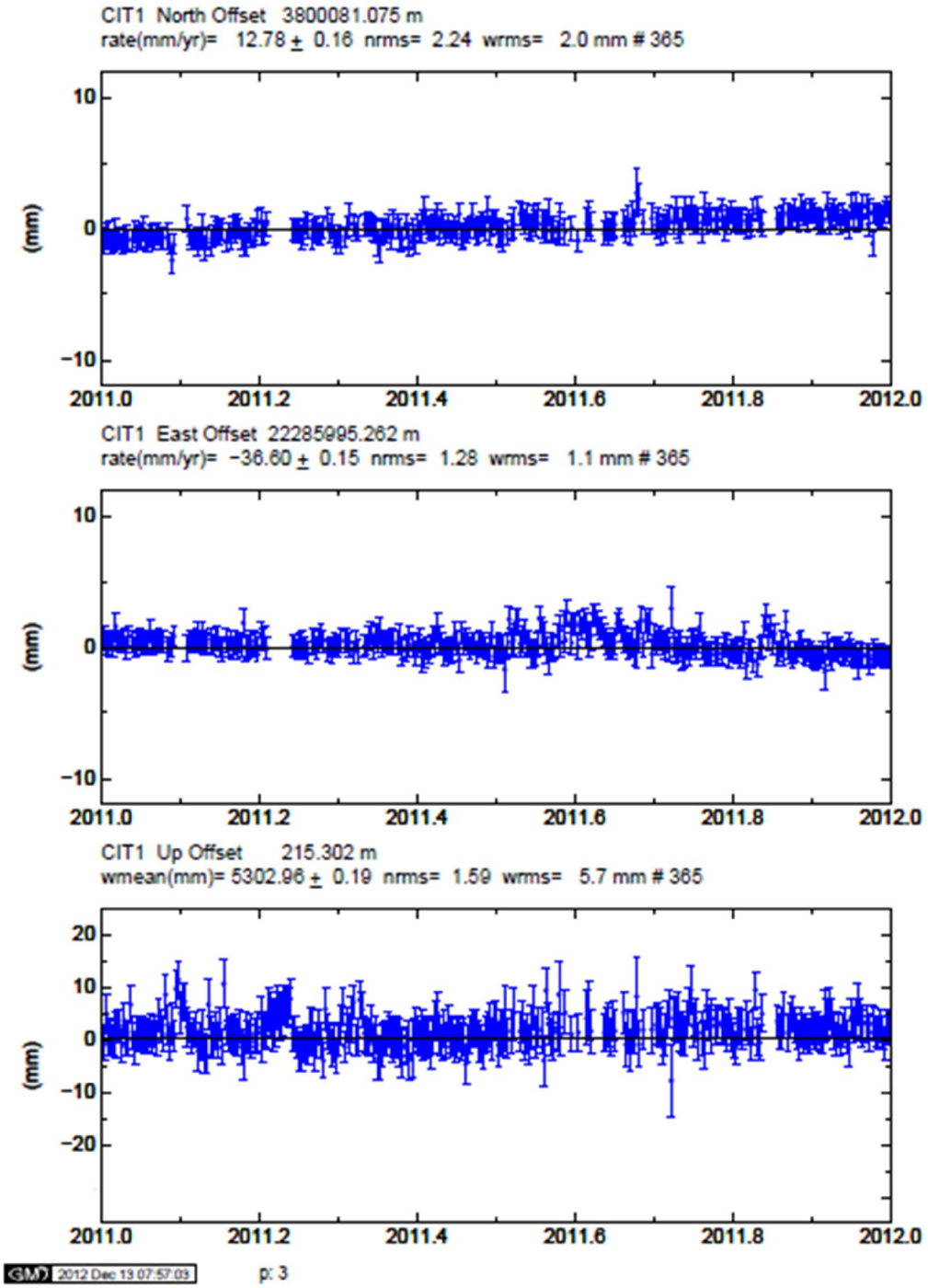

WRMs Residual Plot for NMF-GPT50 Combination gradient 2 for CIT1 station (North America)

APPENDIX 4

UGANDA DATA (RAW DATA)

The WRM VMF1-U-FILE gradient 0

GPS Data = Uganda					
Mapping Function = Vienna Mapping Function (VMF1)					
A priori Constraint = (U-File)UFL					
Gradient Value = 0					
Weighted Root Mean Square(WRM)					
Stn no	Name full	Name (Short)	North offset(mm)	East offset(mm)	Up offset(mm)
1	Addis Ababa University	ADIS	0.6	1.2	1.2
2	Hartebeesthoek	HARB	0.6	1.3	1
3	Malindi	MAL2	0.7	1.5	4.5
4	N'Koltang (Gabon)	NKLG	2.3	4.7	6.4
5	Lusaka (Zambia)	ZAMB	1.5	2.5	6.3
6	Jinja	JINJ	1.6	3.7	1.4
7	Kiboga	KIBO	1.8	0.6	3.9
8	Mbarara	MBRA	2.8	2.7	2.4
9	Rhino Camp	RHIN	1.2	0.3	6.8

The WRM VMF1-U-FILE gradient 1

GPS Data = Uganda					
Mapping Function = Vienna Mapping Function (VMF1)					
A priori Constraint = (U-File)UFL					
Gradient Value = 1					
Weighted Root Mean Square(WRM)					
Stn no	Name full	Name (Short)	North offset(mm)	East offset(mm)	Up offset(mm)
1	Addis Ababa University	ADIS	0.4	0.5	1.4
2	Hartebeesthoek	HARB	0.6	0.5	1.1
3	Malindi	MAL2	0.2	2	5.1
4	N'Koltang (Gabon)	NKLG	2.6	3.4	5.3
5	Lusaka (Zambia)	ZAMB	1.7	1.9	5.4
6	Jinja	JINJ	1.1	4.4	1.5
7	Kiboga	KIBO	1.2	0.6	4
8	Mbarara	MBRA	0.8	1.8	2
9	Rhino Camp	RHIN	0.2	0.8	7.7

The WRM VMF1-U-FILE gradient 2

GPS Data = Uganda					
Mapping Function = Vienna Mapping Function (VMF1)					
A priori Constraint = (U-File)UFL					
Gradient Value = 2					
Weighted Root Mean Square(WRM)					
Stn no	Name full	Name (Short)	North offset(mm)	East offset(mm)	Up offset(mm)
1	Addis Ababa University	ADIS	0.2	1.1	2.3
2	Hartebeesthoek	HARB	0.6	0.5	3.1
3	Malindi	MAL2	0.2	2.2	6
4	N'Koltang (Gabon)	NKLG	2.7	1.4	4.5
5	Lusaka (Zambia)	ZAMB	2	1.1	4.6
6	Jinja	JINJ	0.6	0.7	5
7	Kiboga	KIBO	0.2	0.1	4.7
8	Mbarara	MBRA	1	1.3	2.1
9	Rhino Camp	RHIN	1.2	0.8	7.5

The WRM VMF1-U-FILE gradient 3

GPS Data = Uganda					
Mapping Function = Vienna Mapping Function (VMF1)					
A priori Constraint = (U-File)UFL					
Gradient Value = 3					
Weighted Root Mean Square(WRM)					
Stn no	Name full	Name (Short)	North offset(mm)	East offset(mm)	Up offset(mm)
1	Addis Ababa University	ADIS	0.3	0.2	2.7
2	Hartebeesthoek	HARB	0.5	0.5	2.7
3	Malindi	MAL2	0.1	1.8	5.6
4	N'Koltang (Gabon)	NKLG	2.6	1.6	4.2
5	Lusaka (Zambia)	ZAMB	2	1.2	4.5
6	Jinja	JINJ	0.4	1	5.8
7	Kiboga	KIBO	0.2	0.2	5.1
8	Mbarara	MBRA	1.1	1.4	2.8
9	Rhino Camp	RHIN	1.1	0.7	7.1

The WRM VMF1-GPT50 gradient 2

GPS Data = Uganda					
Mapping Function = Vienna Mapping Function (VMF1)					
A priori Constraint = (Global Temperature Pressure) GPT 50					
Gradient Value = 2					
Weighted Root Mean Square(WRM)					
Stn no	Name full	Name (Short)	North offset(mm)	East offset(mm)	Up offset(mm)
1	Addis Ababa University	ADIS	0	0.4	2.8
2	Hartebeesthoek	HARB	0.6	0.6	3.4
3	Malindi	MAL2	0.3	2	6
4	N'Koltang (Gabon)	NKLG	2.6	1.5	4.7
5	Lusaka (Zambia)	ZAMB	1.9	1.1	4.5
6	Jinja	JINJ	0.6	0.7	5.1
7	Kiboga	KIBO	0.3	0	4.8
8	Mbarara	MBRA	0.9	1.3	2
9	Rhino Camp	RHIN	1.3	0.7	7.8

The WRM GMF-GPT50 gradient 2

GPS Data = Uganda					
Mapping Function = Global Mapping Function (GMF)					
A priori Constraint = GPT50					
Gradient Value = 2					
Weighted Root Mean Square(WRM)					
Stn no	Name full	Name (Short)	North offset(mm)	East offset(mm)	Up offset(mm)
1	Addis Ababa University	ADIS	0	0.5	2.9
2	Hartebeesthoek	HARB	0.6	0.6	3.5
3	Malindi	MAL2	0.3	2.1	6.1
4	N'Koltang (Gabon)	NKLG	2.7	1.5	4.7
5	Lusaka (Zambia)	ZAMB	1.9	1.1	4.5
6	Jinja	JINJ	0.6	0.8	5.2
7	Kiboga	KIBO	0.3	0.1	5.1
8	Mbarara	MBRA	0.9	1.3	2.1
9	Rhino Camp	RHIN	1.3	0.7	7.9

The WRM NMF-GPT50 gradient 2

GPS Data = Uganda					
Mapping Function = Niell Mapping Function (NMF)					
A priori Constraint = GPT50					
Gradient Value = 2					
Weighted Root Mean Square(WRM)					
Stn no	Name full	Name (Short)	North offset(mm)	East offset(mm)	Up offset(mm)
1	Addis Ababa University	ADIS	0.2	1.1	2.3
2	Hartebeesthoek	HARB	0.6	0.5	3.1
3	Malindi	MAL2	0.2	2.2	6
4	N'Koltang (Gabon)	NKLG	2.7	1.4	4.5
5	Lusaka (Zambia)	ZAMB	2	1.1	4.6
6	Jinja	JINJ	0.6	0.7	5
7	Kiboga	KIBO	0.2	0.1	4.7
8	Mbarara	MBRA	1	1.3	2.1
9	Rhino Camp	RHIN	1.2	0.8	7.5

APPENDIX 5

EUROPE DATA (RAW DATA)

The WRM VMF1-U-FILE gradient 0

GPS Data = Europe					
Mapping Function = Vienna Mapping Function (VMF1)					
A priori Constraint = (U-File)UFL					
Gradient Value = 0					
Weighted Root Mean Square(WRM)					
Stn no	Name full	Name (Short)	North offset(mm)	East offset(mm)	Up offset(mm)
1	Brussels	BRUS	1.7	2	2.8
2	Frankfurt	FFMJ	1.6	1.6	4.3
3	Matera	MATE	1.4	1.4	4.2
4	Onsala	ONSA	1.4	1.5	3.8
5	Braunschweig	PTBB	1.2	1.2	3.3
6	Villafranca	VILL	1.3	1.4	3.8
7	Zimmerland	ZIMM	1	1.1	2.3

The WRM VMF1-U-FILE gradient 1

GPS Data = Europe					
Mapping Function = Vienna Mapping Function (VMF1)					
A priori Constraint = (U-File)UFL					
Gradient Value = 1					
Weighted Root Mean Square(WRM)					
Stn no	Name full	Name (Short)	North offset(mm)	East offset(mm)	Up offset(mm)
1	Brussels	BRUS	1.6	2	2.9
2	Frankfurt	FFMJ	1.1	1.2	4.2
3	Matera	MATE	1.1	1.1	4.3
4	Onsala	ONSA	1.1	1.1	3.5
5	Braunschweig	PTBB	1	1.1	3.1
6	Villafranca	VILL	1	1.2	3.6
7	Zimmerland	ZIMM	0.8	0.9	2.3

The WRM VMF1-U-FILE gradient 2

GPS Data = Europe					
Mapping Function = Vienna Mapping Function (VMF1)					
A priori Constraint = (U-File)**UFL**					
Gradient Value = 2					
Weighted Root Mean Square(WRM)					
Stn no	Name full	Name (Short)	North offset(mm)	East offset(mm)	Up offset(mm)
1	Brussels	BRUS	1.7	1.9	3
2	Frankfurt	FFMJ	1.1	1.1	4.2
3	Matera	MATE	1	1	4.6
4	Onsala	ONSA	1.2	1	3.5
5	Braunschweig	PTBB	1	0.9	3.2
6	Villafranca	VILL	1	1.1	3.7
7	Zimmerland	ZIMM	0.8	0.9	2.4

The WRM VMF1-U-FILE gradient 3

GPS Data = Europe					
Mapping Function = Vienna Mapping Function (VMF1)					
A priori Constraint = (U-File)UFL					
Gradient Value = 3					
Weighted Root Mean Square(WRM)					
Stn no	Name full	Name (Short)	North offset(mm)	East offset(mm)	Up offset(mm)
1	Brussels	BRUS	1.7	1.9	3.1
2	Frankfurt	FFMJ	1.1	1.1	4.3
3	Matera	MATE	1	1	4.4
4	Onsala	ONSA	1.1	1	3.5
5	Braunschweig	PTBB	1	0.8	3
6	Villafranca	VILL	1	1.1	3.7
7	Zimmerland	ZIMM	0.8	0.9	2.3

The WRM VMF1-GPT50 gradient 2

GPS Data = Europe					
Mapping Function = Vienna Mapping Function (VMF1)					
A priori Constraint = (Global Temperature Pressure) **GPT 50**					
Gradient Value = 2					
Weighted Root Mean Square(WRM)					
Stn no	Name full	Name (Short)	North offset(mm)	East offset(mm)	Up offset(mm)
1	Brussels	BRUS	1.7	1.9	3
2	Frankfurt	FFMJ	1.1	1.1	4.3
3	Matera	MATE	1	1	4.5
4	Onsala	ONSA	1.1	1	3.4
5	Braunschweig	PTBB	1	0.8	3.1
6	Villafranca	VILL	1	1.1	3.6
7	Zimmerland	ZIMM	0.8	0.9	2.4

The WRM GMF-GPT50 gradient 2

GPS Data = Europe					
Mapping Function = Global Mapping Function (GMF)					
A priori Constraint = (Global Temperature Pressure) **GPT 50**					
Gradient Value = 2					
Weighted Root Mean Square(WRM)					
Stn no	Name full	Name (Short)	North offset(mm)	East offset(mm)	Up offset(mm)
1	Brussels	BRUS	1.7	1.9	3.1
2	Frankfurt	FFMJ	1.1	1.1	4.2
3	Matera	MATE	1.1	1	4.6
4	Onsala	ONSA	1.2	1	3.7
5	Braunschweig	PTBB	1	0.9	3.2
6	Villafranca	VILL	1	1.1	3.7
7	Zimmerland	ZIMM	0.8	0.9	2.4

The WRM NMF-GPT50 gradient 2

GPS Data = Europe					
Mapping Function = Niell Mapping Function (NMF)					
A priori Constraint = (Global Temperature Pressure) **GPT 50**					
Gradient Value = 2					
Weighted Root Mean Square(WRM)					
Stn no	Name full	Name (Short)	North offset(mm)	East offset(mm)	Up offset(mm)
1	Brussels	BRUS	1.7	1.9	3
2	Frankfurt	FFMJ	1.1	1.1	4.2
3	Matera	MATE	1	1	4.6
4	Onsala	ONSA	1.2	1	3.5
5	Braunschweig	PTBB	1	0.9	3.2
6	Villafranca	VILL	1	1.1	3.7
7	Zimmerland	ZIMM	0.8	0.9	2.4

APPENDIX 6

NORTH AMERICA DATA (RAW DATA)

The WRM VMF1-U-FILE gradient 0

GPS Data = North America					
Mapping Function = Vienna Mapping Function (VMF1)					
A priori Constraint = (U-File)UFL					
Gradient Value = 0					
Weighted Root Mean Square(WRM)					
Stn no	Name full	Name (Short)	North offset(mm)	East offset(mm)	Up offset(mm)
1	Blythe	BLYT	2.5	2	6.5
2	Brand Basin	BRAN	2.4	1.5	13.2
3	Caltech	CIT1	2.1	1.2	5.9
4	JPL Mesa	JPLM	1.7	0.7	7.3
5	Mt. Wilson	WSLN	2.8	2.7	12.4

The WRM VMF1-U-FILE gradient 1

GPS Data = North America					
Mapping Function = Vienna Mapping Function (VMF1)					
A priori Constraint = (U-File)UFL					
Gradient Value = 1					
Weighted Root Mean Square(WRM)					
Stn no	Name full	Name (Short)	North offset(mm)	East offset(mm)	Up offset(mm)
1	Blythe	BLYT	2	1.7	5.2
2	Brand Basin	BRAN	2.4	1.3	14.3
3	Caltech	CIT1	2	1.3	5.6
4	JPL Mesa	JPLM	1.9	0.7	7.4
5	Mt. Wilson	WSLN	2.6	2.5	12

The WRM VMF1-U-FILE gradient 2

GPS Data = North America					
Mapping Function = Vienna Mapping Function (VMF1)					
A priori Constraint = (U-File)**UFL**					
Gradient Value = 2					
Weighted Root Mean Square(WRM)					
Stn no	Name full	Name (Short)	North offset(mm)	East offset(mm)	Up offset(mm)
1	Blythe	BLYT	2.1	1.6	5.3
2	Brand Basin	BRAN	2.1	1.4	13.5
3	Caltech	CIT1	2	1.1	5.6
4	JPL Mesa	JPLM	1.9	0.8	7.8
5	Mt. Wilson	WSLN	2.6	2.3	12.6

The WRM VMF1-U-FILE gradient 3

GPS Data = North America					
Mapping Function = Vienna Mapping Function (VMF1)					
A priori Constraint = (U-File)UFL					
Gradient Value = 3					
Weighted Root Mean Square(WRM)					
Stn no	Name full	Name (Short)	North offset(mm)	East offset(mm)	Up offset(mm)
1	Blythe	BLYT	2.1	1.6	5.3
2	Brand Basin	BRAN	2.1	1.4	13.5
3	Caltech	CIT1	2	1.2	5.7
4	JPL Mesa	JPLM	1.9	0.8	7.7
5	Mt. Wilson	WSLN	2.6	2.3	12.3

The WRM VMF1-GPT50 gradient 2

GPS Data = North America					
Mapping Function = Vienna Mapping Function (VMF1)					
A priori Constraint = (Global Temperature Pressure) **GPT 50**					
Gradient Value = 2					
Weighted Root Mean Square(WRM)					
Stn no	Name full	Name (Short)	North offset(mm)	East offset(mm)	Up offset(mm)
1	Blythe	BLYT	2.1	1.6	5.4
2	Brand Basin	BRAN	2.1	1.4	13.6
3	Caltech	CIT1	2	1.1	5.8
4	JPL Mesa	JPLM	1.9	0.8	7.9
5	Mt. Wilson	WSLN	2.6	2.2	12.7

The WRM GMF-GPT50 gradient 2

GPS Data = North America					
Mapping Function = Global Mapping Function (GMF)					
A priori Constraint = (Global Temperature Pressure) **GPT 50**					
Gradient Value = 2					
Weighted Root Mean Square(WRM)					
Stn no	Name full	Name (Short)	North offset(mm)	East offset(mm)	Up offset(mm)
1	Blythe	BLYT	2.1	1.6	5.4
2	Brand Basin	BRAN	2.1	1.4	13.6
3	Caltech	CIT1	2.0	1.1	5.7
4	JPL Mesa	JPLM	1.9	0.8	7.8
5	Mt. Wilson	WSLN	2.6	2.3	12.6

The WRM NMF-GPT50 gradient 2

GPS Data = North America					
Mapping Function = Niell Mapping Function (NMF)					
A priori Constraint = (Global Temperature Pressure) **GPT 50**					
Gradient Value = 2					
Weighted Root Mean Square(WRM)					
Stn no	Name full	Name (Short)	North offset(mm)	East offset(mm)	Up offset(mm)
1	Blythe	BLYT	2.1	1.6	5.4
2	Brand Basin	BRAN	2.1	1.4	13.6
3	Caltech	CIT1	2.0	1.1	5.7
4	JPL Mesa	JPLM	1.9	0.8	7.9
5	Mt. Wilson	WSLN	2.6	2.3	12.6

APPENDIX 7

UGANDA DATA (Plotted)

Different Combinations with gradient 2 for the North offset

North Offset	Gradient=2	Uganda Data		Units=(mm)					
	ADIS	HARB	MAL2	NKLG	ZAMB	JINJ	KIBO	MBRA	RHIN
VMF1-U-FILE	0.2	0.6	0.2	2.7	2	0.6	0.2	1	1.2
NMF-GPT50	0.2	0.6	0.2	2.7	2	0.6	0.2	1	1.2
GMF-GPT50	0	0.6	0.3	2.7	1.9	0.6	0.3	0.9	1.3
VMF1-GPT50	0	0.6	0.3	2.6	1.9	0.6	0.3	0.9	1.3

Different Combinations with gradient 2 for the East offset

East Offset	Gradient=2	Uganda Data		Units=(mm)					
	ADIS	HARB	MAL2	NKLG	ZAMB	JINJ	KIBO	MBRA	RHIN
VMF1-U-FILE	1.1	0.5	2.2	1.4	1.1	0.7	0.1	1.3	0.8
NMF-GPT50	1.1	0.5	2.2	1.4	1.1	0.7	0.1	1.3	0.8
GMF-GPT50	0.5	0.6	2.1	1.5	1.1	0.8	0.1	1.3	0.7
VMF1-GPT50	0.4	0.6	2	1.5	1.1	0.7	0	1.3	0.7

Different Combinations with gradient 2 for the Up offset

Up Offset	Gradient=2	Uganda Data		Units=(mm)					
	ADIS	HARB	MAL2	NKLG	ZAMB	JINJ	KIBO	MBRA	RHIN
VMF1-U-FILE	2.3	3.1	6	4.5	4.6	5	4.7	2.1	7.5
NMF-GPT50	2.3	3.1	6	4.5	4.6	5	4.7	2.1	7.5
GMF-GPT50	2.9	3.5	6.1	4.7	4.5	5.2	5.1	2.1	7.9
VMF1-GPT50	2.8	3.4	6	4.7	4.5	5.1	4.8	2	7.8

Different gradients for VMF1-U-FILE Combinations for the North offset

North Offset		Uganda Data			Units=(mm)				
	ADIS	HARB	MAL2	NKLG	ZAMB	JINJ	KIBO	MBRA	RHIN
VMF1-U-FILE (0)	0.6	0.6	0.7	2.3	1.5	1.6	1.8	2.8	1.2
VMF1-U-FILE (1)	0.4	0.6	0.2	2.6	1.7	1.1	1.2	0.8	0.2
VMF1-U-FILE (2)	0.2	0.6	0.2	2.7	2	0.6	0.2	1	1.2
VMF1-U-FILE (3)	0.3	0.5	0.1	2.6	2	0.4	0.2	1.1	1.1

Different gradients for VMF1-U-FILE Combinations for the East offset

East Offset		Uganda Data			Units=(mm)				
	ADIS	HARB	MAL2	NKLG	ZAMB	JINJ	KIBO	MBRA	RHIN
VMF1-U-FILE (0)	1.2	1.3	1.5	4.7	2.5	3.7	0.6	2.7	0.3
VMF1-U-FILE (1)	0.5	0.5	2	3.4	1.9	4.4	0.6	1.8	0.8
VMF1-U-FILE (2)	1.1	0.5	2.2	1.4	1.1	0.7	0.1	1.3	0.8
VMF1-U-FILE (3)	0.2	0.5	1.8	1.6	1.2	1	0.2	1.4	0.7

Different gradients for VMF1-U-FILE Combinations for the Up offset

Up Offset		Uganda Data			Units=(mm)				
	ADIS	HARB	MAL2	NKLG	ZAMB	JINJ	KIBO	MBRA	RHIN
VMF1-U-FILE (0)	1.2	1	4.5	6.4	6.3	1.4	3.9	2.4	6.8
VMF1-U-FILE (1)	1.4	1.1	5.1	5.3	5.4	1.5	4	2	7.7
VMF1-U-FILE (2)	2.3	3.1	6	4.5	4.6	5	4.7	2.1	7.5
VMF1-U-FILE (3)	2.7	2.7	5.6	4.2	4.5	5.8	5.1	2.8	7.1

APPENDIX 8

EUROPE DATA (Plotted)

Different Combinations with gradient 2 for the North offset

North Offset	Gradient=2	Europe Data		Units=(mm)			
	BRUS	FFMJ	MATE	ONSA	PTBB	VILL	ZIMM
VMF1-U-FILE	1.8	1.4	1.1	1.1	1	1	0.9
NMF-GPT50	1.7	1.1	1	1.2	1	1	0.8
GMF-GPT50	1.7	1.1	1.1	1.2	1	1	0.8
VMF1-GPT50	1.7	1.1	1	1.1	1	1	0.8

Different Combinations with gradient 2 for the East offset

East Offset	Gradient=2	Europe Data		Units=(mm)			
	BRUS	FFMJ	MATE	ONSA	PTBB	VILL	ZIMM
VMF1-U-FILE	2	1.4	1	1	0.8	1.2	0.9
NMF-GPT50	1.9	1.1	1	1	0.9	1.1	0.9
GMF-GPT50	1.9	1.1	1	1	0.9	1.1	0.9
VMF1-GPT50	1.9	1.1	1	1	0.8	1.1	0.9

Different Combinations with gradient 2 for the Up offset

Up Offset	Gradient=2	Europe Data		Units=(mm)			
	BRUS	FFMJ	MATE	ONSA	PTBB	VILL	ZIMM
VMF1-U-FILE	3	4.3	4.4	3.4	3.1	3.8	2.4
NMF-GPT50	3	4.2	4.6	3.5	3.2	3.7	2.4
GMF-GPT50	3.1	4.2	4.6	3.7	3.2	3.7	2.4
VMF1-GPT50	3	4.3	4.5	3.4	3.1	3.6	2.4

Different gradients for VMF1-U-FILE Combinations for the North offset

North Offset		Europe Data		Units=(mm)			
	BRUS	FFMJ	MATE	ONSA	PTBB	VILL	ZIMM
VMF1-U-FILE (0)	1.7	1.6	1.4	1.4	1.2	1.3	1
VMF1-U-FILE (1)	1.6	1.1	1.1	1.1	1	1	0.8
VMF1-U-FILE (2)	1.8	1.4	1.1	1.1	1	1	0.9
VMF1-U-FILE (3)	1.7	1.1	1	1.1	1	1	0.8

Different gradients for VMF1-U-FILE Combinations for the East offset

East Offset		Europe Data		Units=(mm)			
	BRUS	FFMJ	MATE	ONSA	PTBB	VILL	ZIMM
VMF1-U-FILE (0)	2	1.6	1.4	1.5	1.2	1.4	1.1
VMF1-U-FILE (1)	2	1.2	1.1	1.1	1.1	1.2	0.9
VMF1-U-FILE (2)	2	1.4	1	1	0.8	1.2	0.9
VMF1-U-FILE (3)	1.9	1.1	1	1	0.8	1.1	0.9

Different gradients for VMF1-U-FILE Combinations for the East offset

Up Offset		Europe Data		Units=(mm)			
	BRUS	FFMJ	MATE	ONSA	PTBB	VILL	ZIMM
VMF1-U-FILE (0)	2.8	4.3	4.2	3.8	3.3	3.8	2.3
VMF1-U-FILE (1)	2.9	4.2	4.3	3.5	3.1	3.6	2.3
VMF1-U-FILE (2)	3	4.3	4.4	3.4	3.1	3.8	2.4
VMF1-U-FILE (3)	3.1	4.3	4.4	3.5	3	3.7	2.3

APPENDIX 9

NORTH AMERICA DATA (Plotted)

Different Combinations with gradient 2 for the North offset

North Offset	Gradient =2	North America Data (mm)			
	BLYT	BRAN	CIT1	JPLM	WSLN
VMF1-U-FILE	2.1	2.1	2	1.9	2.6
NMF-GPT50	2.1	2.1	2.0	1.9	2.6
GMF-GPT50	2.1	2.1	2.0	1.9	2.6
VMF1-GPT50	2.1	2.1	2	1.9	2.6

Different Combinations with gradient 2 for the East offset

East Offset	Gradient =2	North America Data(mm)			
	BLYT	BRAN	CIT1	JPLM	WSLN
VMF1-U-FILE	1.6	1.4	1.1	0.8	2.3
NMF-GPT50	1.6	1.4	1.1	0.8	2.3
GMF-GPT50	1.6	1.4	1.1	0.8	2.3
VMF1-GPT50	1.6	1.4	1.1	0.8	2.2

Different Combinations with gradient 2 for the Up offset

Up Offset	Gradient =2	North America Data(mm)			
	BLYT	BRAN	CIT1	JPLM	WSLN
VMF1-U-FILE	5.3	13.5	5.6	7.8	12.6
NMF-GPT50	5.4	13.6	5.7	7.9	12.6
GMF-GPT50	5.4	13.6	5.7	7.8	12.6
VMF1-GPT50	5.4	13.6	5.8	7.9	12.7

Different gradients for VMF1-U-FILE Combinations for the North offset

North Offset		North America Data(mm)			
	BLYT	BRAN	CIT1	JPLM	WSLN
VMF1-U-FILE (0)	2.5	2.4	2.1	1.7	2.8
VMF1-U-FILE (1)	2	2.4	2	1.9	2.6
VMF1-U-FILE (2)	2.1	2.1	2	1.9	2.6
VMF1-U-FILE (3)	2.1	2.1	2	1.9	2.6

Different gradients for VMF1-U-FILE Combinations for the East offset

East Offset		North America Data(mm)			
	BLYT	BRAN	CIT1	JPLM	WSLN
VMF1-U-FILE (0)	2	1.5	1.2	0.7	2.7
VMF1-U-FILE (1)	1.7	1.3	1.3	0.7	2.5
VMF1-U-FILE (2)	1.6	1.4	1.1	0.8	2.3
VMF1-U-FILE (3)	1.6	1.4	1.2	0.8	2.3

Different gradients for VMF1-U-FILE Combinations for the Up offset

Up Offset		North America Data(mm)			
	BLYT	BRAN	CIT1	JPLM	WSLN
VMF1-U-FILE (0)	6.5	13.2	5.9	7.3	12.4
VMF1-U-FILE (1)	5.2	14.3	5.6	7.4	12
VMF1-U-FILE (2)	5.3	13.5	5.6	7.8	12.6
VMF1-U-FILE (3)	5.3	13.5	5.7	7.7	12.3

APPENDIX 10

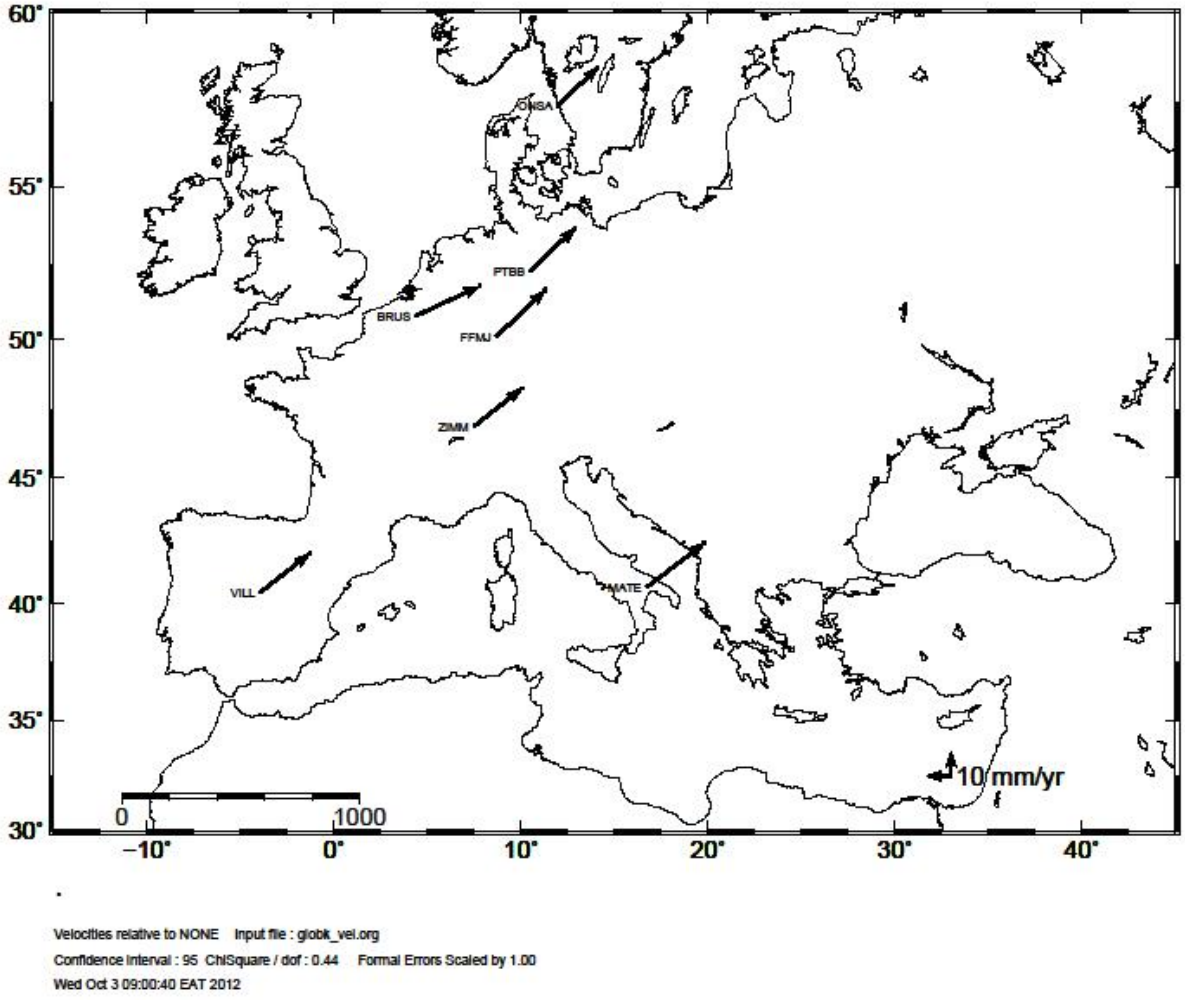

Velocity plot for the seven IGS stations located in Europe

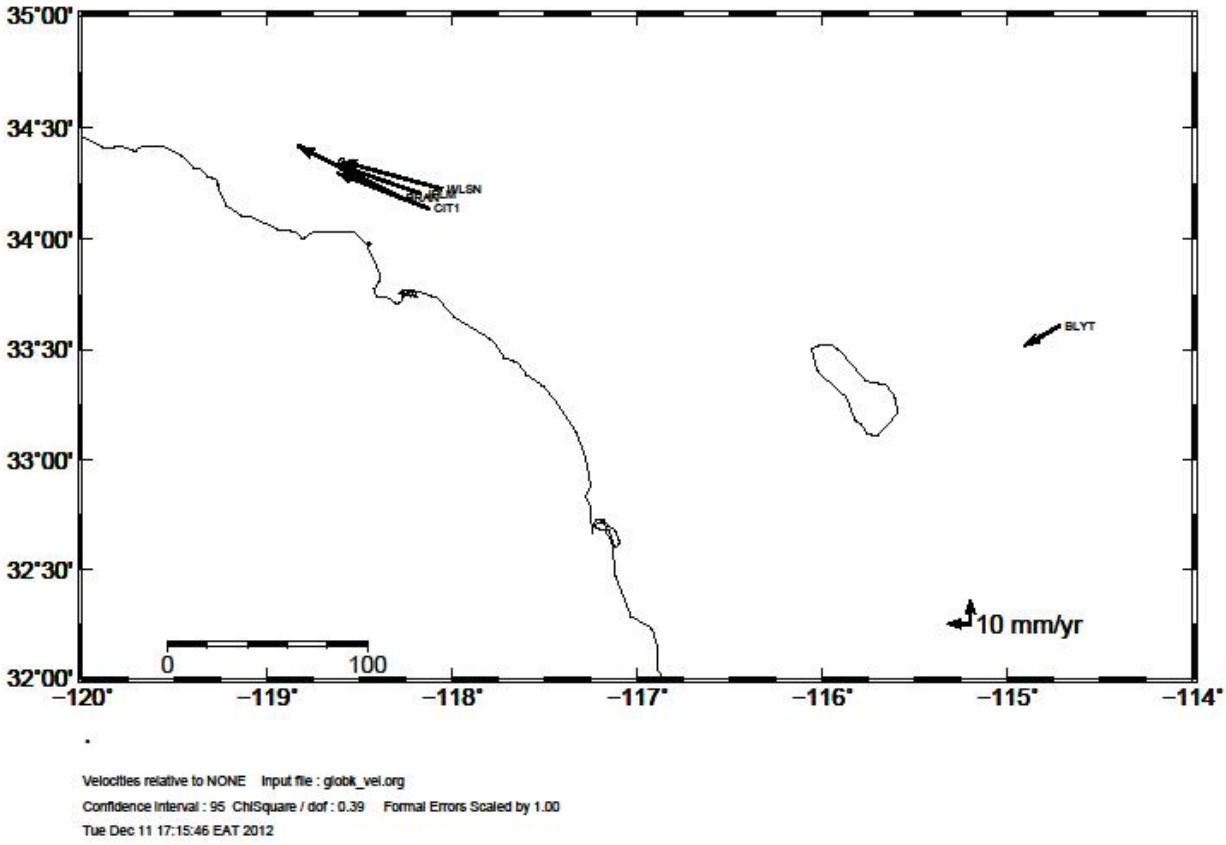

Velocity plot for the seven IGS stations located in North America

Declaration

"This thesis is my original work and has not been presented for a degree in any other university, and that all sources of material used for the thesis have been duly acknowledged."

SUBMITTED BY:

Makabayi Brian _____ _____

Signature Date

CONFIRMATION:

Dr. Addisu Hunegnaw _____ _____

Advisor(s) Signature Date